SELF - SIMILAR OPEN CHANNEL FLOW AND SAND RIBBONS WITH INFLUENT / EFFLUENT SEEPAGE

A Thesis Submitted
In Partial Fulfilment of the Requirements
for the Degree of
DOCTOR OF PHILOSOPHY

By

GAUTAM ROY

to the

DEPARTMENT OF CIVIL ENGINEERING
INDIAN INSTITUTE OF TECHNOLOGY KANPUR

NOVEMBER 1992

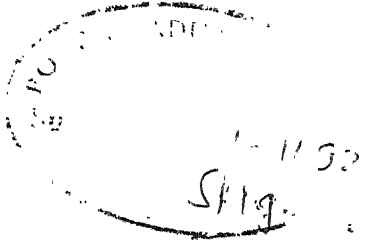

CERTIFICATE

It is certified that the work contained in this thesis entitled "Self-similar open channel flow and sand ribbons with influent/effluent seepage", by Mr. Gautam Roy, has been carried out under my supervision and that this work has not been submitted elsewhere for a degree.

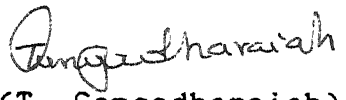

(T. Gangadharaiah)
Department of Civil Engineering
Indian Institute of Technology, Kanpur

November , 1992

SYNOPSIS

Flow in alluvial channals is often accompanied by influent/effluent seepage through the channel bed due to different free surface levels in channel and ambient ground water table. The problem of quantifying the effect of cross-bed seepage on open channel (OC) flow superficially resembles that of distributed suction/injection on a turbulent boundary layer (TBL), but the usual TBL assumption of constant V(y) (= injection rate V_w) is invalid in OC flow. The one-dimensional analysis commonly used in OC hydraulics is also unsatisfactory due to non-description of the mean flow and stress fields and assumptions on friction slope, S_f. In this work streamwise velocity, U, bed shear velocity, U_*, and energy gradient velocity, $\sqrt{a_g HS}$ (a_g is gravitational acceleration, H is flow depth and S is free surface slope) are assumed to be piecewise linear in X,

$$\left.\begin{aligned} U(x,y) &= F(y) + x\,G(y), \quad x = X/H_o, \quad y = Y/H_o; \\ U_*(x) &= U_* \ (1 + \beta x); \ \sqrt{a_g HS} = \sqrt{a_g H_o S_o}\ (1+\alpha x) \end{aligned}\right\} \quad (1)$$

It is shown that when $S \simeq S_o$ (bed slope boundary layer type equations are obtained if $|V_w/U_o| \ll 1$, which yield two coupled ODEs involving F(y) and G(y). Approximate solution of the ODEs for $|v_w| \ll 1$, where $v_w = V_w/\sqrt{a_g H_o S_o}$, shows that the flow is nearly self-similar with $G(y) \simeq \alpha F(y)$ and

$$F(y) = m\,[y^n - y_o^n - 6n^2\,(\sqrt{y} - \sqrt{y_o})] \quad (2)$$

where n varies directly with v_w, y_o is determined using Rubesin's criterion of invariant Reynolds number at sublayer-turbulent interface, and $\alpha \simeq \beta \simeq V_w/U_{av}$. F(y) and G(y), which resemble power laws, approach the log-law identically as $v_w \to 0$.

A set of flume experiments with immobile bed was conducted to verify the above model. Hydraulically rough, subcritial OC flow was subjected to influent/effluent seepage through permeable sand bed. Sand bed thickness was varied with X to ensure uniform V_w. Discharge, flow depth and water surface profiles were measured. It was found that, within limits of experimental error, both the water surface curvature and the change in H_o from uniform flow depth (for same discharge) compare favourably with analytical results.

The following results follow from the analysis :

(i) $U_*^2/(a_g H_o S_o)$, or S_f/S_o where S_f is friction slope, increases/decreases with suction/injection in agreement with one-dimensional OC analysis and TBL data.

(ii) α and β are comparable, but deviate as $|v_w|$ increases.

(iii) Dimensionless velocity u(y) increases and has a fuller profile for suction; conversely for injection.

(iv) $\tau(y)$ sharply increases/decreases near the bed with suction/injection.

(v) The above changes magnify with increase in $H_o \sqrt{a_g H_o S_o}/\nu$ and with decrease in relative roughness, K_s/H_o.

(vi) Water surface has concave/convex curvature for suction/injection. Flow depth varies as

$$H \simeq H_o \left[1 - \alpha S_o x^2 \left(1 + (\alpha/3)x\right)\right] \qquad (3)$$

(vii) The analysis suggests that in duct flow dP/dX decreases/increases with suction/injection for same discharge.

(viii) From a physical interpretation of parabolic eddy viscosity distribution it is reasoned that the flow is nearly self-

preserving in all respects -- mean flow, turbulence field and coherent structures -- if $|v_w^2 U/U_*| << 1$, and an estimate of inner boundary layer length with change in wall inputs is suggested.

(ix) It is suggested that effluent seepage increases flow depth and enhances chances of flood waves overflowing stream banks, while infiltration may be the cause exponentially decreasing bed slope in graded streams.

Seepage effects were included in an investigation of longitudinal ribbons (or stripes/lineations) of lateral grain sorting and relief on non-uniform sand beds. Subcritical flow experiments with equilibrium sediment transport rates (Q_s) were conducted with beds of three different sand mixtures S1, S2 and S3 having median diameters, D_{50} = 0.28, 0.52 and 1.14 mm and Kramer's uniformity coeffcient of 0.48, 0.35 and 0.18 respectively.

Flume runs with and without seepage produced ripple bedforms on S1 sands even at low Q_s. For S2 and S3 sands stable, uniform streamwise stripes developed at low Q_s, which broke down into primary ripples/dunes at higher sediment load. The lateral stripe spacing, L_z, was typically about 1.94H to 2.15H, with relief, L_y, of about 1.5 to 3.0 D_{50}, and with considerable grain sorting (fine grains on ridges and coarse grains in furrows). Q_s was found to increase/decrease with effluent/influent seepage but was in reasonable agreement with the Einstein-Brown relation. Lateral grain sorting and L_y were weakly dependent on Q_s (and hence on V_w). The lineations covered a significant region of the lower and transition bedform regime as delineated by Simons and

Richardson. It was concluded that the appearance of three-dimensional bedforms at low to moderate Q_s is inhibited for very coarse sand-fine sand or sand-gravel mixtures, which complements a similar finding by Chiew for supercritical flow conditions.

The flow dynamics governing lineations has been related to secondary flow of Prandtl's second type by several researchers, whose modelling of the flow and boundary stresses involve assumptions on U(y) and W(y), or on $V'^2(y,z)$ and $W'^2(y,z)$, besides other approximations. It is suggested here that an eddy viscosity (or mixing length) formulation with other appropriate assumptions may be used in the X-momentum equation to obtain the approximate flow field and boundary stresses.

The major conclusions of the thesis are :

(i) OC flows over long stretches with low seepage rates are almost self-similar. The present results for U(y), $\tau(y)$, H(x) and S_f can be directly used for known seepage rates in unlined canals, alluvial streams and other OC applications with clear water flow.

(ii) Nonuniform or sand-gravel beds develop stripes of lateral grain sorting and remain nominally plane at low to moderate sediment load in subcritical flow. Lateral sorting and secondary flow cells are dynamically related through the redistributed stress field.

(iii) Mixing length or eddy viscosity approach may be gainfully applied to OC (and other wall turbulent) flows when secondary velocities (V and/or W) are small in comparison to the streamwise velocity.

ACKNOWLEDGEMENTS

I am deeply indebted to my thesis supervisor, Prof. T. Gangadharaiah, whose constant help, encouragement, guidance and faith were invaluable for my thesis work. I gratefully acknowledge his patient guidance and affirmative support throughout the thesis work.

I am sincerely thankful to all my teachers, in particular, Prof. (retired) V. Lakshminarayana, Prof. S. Surya Rao, Prof. K. Subramanya, Prof. S. Ramaseshan, Dr. B.Datta, and Dr. B.S.Murty, who taught me several useful subjects and helped me many a time during my thesis work.

My sincere thanks are due to Mr. S. Kumar, Mr. Satyanarayana and other staff of Hydraulics laboratory who gave me their unqualified help during my thesis experiments and on many other occasions. I am also indebted to the staff of Civil Engineering Office for their kindly help whenever need arose; Mr. A.C. Pandey for meticulously typing the thesis; and M/s R.K. Bajpai and J.C. Verma for their elegant figure preparation.

Finally, I thank all my friends and colleagues who cheered me all the way, M/s S.K. Verma, Lecki, K.K., Gagan-master, Vivekanand Singh, S.P.Sharma, Muzzammil, Jayakumar, Pranab, Ravindra, Bala, Alauddin, Sunu, Bramhaji and many others.

Gautam Roy

CONTENTS

LIST OF FIGURES

LIST OF TABLES

NOTATIONS

The following symbols/notations have been used in the thesis.

a	:	designation for eddy viscosity formula (a=1 for parabolic eddy viscosity ; a=2 for Prandtl-type mixing length)
a_g	:	acceleration due to gravity
a_o	:	constant in equation for vertical velocity distribution
A	:	van Driest damping coefficient; also cross-sectional area of channel flow
B	:	additive constant in log-law velocity
C	:	arbitrary or empirical constant
C_e	:	energy correction factor for velocity
C_f	:	coefficient of skin friction
c_k	:	Kramer's uniformity coefficient
C_m	:	momentum correction factor for velocity
D	:	grain size
e_s	:	void ratio of permeable material
f,F	:	functional representation
F_m, F_p	:	depth-integrated momentum, pressure force in OC flow
F_s	:	vertical seepage force on sand grains
G, g	:	functional representation
H	:	flow depth
H_b	:	thickness of sand bed
H_p	:	seepage pressure head in saturated medium
k	:	wave number of transverse bed roughness variation
K	:	sand permeability
K_s	:	Nikuradse's grain roughness

l	:	constant (coefficient in velocity distributions); mixing length
L_y, L_z	:	vertical spanwise dimension of bed lineations
m	:	exponents or constant in expressions for velocity distribution
n	:	as above; Manning's rugosity
P	:	pressure
Q	:	discharge per unit channel width
Q	:	channel discharge
R	:	hydraulic radius
s_s	:	ratio of densities of sand and water
S	:	channel (bed or water surface) slope
S_r	:	relative slope of free surface to bed
t	:	dummy variable of integration
T	:	top width of channel flow
u, v, w,	:	U,V,W normalized by $\sqrt{a_g H_o S_o}$
U,V,W	:	Time-mean velocity components in X-, Y- and Z-directions.
U',V',W'	:	Fluctuating components of velocity
U_*	:	bed shear velocity
U_{*1}	:	spanwise varying component of U_* on sand ribbon bed
W_c	:	Coles wake law component of U
X,Y,Z	:	Catesian cases in streamwise, wall-normal and spanwise directions
x,y,z,	:	X/H, Y/H, Z/H
y_o	:	apparent origin of turbulent velocity distribution above bed level
y_{om}	:	spanwise mean value of y_o
Z_o	:	spanwise spacing of sand ribbons
α	:	rate of change of $\sqrt{a_g HS}$ with X

β	:	rate of change of U_* with X
γ	:	unit weight of fluid
γ_s	:	unit weight of sediment
Γ	:	Coles wake function
δ_*	:	displacement thickness
Δ	:	change in variable over a reference value
ε	:	mean spanwise variation of bed roughness
χ	:	Karman constant in log-law
λ	:	rate of change of V_w with x; also, empirical constant in eddy viscosity equation
λ	:	spanwise sublayer streak spacing
ν	:	kinematic viscosity
σ_d	:	standard deviation of grain size distribution
τ, σ	:	shear stress, normal stress
ϕ	:	operator as defined in Equation 3.20.

Subscripts

Unless otherwise mentioned the subscripts denote the following

av	:	depth-average
h	:	free surface or boundary layer edge
o	:	X = 0
s	:	sediment
t	:	turbulent flow
w	:	wall (bed in open channel flow)

Abbreviations

OC	:	open channel
TBL	:	turbulent boundary layer.

CHAPTER 1

INTRODUCTION

1.1 General

Surface water movement through natural and artificial open channels plays a fundamental role in the distribution and availability of water for human needs and concerns, such as domestic, agricultural and industrial use, aquatic life, sediment transportation, navigation, power generation, waste disposal and ecology. While the complexity of these processes in the natural environment is daunting, considerable understanding of alluvial channel mechanics has been achieved by applying the basic principles of fluid motion. Application of these principles to open channel flow is mainly governed by the nature of flow -- laminar or turbulent, the surface and body forces acting in a given fluid domain, and the characteristics of the free surface and the solid boundary.

Flow in alluvial channels is usually turbulent, the instantaneous velocities of small fluid "elements" being random and three dimensional even when the mean flow is steady and rectilinear. Moreover, in turbulent flow, fluid stresses act predominantly through correlated velocity fluctuations rather than mean velocity gradients. As velocity fluctuations tend to die out in a region very close to the boundary -- the viscous sublayer, the impulse of these fluctuations contribute to much shear stress and pressure fluctuations at the boundary. The process is more complex when the boundary is hydraulically rough which is common in gravel- and sand-bed channels. In such cases random protrusions on the boundary extend beyond the sublayer,

effectively destroying it, and affect the near-bed turbulence generation. The effects of a rough boundary, transmitted through turbulent eddies, may permeate the entire boundary layer.

Since fluid particles immediately adjacent to a solid boundary tend to adhere to it in both laminar and turbulent flows, the flow is bounded by the no-slip and no-penetration conditions at a rigid, impervious surface. However, a boundary composed of layers of loose sediment, as often encountered in sedimentary hydraulics, is often permeable, which generally implies non-zero mean and turbulent velocities at the boundary. Even if the mean velocity vector at the boundary be known, the corresponding fluctuating quantities are difficult to determine.

Alluvial channel mechanics also involve processes other than these encountered in pure fluid mechanics, chiefly because of sediment transported by the flow. Sediment is mainly transported in two ways -- as suspended sediment and as bedload. Suspended sediment grains are believed to be sufficiently small as to respond directly and continually to small scale velocity fluctuations. Hence their effects can be accommodated in the equations of motion for turbulent flow. The pre-eminent view considers suspended sediment as passive elements or contaminants which, while responding to the fluid forces exerted on them, can significantly alter flow properties through some form of passive resistance. In contrast to suspended sediment, bedload motion consists of intermittent sliding, rolling and saltating movements of individual grains, which, being discrete events in space and time, are not amenable to continuum analysis. However, by looking

at bedload motion as essentially a random, surface phenomenon, it is possible to assimilate its effect in bulk or average terms.

Apart from its direct effect on flow properties, sediment motion can have an indirect but important effect on the flow. This is because sediment motion often leads to the development of bedforms. Bedforms are relatively immobile or slow-moving sundry deposits of sediment on the bed with fairly regular dimensions and patterns. Bedforms may be sufficiently large as to decelerate the flow and offer considerable form drag in addition to the native skin friction of the bed. Their effects on the mean and turbulent velocity and stress fields are also significant.

1.2 Statement of the problem

The flow in an alluvial channel is often subjected to seepage or infiltration through the porous channel boundary. Seepage occurs due to piezometric gradient between the channel and the ambient water table. Higher ground water table results in discharge into the channel (effluent seepage or injection) while a lower ground water table causes abstraction from the channel (influent seepage or suction). Available information [eg. Watters and Rao, 1971; Brink and Oldenziel, 1974] indicate that seepage affects the hydrodynamic forces on the bed and, possibly, the flow and stress fields. There may thus be significant changes in bulk flow properties such as flow depth, bed shear stress and the balance between the flow, sediment discharge and bedforms. Correct prediction of the channel regime for different seepage conditions will necessitate quantitative modelling of suction/injection on loose boundary open channel flow.

In addition to seepage, the flow in alluvial channels is commonly associated with bedforms. While most bedforms exert considerable pressure drag on the flow, sand ribbons (stripes or lineations) which are flow-aligned structures on the bed, offer little additional flow resistance. Consequently, the discharge carrying capacity of channels is not much affected by these structures in contrast to other types of bedforms such as ripples and dunes. While some researches have been conducted in the past few decades [eg., Mantz, 1978; McLean, 1981; Allen, 1982; Tsujimoto, 1989], the bedform regime (existence criteria) of sand ribbons, their mechanics of formation, and the associated structuring of the flow remain incompletely understood.

1.3 Scope of the work

The present work attempts to study the above problems theoretically and experimentally with a view to gain practical insight. Earlier studies have shown that secondary velocities introduced in the cross-flow plane by seepage and sand ribbons are much smaller than the streamwise velocity component almost throughout the flow region. The low secondary velocities are unlikely to cause significant flow curvature or altered turbulence generation processes, and it may be anticipated that no fundamentally new assumptions are necessary to analyze the flow. The analytical work attempted herein is limited to defining the time averaged velocity and stress fields from the equations of motion, and detailed understanding of the turbulent flow structure is beyond the scope of this work. The analysis is restricted to the case of steady, clear water flow in wide channels.

The theoretical work has been augmented by experiments designed to verify the analytical results as well as to provide an independent data base for drawing empirical conclusions. In particular, experiments were needed to quantify the existence criteria and physical properties of sedimentary bedforms with equilibrium sediment transport. Measurement of the flow structure associated with sand ribbons, which has been reported by earlier researchers, was not attempted in this work.

1.4 Thesis presentation

The thesis has been presented in six chapters. In the following chapter the literature on open channel (and other types of wall-bounded) flow has been reviewed. The effects of seepage on open channel flow and the dynamics of channel flow with sand ribbons as reported in the literature have also been reviewed in Chapter 2. In Chapter 3 analysis of the mean flow field subjected to suction/injection of fluid through bed and in the presence of sand ribbons have been separately carried out. The experiments that were conducted are described in Chapter 4. In Chapter 5 experimental results as well as data from literature have been analyzed and discussed in association with the analytical models of Chapter 3. A brief summary and major conclusions of the thesis have been presented in Chapter 6 along with a mention of certain issues for potential research ensuing from this study.

CHAPTER 2

LITERATURE REVIEW

In a fluvial channel the hydrodynamic forces acting on the boundary, the rates of sediment erosion and deposition, and the water and sediment discharges are intricately related. Hence, simplifications and idealizations are necessary to study any of the component processes. In this chapter literature on the effect of suction and injection on channel flow and the mechanics of streamwise bedforms has been surveyed. Some of the basic assumptions involved in most studies, which are not specifically mentioned in this survey, are the conditions of steady, uniform rectilinear flow, steady and uniform sediment transport rate, and no long-term channel adjustment or time-dependent environmental inputs (such as temperature). The literature has been broadly grouped under the following heads:

* Mean, i.e time-average, velocity and boundary forces in open channel flow (hereinafter, OC flow).
* Hydrodynamic effects of seepage inflow/outflow on channel bed.
* Mechanics of longitudinal bedforms.

2.1 Mean velocity and boundary forces

2.1.1 Depth averaged mean velocity

Empirical equations for the depth averaged mean velocity, U_{av}, have been widely used in OC hydraulics. Among them the most familiar ones are the Chezy's and Manning's equations [Chow, 1959]:

$$U_{av} = C\,(RS)^{1/2} \quad : \text{Chezy} \qquad 2.1$$

$$U_{av} = \frac{1}{n}\,R^{2/3}\,S^{1/2} \quad : \text{Manning} \qquad 2.2$$

where R is hydraulic radius, S is the energy gradient of flow, and C and n and Chezy's and Manning's respective resistance coefficients. For coarse channel material, C and n may be estimated from grain size, but in general both coefficients are determined empirically to account for a host of channel properties [Chow, 1959]. Thus, despite their simple form and ease of use, Equations 2.1 and 2.2 are not ideal for making accurate predictions or to study the effect of specific variables on the flow. A better understanding of the flow process and description of mean velocity and stresses have been acheived by drawing upon diverse studies on turbulent wall (or wall-bounded) flows since the beginning of this century. A brief review of turbulent boundary layer, open channel and pipe flows is made here, focussing particularly on the mean flow structure.

2.1.2 Mean velocity in wall flows

Turbulence in wall flows is characterized by a non-random flow field that is apparently related to the local mean velocity gradients and stresses, and is governed by the no-slip and no-penetration conditions at a rigid, impermeable wall. In terms of the mean properties of flow, a turbulent boundary layer (herinafter, TBL) consists of the following main divisions (Cantwell, 1981; Hinze, 1975]:

(i) The viscous sublayer is a thin region immediately adjacent to the wall and about five wall units, i.e. $5\,\nu/U_*$, thick, -- ν

is kinematic viscosity of fluid and U_* is the wall shear velocity. Due to the no-slip condition at the wall the mean velocity in sublayer is small as compared to the outer flow, and the shear stress is mainly viscous or "laminar" stress. U(y) is well described by the laminar flow equation :

$$\tilde{u} = \tilde{y} \quad : \quad 0 < y < 5 \qquad 2.3$$

where $\tilde{u} = U/U_*$, $\tilde{y} = YU_*/\nu$, $U_* = \tau_w / \rho$, Y being the normal distance from the wall, τ_w, the wall shear stress and ρ , the density of the fluid.

(ii) The buffer layer, extending from the outer edge of the viscous sublayer to the edge of the turbulent region, has typically the properties of both adjoining regions, the viscous and turbulent stresses being of comparable orders of magnitude in this zone. In the buffer layer U(y) is best described as a smooth changeover from Equation 2.3 to Equation 2.4 (stated below).

(iii) The turbulent region covers the boundary layer from $\tilde{y} \simeq 30$ outwards, and predominantly governed by turbulent or Reynolds stresses. Significant correlations of velocity fluctuations [see, e.g., Sabot and Comte-Bellot, 1976] clearly indicate a time-mean structuring of the flow, which may be described by suitable length and time scales of the time-averaged flow (eg., mixing length and wall shear velocity), or by turbulence scales (e.g. integral length scale and Taylor microscale), or by scales of identifiable coherent structures (eg., the dimensions, lifetimes and vorticity of persistent eddies), all of which are related in a

composite flow process. The turbulent region may be further subdivided into two zones, namely:

(a) An inner or logarithmic region extending upto about 0.1H to 0.2H, H being the TBL thickness, having the mean velocity distribution

$$\tilde{u} = \frac{1}{\varkappa} \ln \tilde{y} + B \qquad 2.4$$

where ln denotes natural logarithm and $\varkappa$ and B are empirical constants nearly independent of the flow Reynolds number, Re, in canonical TBLs. In the major part of the inner region $\tilde{u}$ also varies logarithmically with the outer variable y = Y/H

$$\tilde{u} = \frac{1}{\varkappa} \ln \tilde{y} + C \qquad 2.5$$

C being an empirical constant. Thus the inner region is also an overlap region where the velocity scales with both inner and outer flow variables.

(b) An outer turbulent zone, $0.15 < y \leq 1.0$, where $\tilde{u}$ scales on y though not logarithmically, the flow turbulence is intermittent, and the outer edge undulates along its boundary with the irrotational flow region. For constant pressure flows the velocity is well described by Hama's defect law [refer Hinze, 1975] :

$$\tilde{u}_h - \tilde{u} = 9.6\ (1-y)^2 \qquad 2.6$$

where U_h is the velocity at the TBL edge. For pressure gradient flows ie., $\partial P / \partial X \neq 0$, where P is the freestream pressure and X is the downstream direction, the velocity profile is aptly described by Coles' law of the wake :

$$u = \frac{1}{\varkappa} \ln y + C + \frac{\Gamma}{\varkappa} W_c(y) \qquad 2.7$$

where $W_c(y) = 2 \sin^2(\pi y/2)$ and Γ is a wake parameter whose value depends on $\partial P / \partial X$. For Γ, White [1974] suggested the following empirical relation:

$$\Gamma = 0.8 \left(\frac{\delta^*}{\tau_w} \frac{\partial P}{\partial x} + 0.5\right)^{0.75} \qquad 2.8$$

where δ^* is the displacement thickness. For nearly equilibrium TBL flow in adverse pressure gradient, Schofield [1981] indicated that the outer region velocity profile can be collapsed into a single relation between U/U_h and Y/δ^*, but the universality of this relation has been questioned by Dengel and Fernholz [1990].

For turbulent flow in smooth-walled pipes (as also in other prismatic ducts), there is neither any intermittency in the flow nor any variation of kinematic quantities in the flow direction. The sublayer velocity distribution is identical to that in a TBL, and the log-law holds in a major part of the turbulent region, with some change in the additive constant. Thus in terms of wall variables and in defect form,

$$\tilde{u} = \frac{1}{\varkappa} \ln \tilde{y} + 5.5 \qquad 2.9$$

$$\tilde{u}_h - \tilde{u} = -\frac{1}{\varkappa} \ln y + 0.8 \qquad 2.10$$

where H is the pipe radius. In the core region the velocity deviates from the above distributions. Nikuradse had empirically shown that in the log-region the velocity can also be approximated by a power law,

$$\tilde{u} = C_n y^n \qquad 2.11$$

where C_n is an empirical constant dependent on n, and $0 < n < 1$. Typically n decreases with increase in Re so that Equation 2.11 approaches the log-law asymptotically.

Equations 2.3 through 2.11 are valid for flow over smooth boundaries. For flow over rough surfaces the sublayer flow is disrupted while in the turbulent region the velocity is depreciated. Based on the early works of Nikuradse [refer Schlichting, 1979] and subsequent experiments by many researchers [eg., Bayazit, 1976; Stukel, Hopke and Nourmohammadi, 1984] the modified log-law over fully rough surfaces

$$\tilde{u}_r = \frac{1}{\chi} \ln \left(\frac{Y - \Delta Y_o}{K_s} \right) + B_1 \qquad 2.12$$

where subscript r denotes rough boundary, K_s is Nikuradse's roughness scale, B_1 is a function of K_s, and ΔY_o is a downward shift of apparent velocity origin. On comparison with Equation 2.4, the velocity shift $\Delta\tilde{u} = \tilde{u}_r - \tilde{u}$ is

$$\Delta \tilde{u} = B_1 - B - \frac{1}{\chi} \ln \tilde{k}_s \qquad 2.13$$

Physically three flow regimes are distinguishable depending on the magnitude of $\tilde{k}_s$, viz.

* Hydrodynamically smooth regime, $\tilde{k}_s \lesssim 5$, where the sublayer flow is virtually undisturbed; and $B_1 = B = 5.5$.
* Transition regime, $5 \lesssim \tilde{k}_s \lesssim 70$, where the sublayer is partially destroyed; B_1 increases monotonically to about 9.6 at $\tilde{k}_s \simeq 12$ before decreasing to about 8.5 at $\tilde{k}_s \simeq 70$.
* Rough flow regime, $\tilde{k}_s > 70$, where the sublayer is effectively destroyed; $B_1 \simeq 8.5$.

In contrast to Nikuradse's three dimensional k-type roughness, Perry, Schofield and Joubert [1969] distinguished two-dimensional d-type transverse roughness elements where the roughness scale determining the velocity shift -- logarithmic asymptote -- is proportional to H rather than the roughness height. Perry et al postulated that the vortices formed behind d-type roughness elements are stable and do not shed periodically. Their empirical results have been confirmed by later studies, eg. Stukel et al [1984].

2.1.3 Turbulence structure in wall flows

Spatial and temporal correlations of different flow variables, referred to as coherent motion [Robinson, 1991], indicate a stable mechanism in the maintenance of Reynolds stresses and the production, convection, diffusion and dissipation of turbulence in wall flows. Major results of coherent flow studies have been extensively discussed and reviewed in literature, in particular by Cantwell [1981] and Robinson [1991], and are discussed here briefly and selectively in order to highlight some complexities of near wall flow vis-a-vis the mean flow description of the previous section. In terms of persistent flow vortices with a directional preference, the outer region of a TBL is characterized by weak spanwise vorticity of relatively long lifetimes. The bulges and vorticity at the outer edge of TBL enable entrainment of freestream fluid into the boundary layer.

At the other extreme, the quiescent sublayer is densely covered with high and low speed streaks ie, alternate elongated regions of high- and low-streamwise velocity, with spanwise

wavelength of about $100\,\nu/U_*$. The streaky sublayer structure is believed to be associated with contra-rotating pairs of streamwise vortices, which are probably the stretched limbs of U- or V-shaped horseshoe or hairpin vortices [Blackwelder and Eckelman, 1979; Gupta et al., 1971; Kline et al, 1967]. As compared to outer region eddies, the lifetime of sublayer eddies is rather short due to quasi-periodic disturbances (the burst cycle) when high speed fluid from the turbulent region invade the sublayer, followed by lift-up and ejection of low speed streaks into the turbulent region. As of now there appears to be no clear consensus about whether the period of turbulence bursts scales with inner or outer flow variables [Shah and Antonia, 1989]. Moreover, though sublayer vortices are believed to break down or to merge with neighbouring eddies during bursts [Perry, Henbest and Chong, 1986; Smith and Metzler, 1983; Wark and Nagib, 1991], they are also reported to be significantly present in most of the TBL [Head and Bandyopadhyay, 1981].

Near-wall measurements indicate high correlations between instantaneous wall pressure, shear stress and velocity components. High wall shear is associated with high spanwise vorticity near the wall, the rms wall shear fluctuation, $\tau'_{w,rms}$ being about 0.4 τ'_w [Alfredsson, Johansson, Haritonidis and Eckelman, 1988]. High wall pressure, associated with the passage of inclined shear layers in the inner turbulent region, have rms values, $P'_{w,rms}$, of about 2 to 4 τ_w [Hinze, 1975; Willmarth, 1975]. This value is much higher than $\tau'_{w,rms}$ probably due to significantly higher contribution of high frequency P'_w as compared to τ'_w [Yefimtsov, Kuzentsov and Sysoyev, 1983].

For turbulent flow over rough surfaces, where the sublayer and buffer layer may be fully disrupted, the wall-normal and spanwise velocity components, V' and W', are an the whole reduced in the logarithmic zone but do not affect the wake region. Apparently, roughness elements increase the mass and momentum exchange in the near-wall region, but do not alter the nature of flow, the mode of turbulence production and Reynolds stress maintenance (Bushnell and McGinley, 1989; Grass, 1971; Nourmohammadi, et al, 1985; Sabot et al, 1977]. For densely packed roughness elements both $P'_{w,rms}$ and τ_w increase with increase in K_s, but the ratio $P'_{w,rms}/\tau_w$ decreases [Blake, 1970].

2.1.4 Mean velocity distribution in OC flow

The mean velocity profile in turbulent open channel flow has been observed to be more or less logarithimic at sufficient distance away from the wall. The effect of bed roughness is also similar to that for the inner region of TBL flow. However, due to natural sediment coming in varying compositions of different shapes and sizes, the estimation of K_s poses considerable difficulty in natural channels. David [1980], Garde and Raju [1985] and Raudkivi [1990] have surveyed various formulae recommended for estimating K_s, a few of which may be cited here :

Ackers and White	:	$K_s = 1.25\ D_{35}$	2.15
Einstein and Barbarossa	:	$K_s = D_{65}$	
Engelund and Hansen	:	$K_s = 2D_{65}$	
Hey	:	$K_s = 3.5D_{84}$	

where D is grain diameter, and its suffix denotes the percentage of finer grains in the mixture. It is evident that the criteria

of Equation 2.15 can give widely divergent results for the same sediment bed. Considering such discrepancy to be due to representation of a heterogeneous sediment mixture by just one statistical size, Mittal [1977], Mittal [19 8], David [1980] and Singh [1981] conducted extensive measurements with fixed beds of non-uniform sand and gravel, in which D_{50} was varied from 0.14 to 3.0 mm combined with variation of the standard deviation of grain sizes, σ_d. Based on their data Gangadharaiah, David and Roy [1991] found that K_s/D_{50} can be related quite accurately to $\tilde{\sigma}_d$ ($= \sigma_d U_*/\nu$). Their plot shows that K_s/D_{50} increases monotonically from 1 to about 4.8 at $\tilde{\sigma}_d \simeq 70$ before decreasing to about 1.7 at $\tilde{\sigma}_d = 1000$. The peaking of the curve at $\tilde{\sigma}_d = 70$ shows similarity of the effect of $\tilde{\sigma}_d$ with that of $\tilde{k}_s$ as it coincides with the value of $\tilde{k}_s$ when a flow becomes fully rough. A suitable empirical fit of Gangadharaiah et al's plot may be

$$\frac{K_s}{D} = 1 + 3.75 \exp\left[-1.3 \left| \log_{10} \left(\frac{\tilde{\sigma}_d}{70} \right) \right|^{1.5} \right] \qquad 2.16$$

The estimation of bed roughness with sediment transport is difficult, but it is known that K_s may change drastically from fixed bed values. In particular, Wilson [1989] has shown that with bedload motion at high shear stresses K_s is about half the shear layer thickness of moving bedload. Wilson also gave the following empirical relation

$$\frac{K_s}{D} \simeq 5 \tau_* \qquad 2.17a$$

with $$\tau_* = \frac{\rho U_*^2}{a_g(\rho_s - \rho) D} \qquad 2.17b$$

where τ_* is the sediment mobility number or Shields dimensionless shear stress parameter, a_g is acceleration due to gravity, and ρ_s and ρ are the densities of sediment and water respectively.

While most OC studies involve subcritical flows, a few studies of supercritical flow velocities on plane beds have indicated some devation from the canonical distribution. In a set of experiments involving mean and fluctuating velocity measurements Tominaga and Nezu [1992] have recently reported that though the velocity distribution follows the log-law in the main, the additive constant of the law decreases substantatially with increase in Froude number, the decrease being more significant for rough bed flows.

Several OC velocity measurements for subcritical flows have also indicated that u deviates from the log-law at distances beyond about 0.15H from the bed, eg. Bronco and Parthenaides [1971], Cardoso, Graf and Gust [1989], Coleman [1981], Finley [refer Townsend, 1976], Nezu and Rodi [1986], and Zippe and Graf [1983]. Coleman proposed to explain the deviations by use of Coles' wake law with the modified value of $\Gamma = 0.191$ for clear water flow. Moreover, in some of the data of Cardoso et al and of Nezu and Rodi the velocity profile deviates from the suggested wake law near the free surface where the flow is apparently retarding. Retarding flow near free surface is, in fact, not uncommon in OC flow, particularly when the bed is hydraulically rough [Chow, 1959], and may be attributed to secondary flow [Cardoso et al] or wind shear at the free surface. The latter possibility is normally discounted in OC flow analysis, but may not be entirely without importance. Several studies, eg. Rashidi

and Banerjee [1990], Street [1979] and Ueda et al [1977] have indicated the possibility of free surface shear producing similar effects as that of a moving wall, and this analogy has been recommended for modelling of surface shear and near surface flow [ASCE Task Committee, 1988].

In addition to log-law and wake law, power laws have also been employed for describing OC velocity distributions. In recent times Chen [1991] has demonstrated the validity of power laws in OC flow. He recommended the use of the 1/7-th power law (ie, n = 1/7 in Equation 2.11) for hydraulically smooth flows, and the 1/4-th power law for hydraulically rough flows. Coleman [1991] has also expressed preference for power laws over the log-law.

2.1.5 Analytical derivation of mean velocity and bed stresses in OC flow

The two dimensional analysis of flow in wide open channels, in its simplest form, uses the continuity and momentum equations, and follows the procedure of Reynolds stress modelling in the inner region of a TBL. Though several analytical methods exist for obtaining the log-law in the inner region, eg., the overlap layer criterion of Millikan [refer Hinze, 1975] and the vorticity transport hypothesis of Taylor [refer Schlichting, 1979], Prandtl's phenomenological approach is the most widely used one due to its insight and simplicity of use. According to Prandtl's hypothesis for TBL flow :

(i) The inner turbulent region is of constant shear stress ($=\tau_w$)

(ii) U' and V' are proportional to the local mean vorticity as

$$|U'| = |V'| = l \frac{\partial U}{\partial Y} \qquad 2.18$$

where $l = \varkappa Y$ is the mixing length. With the above formula the Reynolds stress τ in terms of kinematic eddy viscosity, ν_t, is

$$\frac{\tau}{\rho} = - \overline{U'V'} = \nu_t \frac{\partial U}{\partial Y} \qquad 2.19$$

$$\text{where} \quad \nu_t = \varkappa^2 Y^2 \left| \frac{\partial U}{\partial Y} \right| \qquad 2.20$$

with $- \rho \overline{U'V'}$ being the time-averaged stress. With $\tau = \tau_w$, the logarithmic velocity distribution is readily obtained. Based on Prandtl's approach, alternative formulations of mixing length or eddy viscosity have been proposed by many researchers for other types of wall flows and for non-canonical TBL flows [see eg., Galbraith and Head, 1975].

In order to derive a single velocity distribution for the entire inner region including the sublayer and buffer layer, Prandtl's mixing length formulation has been modified or adapted by several researchers, eg., by Rotta and by Van Driest respectively as [see Hinze, 1975]

$$\nu_t = \nu + \varkappa^2 Y^2 \left| \frac{\partial U}{\partial Y} \right| \qquad 2.21$$

$$\text{and} \quad \nu_t = \varkappa^2 Y^2 \left[1 - \exp\left(- \frac{\tilde{y}}{A}\right)\right] \left| \frac{\partial U}{\partial Y} \right| \qquad 2.22$$

where A is a constant (= 26). More recently Haritonidis [1989] has argued that, instead of Equation 2.18, V' should be determined from the frequency of turbulence bursts. Thus he derived

$$\nu_t = \lambda \tilde{y} Y \qquad 2.23$$

where λ is an empirical constant. With certain assumptions and qualifications his results show good agreement with the distribution of $\tilde{u}$ and τ in the near wall region of both ordinary and drag reducing flows.

Fully developed open channel flow of high aspect ratio is also amenable to the mixing length approach of Prandtl. However since there is virtually no constant stress zone in OC flow -- τ increases linearly from the water surface to the bed -- alternative forms of ν_t or Prandtl's l have been suggested, since Prandtl's hypothesis is, in any case, intuitive and not based on constitutive relations [see eg, Rijn, 1984; Umeyama and Gerritsen, 1992]. Two such commonly employed formulae cited below are the modified mixing length formula and the parabolic eddy viscosity formula respectively :

$$\nu_t = \kappa^2 Y^2 (1-y) \left| \frac{\partial U}{\partial Y} \right| \qquad 2.24$$

and $$\nu_t = \kappa Y (1-y) U_* \qquad 2.25$$

Both equations give the log-law in steady, uniform OC flow for $\tau = \tau_w (1-y)$.

As mentioned in the previous section the inclusion of a wake component in the mean velocity has been suggested in several studies. Thus Vedula and Achanta [1988] included Hama's defect law for $y > 0.15$ in their analysis and found good agreement of observed and computed mean velocity distribution and bed shear stress for both pipe flow and OC flow data. Willis [1985] also included a wake component to obtain fair agreement with outer channel flow data, while for flow in the near-bed region a combination of fluid and eddy viscosities yielded good agreement.

The simple phenomenological approach of Prandtl does not often predict the velocity distribution accurately in non-canonical wall flows. In the past few decades higher order turbulence closure models for the Reynolds stresses have been increasingly used. These models, which are more complex than the one-equation gradient transport formulae, usually need more empirical data (for validation/calibration) and computational effort. They have been reviewed in fair detail elsewhere [ASCE Task Committee, 1988; Speziale, 1991].

The time-averaged pressure, P_w, and shear stress acting on the channel bed is easily computed from the depth-integrated momentum equations in X and Y directions [Chow, 1959]. For channel with small slope, S, and V' = 0 at the free surface,

$$P_w = \gamma H \qquad 2.26$$

and

$$\tau_w = \gamma HS \qquad 2.27$$

where γ is the unit weight of water. The mean shear stress acting an individual bed grains may, however, be significantly different from that of Equation 2.27 depending on the presence or absence of bedforms, and on the arrangement, concentration and sorting of grains on the bed surface. Surface grains are also subjected to considerable pressure and shear stress fluctuations as discussed in Section 2.1.3 and in Vanoni [1977].

In mobile bed channels the bed shear stresses and channel resistance are not merely dependent on the roughness of bed grains. They also depend on the amount and type of sediment load (i.e., suspended sediment load or bedload) and other possible effects such as sidewalls, bank vegetation and free surface shear

produced by winds. Empirical and semi-empirical formulae have been developed by several researchers to account for the effect of sediment motion on OC flow eg, by Einstein and Barbarossa, Engeland and Hansen, and Ackers and White [refer Ackers, 1983; Vanoni, 1977]. However, it may be mentioned that due to lack of in-depth understanding of the processes, there are wide differences in the physical concepts used as well as the sediment load predicted by different formulae [McBean and Al-Nassiri, 1988; Samaga, Raju and Garde, 1986].

2.2 Flow over permeable boundary with distributed suction or injection

2.2.1 General

Turbulent flow over a permeable boundary accompanied by suction or blowing of fluid through the boundary may occur in diverse natural situations. For example, in rivers and canals flowing in granular material, seepage inflow from the channel to the bed (influent seepage, infiltration or suction) or seepage outflow from the bed into the channel (effluent seepage or injection) is a common occurrence due to piezometric head difference between the channel and ground water table. Suction/injectin have also found many applications in modern life. For instance, water is sometimes abstracted from lined irrigation canals or pipes through perforated boundaries. In aerodynamic and internal flows injection has been found effective in reducing skin friction and heat transfer to the walls (transpiration cooling), whereas suction has been employed to reduce flow turbulence and prevent flow separation [Jeromin, 1970;

Fiedler and Fernholz, 1990; Narasimha and Sreenivasan, 1979; Subramanya, 1986].

In studying the effect of suction and injection -- hereinafter suction/injection is used synonymously with uniformly distributed suction/injection through the boundary unless otherwise specified -- two aspects are worthy of note. First, for flow over a permeable boundary without any net transfer across the boundary -- referred to as passive porosity -- the flow properties may be noticeably affected as compared to flow over a similar, but impermeable, boundary. This is probably because

(i) the no-slip condition is not strictly met at the boundary;

(ii) the no-penetration condition too may be inaccurate for the mean velocity (due to possible local variations in U) and invalid for the fluctuating velocity component, U'.

Empirical results indicate that passive porosity increases the skin friction, and changes the constants of log-law [Beavers and Joseph, 1967; Bushnell and McGinley 1989; Gupta and Paudyal, 1985; Schetz and Nerney, 1977; Zagni and Smith, 1976; Zippe and Graf, 1983]. Much of the experimental conclusions reported in literature are, however, conflicting, and some later work eg, Richardson and Parr [1991], has indicated that the friction factor may increase or decrease with passive porosity depending on boundary roughness or pore size. Evidently, a simple correspondence between passive porosity and its effect on the flow can not be expected.

Secondly, self-preserving flow is not established immediately after commencement of suction/injection. Experiments suggest that the internal boundary layer that develops from the point of

application of injection may not merge with the outer boundary layer before a distance $X_d \simeq$ 30H to 40H downstream [Simpson, 1971]. Since the establishment of self-similarity with change in other wall variables, such as roughness, spans a length of the same order of magnitude, $X_d \sim$ 20H to 60H [Smits and Wood, 1985], it may be inferred that in the case of suction, as for injection, X_d is not less than 20H or 30H. Unfortunately, many experimental measurements with suction/injection are at X considerably less than 20H eg, Elena [1984] and Fulachier et al [1987]. This limits the utility of these data in studying flows with wall mass transfer to localized phenomena.

2.2.2 Fluid dynamic effects of wall suction/injection

A considerable body of experimental measurements reported in literature show that the gross effects of suction/injection in TBL flow are similar to those of favourable/adverse pressure gradients. These effects are summarized in Table 2.1. Though most of the observed effects are similar in TBL and pipe flows, some differences have been reported. To cite, Pennel, Eckert and Rodi's [1972] pipe flow experiments with injection showed an initial tendency towards laminarization upto X $\simeq$ 5H. More significantly Eckert and Rodi [refer Narasimha and Sreenivasan, 1979] indicated that after proper development of pipe flow with injection, the skin friction exceeds that of flows without wall mass transfer.

Table 2.1: Hydrodynamic effects of suction/injection on wall flow

Parameter	Effect of suction	Effect of injection
τ_w, C_f	Increase	Decrease
Shear stress profile	Tends to bulge near the wall.	---
Mean velocity profile	Fuller	More uniformly curved.
Turbulence characteristics	Production, intensity and frequency of bursts reduce	---
Developing length	---	~ 30H to 40H
TBL thickness as compared to canonical TBL thickness	Decreases	Increases

In an effort to understand the effect of suction on TBL flow structure Gad-el-Hak and Blackwelder [1989] applied continuous suction and strong, impulsive suction respectively through two wall slots spaced about $100\,\nu/U_*$ apart (equal to sublayer streak spacing in laminar boundary layer flow). In the first case flow visualization showed a train of hairpin vortices behind the slots suggesting a spatial structuring of the near wall flow similar to that in TBL flow. Moreover, the boundary layer had a fuller velocity profile than the Blasius boundary layer. In the second case the main change observed was turbulence burst-like events detected by hot film anemometry. In sum, localized slot suction indicated some developments similar to turbulent coherent structures depending on how the suction was applied.

There have been several studies on the effect of suction and injection on loose boundary open channels, though detailed

measurements of U(y) and τ(y) have not been made in most cases. Martin [1970] and Martin and Aral [1971] indicated that the vertical seepage force, F_s, acting on surface grains of a sand bed can be expressed as

$$F_s = - C_1 (1+e_s) \frac{\partial P}{\partial Y} \qquad 2.28$$

where the coefficient C_1 is about 0.35 to 0.5, e_s is the void ratio and $\partial P/\partial Y$ is the vertical pressure gradient.

Inserting Equation 2.28 into Shields parameter Brink and Oldenziel [1974] obtained a modified mobility number, τ_*, as

$$\tau_* = \frac{U_*^2}{a_g D \left[s_s - 1 + C_1 (1+e_s) \frac{dH_p}{dY}\right]} \qquad 2.29$$

where a_g is the gravitational acceleration, D is grain diameter and $s_s = \rho_d/\rho$, ρ_d and ρ being the mass densities of grains and water respectively, and H_p is piezometric head. The authors did not attempt to measure the bed shear stress. Assuming that the bed shear stress increases with suction and decreases with injection, since the denominator in Equation 2.29 also increases with suction and decreases with injection, Equation 2.29 does not readily indicate whether sediment mobility is enhanced or reduced on applying suction (or injection). However, Brink and Oldenziel's experimental data consistently show increase in sediment transport rate with injection and its decrease with suction. An illustrative set of velocity profiles given by the authors shows that the velocity profile is fuller for suction and more gently curved for injection in comparison to that of uniform flow. This agrees, at least quatitatively, with TBL flows.

Maclean and Willetts [1986] conducted OC flow measurements with relatively high rates of suction through a porous bed. Their indirect measurement of τ_w from suction-free grains, indirect estimation of τ_w from bedload and estimation of τ_w from momentum balance indicated monotonic increase in τ_w with suction rate. However, each of these estimates differed widely from the others, with the momentum balance estimate being several times the estimate from the threshold state of grains shielded from suction. The intermediate estimate of τ_w was from an equation for bedload motion based on sediment mobility similar to Equation 2.29. Further velocity measurements by Maclean [1991] for OC and TBL flows with high suction rates bring out some basic differences in the two flow situations. In contrast to OC flows where $|V(y)|$ decreased monotonically with increase in y, in TBL flow V(y) bulged slightly in the inner region but was relatively constant thereafter.

Direct measurements of the change in hydrodynamic drag and lift forces on surface grains was carried out by Watters and Rao [1971] using 3.75 inch spheres in turbulent flow. Their results showed that the drag force decreased considerably with injection and increased with suction, while the lift force increased with injection and decreased with suction. In both cases the changes are more pronounced at low R_e, and, at least for the lift force, the relative change in magnitude approached a limiting value at high R_e. Surprisingly, the lift force was found to be always negative.

2.2.3 Analysis of TBL flow with suction/injection

Theoretical studies of the effect of wall suction and injection on TBL flow generally assume the mean vertical velocity to be constant ($V=V_w$) throughout the boundary layer, and use Prandtl's mixing length method to model the Reynolds stress term in the inner region of flow. Most of these models, developed in the 1950s and 1960s, have been reviewed in Jeromin [1970] and elsewhere. The basic formulation of these methods, assuming no-slip velocity at the wall, is outlined below.

Considering Prandtl's boundary layer equations to be valid,

$$-\frac{\tau}{\rho} = \nu \frac{\partial U}{\partial Y} - \overline{U'V'} = U_*^2 + V_w U \qquad 2.30$$

Though Equation 2.30 can be solved by relating the Reynolds stress to mean vorticity through a single equation eg, that of Rotta or of van Driest (Equations 2.21 and 2.22), most researchers adopted a two-layer model by solving the velocity distributions separately for the viscous sublayer and turbulent regions and combining them through a common value, U_1, at the sublayer-turbulent interface. Thus, for the sublayer region Equation 2.30 yields

$$\tilde{u} = \frac{1}{\tilde{v}_w} [\exp(\tilde{v}_w \tilde{y}) - 1] \qquad 2.31$$

and for the turbulent region,

$$\tilde{u} = \tilde{u}_{log} \left(1 + \frac{\tilde{v}_w \tilde{u}_{log}}{4}\right) \qquad 2.32$$

where $\tilde{u}_{log} = (\frac{1}{\varkappa})\ln \tilde{y} + B$ is the log-law velocity admitting possible changes in the coefficients $\varkappa$ and B. Equation 2.32, originally developed by Dorrance and Dore, is the so-called

bilogarithmic law. It shows that for any given $\tilde{y}$, $\tilde{u}$ is linearly dependent on $\tilde{v}_w$ if $\varkappa$ and B are constant.

Depending on the boundary conditions applied on Equation 2.32 the coefficients $\varkappa$ and B can be determined. Conceptually, only one boundary condition is available, which is at the sublayer-turbulent interface (alternatively, at the apparent origin of the velocity profile), so that assuming $\varkappa$ to be constant B can be determined. The various criteria suggested -- essentially intended for flow over smooth boundaries -- are as follows [refer Jeromin, 1970; Kocheryzhenkov and Matveyev, 1977] :

(i) Rubesin [1954] proposed that the Reynolds number, R_{ei}, at the sublayer-turbulent interface is independent of v_w,

$$R_{ei} = \frac{U_i Y_i}{\nu} = 13.1^2 \qquad 2.33a$$

(ii) Dorrance and Dore [1954] and Stevenson [1963] recommended that the origin of $\tilde{u}$ on the wall length scale ν/U_* ie, $\tilde{y}$ for $\tilde{u} = 0$, is invariant, implying thereby

$$B = \text{constant} \qquad 2.33b$$

(iii) Black and Sarnecki [1964] suggested that irrespective of V_w, $\tilde{u}_i$ is constant,

$$\tilde{u}_i = 11.0 \qquad 2.33c$$

(iv) Simpson [1966] ignored the modified sublayer velocity distribution and prescribed

$$\tilde{u}_i = \tilde{y}_i = 11.0 \qquad 2.33d$$

Dorrance and Dore's, Rubesin's and Simpson's criteria seem to have been more frequently used by subsequent researchers.

For the defect region of flow [refer Jeromin, 1970] Stevenson proposed $\tilde{u}$ as an extended form of the bilogarithmic law. Mickley and Smith suggested a modified wake law by normalizing the velocity with the maximum shear velocity in the boundary layer rather than the wall shear velocity. McQuaid used an independently computed wall shear velocity taking account of the pressure gradient and transpiration velocity. In contrast to earlier researchers, Torii, Nishikawi and Hirata did not assume V to be constant and, instead related it to U through the continuity equation. They subsequently made some assumptions to obtain U(y) and $\tau(y)$. Most of the analytical solutions for the defect region cited here show fair to good agreement with empirical data [Jeromin,1970].

Kays [1972] studied heat and mass transfer to TBL using a van Driest-type mixing length formula for the inner region and a mixing length scaling on boundary layer thickness for the outer region with a criterion similar to Rubesin's for the sublayer-turbulent interface. The numerical solutions were found to match very well with experimental data of velocity and temperature profiles including measurements in the developing or relaxing length of the inner boundary layer.

2.2.4 Analysis of OC flow with suction/injection

Conventionally, the depth average continuity, momentum and energy equations are used in the analysis of spatially varied flow in open channels. The analysis is valid for inflow to, or outflow from, the channel through the top, sides or bottom of the channel and at any rate of inflow or outflow so long as the channel flow

remains turbulent and the flow does not change from subcritical to supercritical or vice versa. The essential analysis and main results [Chow, 1959; Subramanya, 1986] are discussed below.

For streamwise increasing discharge, the net momentum flux across the channel section is

$$\frac{dF_m}{dX} = -\frac{dF_p}{dX} + \gamma A S_o - \gamma A S_f \qquad 2.34$$

where F_m and F_p are respectively the momentum and pressure forces, γ is unit weight of water, A is cross-sectional area, S_o is the channel slope ($|S_o| << 1$) and S_f is the energy gradient of flow. With $\partial P/\partial X = \gamma A\, dH/dX$ and $F_m = C_m Q^2/A$, where C_m is the momentum correction factor and Q is the discharge, Equation 2.34 gives the water surface gradient as

$$\frac{dH}{dX} = \frac{S_o - S_f - 2 C_m Q Q_* /(a_g A^2)}{1 - C_m Q^2 T/(a_g A^3)} \qquad 2.35$$

where $Q_* = dQ/dX$ (that is, inflow to channel per unit length), and T is the water surface span. For wide rectangular channels with constant Q_* the above equation simplifies to

$$\frac{dH}{dX} = \frac{S_o - S_f - 2C_m v_i u_{av} S_o}{1 - C_m u_{av}^2 S_o} \qquad 2.36$$

where V_i is the inflow rate per unit bed area, and v_i and u_{av} are V_i and U_{av} normalized with $\sqrt{a_g H S_o}$. Holding S_f and C_m constant, the water surface elevations can be easily computed if the depth and mean velocity at a control section are known.

For spatially decreasing discharge, it is contended that the energy content of flow per unit mass is not significantly affected by water withdrawal. Hence the depth-integrated energy equation is applied instead of the momentum equation,

$$-S_f = \frac{dH}{dX} - S_o - \frac{d}{dX}\left(\frac{C_e Q^2}{2a_g A^2}\right) \qquad 2.37$$

$$\Longrightarrow \quad \frac{dH}{dX} = \frac{S_o - S_f - C_e\, v_w\, u_{av}\, S_o}{1 - C_e\, u_{av}^2\, S_o} \qquad 2.38$$

for wide rectangular channels with uniform water withdrawal rate, where C_e is the energy correction factor.

The one dimensional analysis outlined above has several shortcomings. Firstly, other than H and U_{av}, many aspects of the mean flow and stress field, such as U(y), and $\tau(y)$, remain undetermined. Secondly, there is considerable scope of error in assuming S_f based on uniform flow equations, such as Manning's equation, which may not be valid for gradually or spatially varied flow. Thirdly, the coefficients C_e and C_m depend on the shape of the velocity profile and may change significantly with suction/injection; in fact, C_m is known to be much higher for increasing discharges than for uniform flow [Subramanya, 1986]. Finally, the analysis does not throw any light on the turbulence flow field.

An attempt to extend the two dimensional analysis of TBL flow with suction/injection to OC flows was made by Nakagawa [1984], who adopted the bilogarithmic law (Equation 2.32) and prescribed a slip velocity at the bed surface. The slip velocity boundary condition was estimated by considering velocity fluctuations U' and V' (produced by pressure fluctuations of the turbulent channel flow penetrating the bed) to be correlated. The resulting turbulent shear stress in the bed produced

streamwise seepage flow, whose magnitude at the bed surface gave the slip velocity. It may be pointed out that the author did not consider any damping of pressure fluctuations in an uncompacted granular medium; nor were possible correlations between U' and W' or between V' and W' in the bed (which could have induced three dimensional seepage flow) taken into account. Most importantly, consequent upon Nakagawa's adoption of the bilogarithmic law, $V_h = V_w$ at the free surface. Thus, the free surface must have a slope, S_r, relative to the bed,

$$S_r = \frac{V_w}{U_h} \qquad 2.39$$

This contradicts the author's assumption of the free surface being parallel to the bed. Hence the validity of a self-similar solution (Equation 2.32) for the entire flow depth is questionable.

As illustrated by the above discussion there are serious difficulties in directly transplanting the transpired boundary layer analysis to OC flows subjected to suction/injection. At the same time there do not appear to have been any successful two-dimensional analysis independent of TBL assumptions. Hence the one-dimensional hydraulic equations remain the most effective tools for even complex problems involving sucked/injected channel flow such as conjunctive modelling of channel flow with subsurface seepage or infiltration [Akan and Yen, 1981] and dynamic analysis of surface irrigation through furrows [Schmitz and Seus, 1992].

2.3 Mechanics of longitudinal bedforms

2.3.1 General

Turbulent fluid flow with sediment motion over a flat bed often leads to a systematic three-dimensional reshaping of the bed by locally unmatched erosion and deposition rates until dynamic equilibrium is achieved. Among several common sedimentary structures formed in such cases, two-dimensional, flow-aligned longitudinal bedforms are common to different sedimentary bedforms. Some of their observed occurrences in nature are [Allen, 1964; 1982; Karcz, 1967; Hanna, 1969; Kenyon, 1970; Glennie, 1987; Werner, et al, 1980] :

* in deserts as longitudinal or self dunes;
* on non-cohesive or weakly cohesive sediment beds in rivers, seas and lakes as longitudinal stripes, ridges, lineations, (sand) ribbons, or mudgrooves;
* on bedding surfaces of fine- to medium-grained sandstone as parting lineation or primary current lineations.

Though longitudinal or streamwise bedforms vary widely in dimension and, to some extent, morphology, depending on their geophysical setting, their common shape and alignment tends to suggest that their mechanism of formation and maintenance are similar, if not identical. Many researchers have described boundary layer as the active agent that sculptures longitudinal bedforms on passive, deformable beds, and suggested that transverse structuring of the flow, probably in association with streamwise helicoidal vortices, are instrumental in this process [eg. Allen, 1982; Folk, 1976; Gupta, Parkash and Garde, 1987; Hanna, 1969; Muller and Studerus, 1979]. Though many details of

the mechanism that enables a close coupling of the flow and the bed may not be understood yet, the importance of longitudinal bedforms can be realized from the following facts [Allen 1982; Folk, 1976; Glennie, 1987; Tsujimoto, 1989] :

* Longitudinal bedforms in contrast to transverse (two or three- dimensional) bedforms exert little form drag on the flow.
* Knowledge of these structures can be used to infer significant aspects of the flow and sedimentological context in which they occur. Such knowledge have been used in paleocurrent analysis and in identifying desert wind direction.

The above results have accrued mainly from empirical knowledge of streamwise bedforms, and further advantages may come with better theoretical understanding of their mechanics. As of now, two main theories of longitudinal bedforms have been proposed by researchers, -- one relating them to coherent structures of the viscous sublayer, and the other to secondary currents of the bulk (or outer) flow. These models are reviewed here.

2.3.2 Low-speed streak model

Based on Sorby's suggestion early this century [refer Allen, 1982], parting lineation on parallel-laminated sandstone have been conceptually linked with bedload streaks and the spanwise organization of quiescent sublayer flow [Allen, 1964, 1982; Jackson, 1976; Mantz, 1978; Weedman and Slingerland, 1985; Williams and Kemp, 1971]. According to this thesis lateral advection by the sublayer vortical flow deflects bedload towards

low-speed streak regions where, due to their increased concentration and low fluid momentum, the bedload tends to deposit in flow-parallel lanes as indicated in Figure 2.1. Jackson [1976] and Allen [1982] have suggested that the main impetus for sediment motion and the ridge-groove formation comes from turbulent bursting events and not the quiescent flow, and that incipient bedforms induce lateral fixing of low-speed streak and/or burst locations.

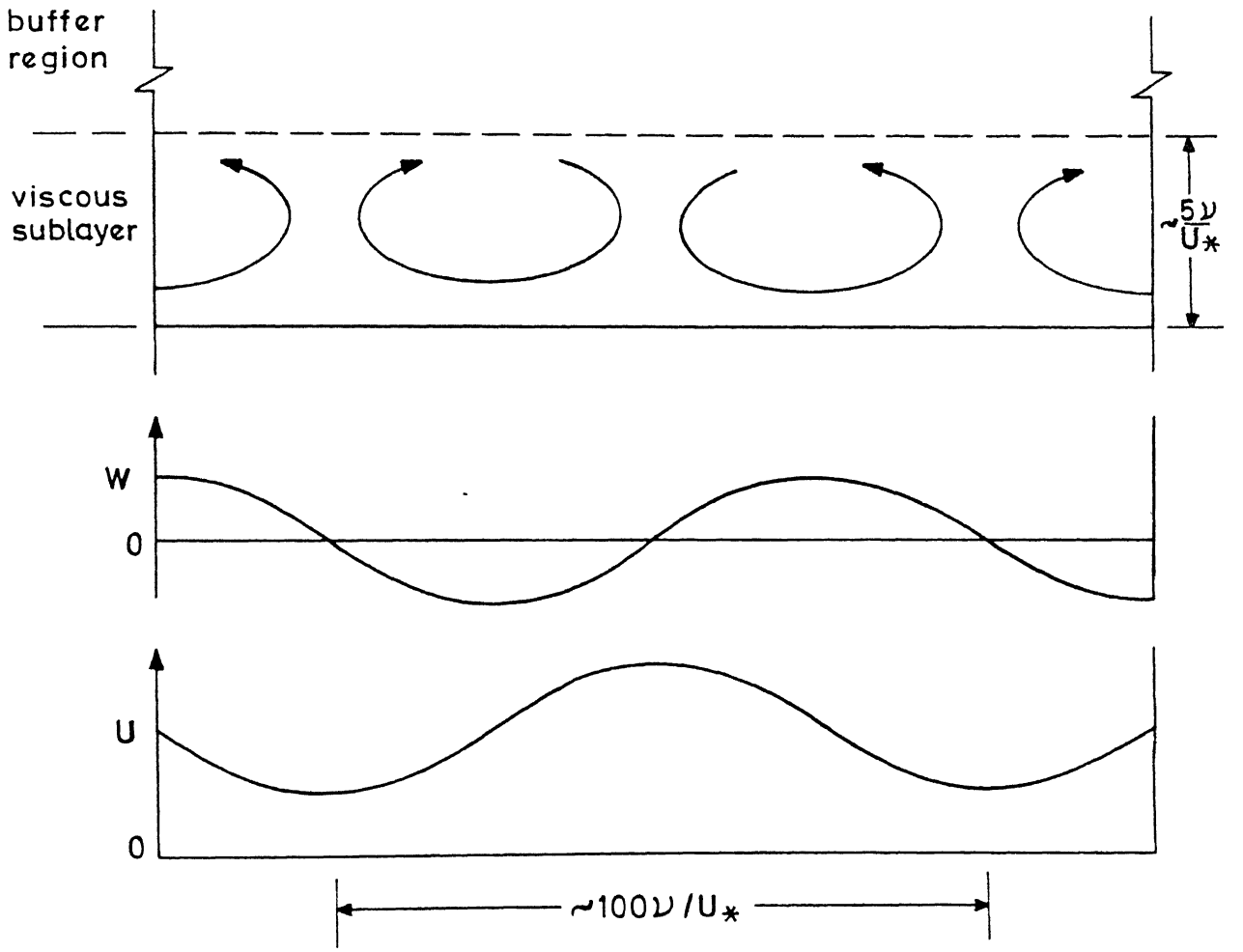

Figure 2.1 : Schematic of sublayer flow structure

The low-speed streak model has been verified in the laboratory by Allen [1969], Mantz [1978] and Weedman and Slingerland [1985]. These studies reveal that the characteristic spacing, L_z, of bedload streaks and sediment ridges produced on the flume bed is about $100\,\nu/U_*$ which is the same as that of sublayer streak spacings, λ_z. Further, shape-fabric studies of sandstone deposits showed that the long axes of grains on parting lineations were oriented at small angles to the lineations, which is indicative of the impact of weak lateral flow on the lineations [Allen, 1982].

The evidence cited above does not validate the low-speed streak model completely, particularly since the mechanism of sublayer flow structuring is insufficiently understood at present. Thus, it is yet to be demonstrated that incipient ridge-groove formations can control the spanwise organization of sublayer flow and turbulence bursts. Without such control, bed lineations will disappear almost as soon as they begin to appear without leaving any trace. Secondly, it is not very clear why in the experiments of Mantz bedload streaks were observed with micaceous flakes whereas ripple bedforms developed with granular sediment. Thirdly, Gupta et al. [1987] reported lineations with grain shear Reynolds number, $\tilde{d}$, in the range $11 < \tilde{d} < 70$. This corresponds, for a static bed, to transitional bed roughness when the sublayer flow structure is at least partially destroyed [Grass, 1971]. Hence it is difficult to fully account for Gupta et al's lineations in terms of the sublayer flow. These and other questions that may arise, such as the possible correspondence between the dimensions (length and relief) of lineations and of

sublayer streaks, underscore the need for detailed hydrodynamic and sedimentological studies of lineations and their relation to sublayer flow.

2.3.3. Secondary current model

Secondary currents in straight open channels usually occur as counter-rotating pairs of streamwise vortices whose vertical dimensions are on the order of flow depth. They may be caused by a number of factors such as asymmetric channel boundary (sidewalls or channel banks), the effects of corners and bed disturbances, and, in general, any physical condition that produces unbalanced hydrodynamic forces in a rectilinear flow configuration. These forces result from the inhomogeneity in anisotropic wall turbulence and produce Prandtl's second type of secondary flow, as opposed to secondary currents of Prandtl's first type caused by skewing of the mean flow eg., in channel bends [Perkins, 1970]. Proponents of the secondary current model for streamwise bedforms attribute the existence of the latter to lateral redistribution of streamwise momentum and shear stress near the wall by secondary flow, with generation of secondary flow being possibly aided by the existence of bedforms or lateral grain sorting [Glennie, 1987; Hanna, 1969; McLean, 1981; Muller and Studerus, 1979; Nezu, Nakagawa and Tomingaga,1985; Tsujimoto, 1989].

The secondary current hypothesis is empirically supported by the direct or indirect detection of secondary flow cells in the presence of lineations, and the correlation of the lateral spacing of cells with L_z. Flume studies show that the spacing of pairs of secondary cells with bed roughness strips sim ulating sand ribbons

is equal to L_z, suggesting that sand ribbons are produced in the low momentum regions where bedload tends to deposit [Muller and Studerus, 1979; Studerus,1982]. Moreover, measurements by the above authors and flow visualization by McLean [1981] showed the near-bed flow to be directed away from the roughness strips indicating the likelihood of greater bedload concentration and lineation development in the smooth zones.

Nezu et al [1985] reported secondary flow cells in experiments with flow-parallel ridges placed on a channel bed. They found the near-bed secondary flow to be directed towards the ridges which supports the above hypothesis if the ridges are considered analogous to lineations. However, the local effect of bed ridges should be a decrease in the log-law velocity similar to that of roughness strips. Thus Nezu et al's measured direction of the near bed secondary velocity is not quite equivalent to those of Muller and Studerus and of McLean.

Unlike the low-speed streak model, attempts have been made in the case of the secondary current hypothesis to make quantitative analysis or estimates of velocities and shear stress. Odgaard [1984] proposed a shear induced secondary flow model that makes simplifying assumptions about the distribution of V(y) and the profiles of $\tau(y)$ and U(y). Though these assumptions are not rigorously justified and, in fact, give a considerable slip velocity for W at the channel bed, the resulting shear stress and mean velocity distributions show good agreement with the data of Muller and Studerus.

McLean [1981] developed a more elaborate mathematical model for the mean flow field and stress on a flat bed with spanwise periodically varying roughness. With an assumed form of the variation of turbulent normal stresses and with an eddy viscosity formulation for shear stresses he obtained secondary flow velocities as functions of some undetermined coefficients. Assuming the secondary velocities and a secondary component of the streamwise velocity to be the perturbed mean flow components due to variation in bed roughness, he obtained the streamwise velocity and shear stress from the X-momentum equation using eddy viscosity formula. The unknown coefficients were evaluated by matching computed U(y) with his experimental data, and he thus showed the mean flow field to be uniquely related to bed roughness variation. McLean also suggested that the most likely ribbon spacing is ~ 3H conforming to field observations, and that, though the secondary circulation is weak compared to the mean flow, the ratio of τ_w over rough and smooth strips could be as high as 2 or 3.

In contrast to McLean's and Odgaard's approach Tsujimoto [1989] assumed secondary flow cells and showed that it produces lateral grain sorting on a non-uniform grain bed. By assuming an oblique near-bed velocity vector, and with empirical estimates of entrainment rates and saltation distances of different size fractions, Tsujimoto's analysis indicated the development of lateral grain sorting and their attenuation with equilibrium transport rates of bedload composed of sand and gravel.

In concluding, it may be mentioned that whereas the scales of bedload streaks and parting lineations suggest that they are related to sublayer or wall layer flow structures, secondary

currents of the bulk flow seem to be the likely cause of sand ribbons. However, though secondary currents are purported to produce sand ribbons on non-uniform grain beds, such ribbons (or lineations or ridges) on graded material beds have not been reported in literature.

CHAPTER 3

THEORETICAL CONSIDERATIONS AND MODELLING

3.1 Analysis of flow with suction/injection

As discussed in the previous chapter the present analytical solutions for flows with suction/injection are essentially suited for TBL flows. In OC and duct flows the vertical velocity does not transpire through the boundary layer uniformly ie, $V(Y) \neq V_w$, and the intermittency of the outer TBL region is absent or much less in these cases. Herein an attempt is made to analyse spatially varied OC flow with uniformly distributed suction/injection and with water surface nearly parallel to the channel bed. It is assumed that the turbulence generation, diffusion and dissipation mechanisms are fundamentally unchanged from those of uniform OC flow, so that turbulence quantities can be modelled identically in both cases.

3.1.1 Basic formulation

Consider turbulent flow in a wide, rectangular channel with small bed slope, S_o ($\simeq \sin\theta$), as shown in Figure 3.1, subjected to injection or suction at a constant rate V_w over sufficient length of the channel. For a Cartesian coordinate system with Y normal to the bed and X flush with the bed in the streamwise direction having origin at the location where $dH/dX = 0$, let H_o be the flow depth and Q_o the specific discharge (discharge per unit width) at X=0. The following assumptions are made in this analysis :

(i) The flow is incompressible, steady and two-dimensional in the mean.

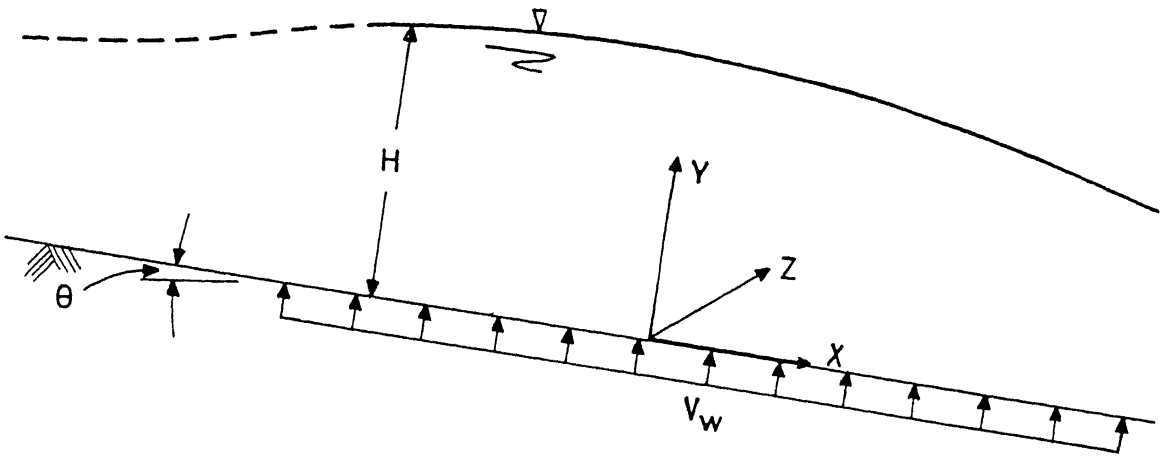

Figure 3.1 : Schematic of open channel flow with suction or injection

(ii) At X=0 water immediately below the bed has the same longitudinal and lateral pressure gradients as those of the overlying fluid, ie,

$$\frac{\partial P}{\partial X} = \frac{\partial P}{\partial Z} = 0 \text{ near } X=0 \qquad 3.1$$

where P is the pressure difference with gauge pressure. Equation 3.1 implies constancy of $\partial P/\partial Y$ across the bed surface, and hence constancy of V_w.

Assumming all quantities to be invariant with Z, the governing equations of motion for the turbulent flow region in the neighbourhood of X=0 are :

$$\frac{\partial U}{\partial X} + \frac{\partial V}{\partial Y} = 0 \qquad 3.2$$

$$\frac{\partial (U^2)}{\partial X} + \frac{\partial (UV)}{\partial Y} = - \frac{\partial P}{\rho \partial X} + a_g S_o - \frac{\partial}{\partial X}(U'^2) - \frac{\partial}{\partial Y}(\overline{U'V'}) \qquad 3.3$$

$$\frac{\partial (UV)}{\partial X} + \frac{\partial (V^2)}{\partial Y} = - \frac{\partial P}{\rho \partial Y} + a_g - \frac{\partial}{\partial X}(\overline{U'V'}) - \frac{\partial (\overline{V'^2})}{\partial Y} \qquad 3.4$$

with the boundary conditions :

(i) at $Y = H_o$, $V = \overline{V'^2} = \overline{U'V'} = P = 0$ 3.5

(ii) at $Y = Y_o$, $V = V_w$ and $U = 0$ 3.6

where a_g is acceleration due to gravity and Y_o is the apparent origin of the turbulent velocity distribution. A simple order of magnitude analysis indicates that when V_w is small, the equations of motion reduce to Prandtl's boundary layer equations albeit, with the inclusion of the gravitational acceleration term. Herein, some empirical considerations will be used to obtain an estimate of V_w for which the boundary layer simplification is valid.

Since $dH/dX = 0$ at $X = 0$ and since the bounds on V at $Y = Y_o$ and $Y = H_o$ are uniform in the neighbourhood of $X = 0$, it may be assumed that $\partial V / \partial X = 0$ for all Y, or $V(X,Y) = V(Y)$. Hence on integrating Equation 3.4 over Y to H_o and differentiating with X,

$$- \frac{1}{\rho} \frac{\partial P}{\partial X} = \frac{\partial \overline{V'^2}}{\partial X} - \frac{\partial}{\partial X} \int_y^{H_o} \frac{\partial}{\partial X} (\overline{U'V'})\, dt \qquad 3.7$$

t being a dummy variable. Subsituting the above in Equation 3.3,

$$a_g S_o + \frac{\partial}{\partial Y}(-\overline{U'V'}) + \frac{\partial}{\partial X}(\overline{V'^2} - \overline{U'^2}) + \frac{\partial}{\partial X}\int_Y^{H_o} \frac{\partial}{\partial X}(-\overline{U'V'})dt$$

$$= \frac{\partial}{\partial X}(U^2) + \frac{\partial}{\partial Y}(UV) \qquad 3.8$$

From empirical TBL and uniform OC flow data it may be assumed that $\overline{U'^2}$ and $\overline{V'^2}$ are at most a few times the kinematic shear stress which, for uniform OC flow, is $a_g H_o S_o$. With water surface slope, $S = S_o - dH/dX$, the third term of Equation 3.8 is thus of order

$$\left[\frac{d}{dX}(a_g HS)\right]_{X=0} = - a_g H_o \left[\frac{d^2H}{dX^2}\right]_{X=o} \qquad 3.9a$$

which is numerically small in comparison to the first term if

$$\left| \frac{H_o}{S_o} \frac{d^2H}{dX^2} \right|_{X=0} << 1 \qquad 3.9b$$

This condition is automatically satisfied if $d^2H/dX^2 = 0$ at $X=0$, ie, if the water surface is uniformly parallel to the bed or has a point of inflexion at $X = 0$. If $|d^2H/dX^2| > 0$, it will be shown later that the condition is fulfilled if

$$\left| \frac{V_w}{U_{av}} \right| << 1 \qquad 3.9c$$

An estimate of the fourth term of Equation 3.8 may be obtained by use of Prandtl's mixing length formulation together with the assumption of a self-similar X-velocity satisfying the continuity equation,

$$- \overline{U'V'} = \varkappa^2 Y^2 \left| \frac{\partial U}{\partial Y} \right| \left| \frac{\partial U}{\partial Y} \right| \qquad 3.10a$$

$$U(X,Y) = U(0,Y)\left(1 + \frac{V_w X}{Q_o}\right) \qquad 3.10b$$

Subsituting Equations 3.10 in the fourth term and dividing by $a_g S_o$

$$\frac{1}{a_g S_o} \frac{\partial}{\partial X} \int_Y^{H_o} \frac{\partial}{\partial X}(-\overline{U'V'})dt \sim O\left[\frac{2V_w^2}{Q_o^2} \cdot \frac{a_g H_o^2 S_o}{a_g S_o}\right] \qquad 3.11a$$

Hence the fourth term may be ignored when

$$\left(\frac{V_w}{U_{av}}\right)^2 << 1 \qquad 3.11b$$

3.1.2. Turbulence stress modelling and governing equations for time-average velocity

With the considerations outlined have, Equations 3.3 and 3.4 yield

$$\frac{\partial}{\partial Y}(- \overline{U'V'}) = - a_g S_o + \frac{\partial}{\partial X}(U^2) + \frac{\partial}{\partial Y}(UV) \qquad 3.12$$

The Reynolds stress term is modelled here by a gradient transport formulation involving kinematic eddy viscosity, ν_t,

$$- \overline{U'V'} = \nu_t \frac{\partial U}{\partial Y} \qquad 3.13$$

$$\text{where } \nu_t = \begin{cases} \varkappa^2 Y^2 \left(1 - \frac{Y}{H}\right) \left|\frac{\partial U}{\partial Y}\right| & 3.14 \\ \varkappa Y \left(1 - \frac{Y}{H}\right) U_* & 3.15 \end{cases}$$

with the last two equations being the mixing length and parabolic eddy viscosity formulae respectively, and U_* being the local bed shear velocity.

Since $\partial V/\partial X = 0$ and since $H(x)$ $(= H_o)$ is constant near X=0, Equation 3.2 implies that U(X,Y) is a linear function of X.

Let $$U(x,y) = F(y) + x\,G(y) \qquad 3.16$$

$$\Longrightarrow \quad V(y) = \int_y^1 G(t)\,dt \qquad 3.17a$$

and $$\int_{y_o}^1 G(t)\,dt = V_w \qquad 3.17b$$

where $x = X/H_o$ and $y = Y/H_o$. Hence from Equations 3.14 or 3.15,

$$U_* = U_{*o}\,[1 + \beta x] \qquad 3.18a$$

where $$U_{*o} = \left[\kappa\, y\sqrt{1-y}\,\frac{\partial F}{\partial y}\right]_{y=y_o} \qquad 3.18b$$

and $$\beta = \left[\frac{\partial G}{\partial y} \Big/ \frac{\partial F}{\partial y}\right]_{y=y_o} \qquad 3.18c$$

Thus, ν_t, is a linear function of x.

On subsituting Equations 3.13, 3.16 and 3.17 in Equation 3.12, integrating from Y to H_o, and dividing by $a_g H_o S_o$,

$$\frac{\nu_t}{H_o\sqrt{a_g H_o S_o}}\left(\frac{df}{dy} + x\,\frac{dg}{dy}\right) = (1-y)\left[\frac{S}{S_o} + \phi_{fg} + x\phi_{gg}\right] \qquad 3.19$$

where $h = H/H_o$, $f(y) = F(y)/\sqrt{a_g H_o S_o}$, $g(y) = G(y)/\sqrt{a_g H_o S_o}$, and ϕ_{f1f2} is the following operation on any two function $f_1(y)$ and $f_2(y)$ that are continuous and integrable in the interval $y_o \le y \le 1$,

$$\phi_{f_1 f_2} = \frac{[f_1(y) \int_y^1 f_2(t)\,dt - 2 \int_y^1 f_1(t) f_2(t)\,dt]}{(1 - y)} \qquad 3.20$$

Since ν_t is linear in x, Equation 3.19 implies that hS/S_o should be quadratic in x. Thus Equation 3.19 becomes, on assuming the following expression for hS/So, where α and α are constants,

$$\frac{S}{S_o} = (1 + \alpha x)^2 + \alpha_1 x^2 \qquad 3.21$$

$$\frac{\nu_t}{H_o \sqrt{a_g H_o S_o}} \left(\frac{df}{dy} + x \frac{dg}{dy}\right) = [1 + \phi_{fg} + x(2\alpha + \phi_{gg}) + x^2(\alpha^2 + \alpha_1)](1 - y) \qquad 3.22$$

On substituting the turbulent viscosity formula of Equation 3.14 or 3.15, and equating terms of order x^0, x^1 and x^2 respectively, three separate equations can be obtained, which, together with boundary conditions, are required to yield the functions f(y), g(y) and the constants α and α_1.

3.1.3 Self-similar solution for U(y)

(a) Mixing length formula : With Equation 3.14 for ν_t, Equation 3.22 yields the following equations of order x^0, x^1 and x^2

$$\kappa^2 y^2 f'^2 = 1 + \phi_{fg} \qquad 3.23a$$

$$\kappa^2 y^2 f' g' = \alpha + \frac{\phi_{gg}}{2} \qquad 3.23b$$

and $$\kappa^2 y^2 g'^2 = \alpha^2 + \alpha_1 \qquad 3.23c$$

together with the boundary conditions

$$\text{(i) at } y = y_o \text{ , } f(y) = g(y) = 0 \qquad 3.23d$$

$$\text{(ii)} \int_{y_o}^{1} g(t)dt = v_w \qquad 3.23e$$

where $f' = df/dy$, $g' = dg/dy$, $v' = dv/dy$, etc. The above equations are in integro-differential forms, but are easily converted to ordinary differential equations, namely,

$$\frac{d}{dy}[\chi^2 y^2 (1-y) f'^2] = 1 + f\, v' + f'(v_w - v) \qquad 3.24a$$

$$\frac{d}{dy}[\chi^2 y^2 (1-y)\, f' v''] = -\alpha + \frac{[v'^2 + v''(v_w - v]}{2} \qquad 3.24b$$

$$\frac{d}{dy}[\chi^2 y^2 (1-y)\, v''^2] = \alpha^2 + \alpha_1 \qquad 3.24c$$

Inspection of Equations 3.23 or Equations 3.24 does not indicate any closed form solutions for f(y) and g(y). However, if $v^2(y) << 1$ then it may be anticipated that $\phi^2_{fg} << 1$. Moreover, if g(y) be of order α f(y), then $\phi^2_{gg} << |\alpha|$. Then Equations 3.23 in binomial series expansion approximate to

$$\chi y f' = 1 + \frac{\phi_{fg}}{2} \qquad 3.25a$$

$$\chi y g' = \alpha + \frac{\phi_{gg} - \alpha \phi_{fg}}{2} \qquad 3.25b$$

and $$\chi y g' = \alpha \left(1 + \frac{\alpha_1}{2\alpha}\right) \qquad 3.25c$$

Equation 3.25b contradicts Equation 3.25c. The latter is ignored as it involves error terms of order x^2 whereas U(y) was assumed linear in x. Making the assumption that the flow is nearly self-

similar, let

$$g(y) = \alpha f(y) \qquad 3.26$$

Thus Equations 3.25a and b imply,

$$\varkappa y \frac{dg}{dy} = \alpha + \frac{\varnothing_{gg}}{2} \qquad 3.27a$$

and

$$\varkappa y \frac{dg}{dy} = \alpha \qquad 3.27b$$

Evidently Equation 3.26 is invalid, but, if $|\varnothing gg| << |\alpha|$, then Equations 3.27a and 3.27b hold approximately. In that case there may be error in g(y) as determined from either of these equations, but the error will be numerically small as $|\varnothing_{fg}| << 1$. More significantly, since $\int_y^1 g(t)dt$ is fixed at both extremes $y = y_o$ and $y = 1$, if g(y) be a monotonic function within these limits, then the error in determining $\varnothing_{fg}$ will be relatively small. Thus f(y) determined from Equation 3.25a will be fairly insensitive to the error in g(y) determined from Equation 3.27a or 3.27b.

Equation 3.27b with Equations 3.23d and e yield the familiar log-law :

$$g(y) = \frac{\alpha}{\varkappa} \ln\left(\frac{y}{y_o}\right) \qquad 3.28$$

From Equation 3.27b an approximate solution can be obtained by taking cue from power laws often used in pipe and OC flows. For $0 < y \leq 1$ and $|n| << 1$ the following relation approximately holds,

$$\int_y^1 t^n dt \simeq \left(\frac{1 + n\sqrt{y}}{1 + n}\right)(1 - y) \qquad 3.29$$

It can be verified numerically that the error in the above equation is less than 0.9 % for $|n| < 0.1$ and 2.2 % for $|n| < 0.2$. Thus it is proposed to seek solutions of the form

$$g(y) \simeq l\,(y^n - c_o \sqrt{y} - c_1) \qquad 3.30a$$

where the constants c_1 and l are determined from the boundary conditions 3.23e and d, respectively as

$$c_1 = y_o^n - c_o \sqrt{y_o} \qquad 3.30b$$

$$l = \frac{v_w}{(1-y_o)\left(\frac{1+n\sqrt{y_o}}{1+n} - \frac{2}{3}c_o - c_1\right)} \qquad 3.30c$$

Substituting Equations 3.30 in Equation 3.27a, and equating terms of order y^1, y^n and y^o respectively, the constants n, c_o and α can be determined.

(b) Parabolic eddy viscosity formula : With Equation 3.15 in Equation 3.22 and proceeding as earlier, the following equations are obtained in place of Equations 3.23a and b :

$$u_{*o}\,\kappa y \frac{df}{dy} = 1 + \emptyset_{fg} \qquad 3.31a$$

$$u_{*o}\,\kappa y \frac{dg}{dy} = (2\alpha - \beta) + \emptyset_{gg} - \beta\emptyset_{fg} \qquad 3.31b$$

Thus, with the relation of Equation 3.26, i.e., $g(y) = \alpha f(y)$,

$$u_{*o}\,\kappa y \frac{dg}{dy} = \alpha + \emptyset_{gg} \qquad 3.32a$$

and $$u_{*o}\,\chi\, y\,\frac{dg}{dy} = \alpha \qquad 3.32b$$

whose solutions can be obtained in the form of Equation 3.30a as in the previous case.

(c) Velocity Profile : The solved dimensionless velocity distributions for the mixing length and parabolic eddy viscosity models can be represented in the common form :

$$g(y) = \frac{\alpha}{u_{*o}^{(2-a)}\chi}\ln\left(\frac{y}{y_o}\right) \qquad 3.33$$

or $$g(y) = l\,[y^n - y_o^n - 6n^2(\sqrt{y} - \sqrt{y_o})] \qquad 3.34$$

and $$f(y) = m\,[y^n - y_o^n - 6n^2(\sqrt{y} - \sqrt{y_o})] \qquad 3.35$$

where
$$n \simeq \frac{v_w\,[1-n-3n^2-c_1]}{a\chi\, u_{*o}^{(2-a)}(1-y_o)[1-n-3n^2+n\sqrt{y_o}-c_1]}$$

$$c_o \simeq 6n^2$$

$$c_1 = y_o^n - c_o\sqrt{y_o}$$

$$l = \frac{v_w}{(1-y_o)\,(1-n-3n^2+n\sqrt{y_o}-c_1)}$$

and
$$m \simeq \frac{a(1-y_o)\,(1-n-3n^2+n\sqrt{y_o}-c_1)}{2(1-n-3n^2-c_1)\,(1-n-3n^2-0.5c_1)v_w} \qquad 3.36$$

with $$a = \begin{cases} 2 & \text{for mixing length formula} \\ 1 & \text{for parabolic eddy viscosity} \end{cases}$$

It can be verified numerically that Equation 3.34 approaches Equation 3.33 and Equation 3.35 approaches the law of the wall in the limit as n --> 0 or, as v_w --> 0. The likely error in estimating g(y) can be reduced by taking the average of Equations

3.33 and 3.34. Alternatively, g(y) can be computed by replacing the exponent n by $n_1 = n/2$ in Equation 3.34 and evaluating the coefficients c_0, c_1 and 1 accordingly.

(d) Parameters α and β : Since there is an error in the assumed equality $g(y) = \alpha f(y)$, the parameters α and β representing water surface curvature and rate of change of bed shear velocity, the parameters α and β will also absorb the error. To reduce the scope of error in α , the depth-average value of g(y) and f(y) may be used in Equation 3.26, so that

$$\alpha = \frac{\int_{y_o}^{1} g(t)dt}{\int_{y_o}^{1} f(t)dt} = \frac{v_w}{u_{av}} \qquad 3.37$$

Substituting $\beta = \left[\frac{dg/dy}{df/dy}\right]_{y=y_o}$ in Equations 3.25 or in Equations 3.31, β is found to be approximately,

$$\beta/\alpha \simeq \left[\frac{2+(a-1)\emptyset_{fg,o}}{2+a\emptyset_{fg,o}}\right] \qquad 3.38a$$

where $\emptyset_{fg,o}$ is the value of $\emptyset_{fg}$ at $y = y_o$,

$$\emptyset_{fg,o} \simeq -2\, v_w\, u_{av} \qquad 3.38b$$

(e) Comments on the analysis : (i) When using the mixing length model, terms of order $\emptyset^2_{fg}$, $\emptyset^2_{gg}$ and higher were ignored in Equations 3.25. This may give rise to significant error in the solution set unless $\emptyset^2_{gg} << 1$. The solution set for the parabolic eddy viscosity formulation is free of this error.

(ii) From Equations 3.21 and 3.37 the water surface curvature at x=0 is found to be positive for suction and negative for injection,

$$\left.\frac{d^2h}{dx^2}\right|_{x=0} = \frac{-2\, v_w\, S_o}{u_{av}} \qquad 3.39$$

From the above relation it follows that the inequalities of Equations 3.9b and 3.11b necessary for the boundary layer approximation are fulfilled when $|v_w/u_{av}| << 1$.

3.1.4 Evaluation of y_o

The velocity distribution derived above is incomplete without defining the apparent origin of the turbulent velocity distribution. Towards this end a two layer model is invoked for hydraulically smooth bed flow assuming uniform transpiration rate in the sublayer and an identical mean velocity, u_i, for the sublayer and turbulent region flows at their interface, y_i. Thus, for the sublayer region $\partial u/\partial x = 0$, and momentum balance in the x-direction gives

$$\frac{du}{dy} = R_* \,(u^2{}_{*o} + v_w u - y) \qquad 3.40a$$

$$\text{where} \quad R_* = \frac{H_o \sqrt{a_g H_o S_o}}{\nu} \qquad 3.40b$$

is a Reynolds number. On integrating Equation 3.40a over y, and letting $u = u_1$ at $y = y_1$,

$$u = \left(u_{*o}{}^2 - \frac{1}{R_* v_w}\right) \frac{[\exp\,(R_* v_w y) - 1]}{v_w} + \frac{y}{v_w} \qquad 3.41$$

$$u_{*o}^2 = \frac{[v_w\, u_i - y_i]}{[\exp\,(R_*\, v_w\, y_i) - 1]} + \frac{1}{R_*\, v_w} \qquad 3.42$$

An independant relation between u_i and y_i may be defined by one of several suggestions made by researchers cited in Chapter 2. Herein Rubesin's criterion is adopted with a modified value at the turbulent-laminar interface corresponding to the values of $\varkappa$ and B in the log-law in a given uniform flow situation. For example, with $\varkappa$ = 0.4 and B = 5.5,

$$\tilde{u}_i \, \tilde{y}_i = 135.373$$

or,
$$u_i \, y_i = \frac{135.373}{R_*} \qquad 3.43$$

Thus, if u_{*o} is known then Equations 3.42 and 3.43 together yield the values y_i and u_i from which y_o can be determined using Equations 3.35 and 3.36. Since u_{*o} is also implicity defined by Equation 3.35 and 3.36, y_o can be determined from the above equations. However, since u_{*o}, y_o, n and c_1, are interdependent, an iterative scheme has to be used for determining the various constants. A suitable procedure is outlined below.

Step 1 : Given $\varkappa$, B, R_* and v_w, compute initial values of y_o and y_i from uniform flow criteria.

Step 2 : Compute u_{*o} from Equation 3.42 and u_i from Equation 3.43.

Step 3 : Compute n, c_o and c_1 from Equations 3.36 and 3.34 with $f(y_i) = u_i$.

Step 4 : Compute y_o and u_{*o} from Equations 3.36 and 3.48 (given later).

Step 5 : If y_o and u_{*o} are almost same as in Step 2 then terminate computation; else repeat Steps 2 through 5 with new value of y_i.

It may be noted here that the shear stress distribution derived from Equation 3.40a for the viscous sublayer may be different from that of the turbulent region, so that the shear stress of the two regions at the interface is not equal. This apparently contradicts the notion of a two layer flow with common properties at the interface. However, the two layer approach is essentially an approximation to overcome the problem of exact stress modelling near the bed. The discontinuity in stress can be overcome by using a van Driest type of mixing length formula [see, for example, Kays, 1972], but this is not attempted here in order to eliminate analytical difficulties. As will be seen in Chapter 5 the divergence between "laminar" and turbulent shear stresses at the interface, assuming identical bed shear stress for the two cases, is not sufficiently large to warrant a modified eddy viscosity formulation.

For hydraulically rough flow regime ($\tilde{k}_s > 70$) the sublayer flow is believed to be completely destroyed or, at least inconsequential in defining the velocity distribution origin. Hence it may be assumed that, for a given bed roughness y_o is independent of v_w. For the transition regime a priori definition of y_o in the absence of empirical evidence is difficult.

3.1.5 Computation of flow parameters

(a) Mean velocity and flow depth : From Equations 3.35 and 3.36 the depth-average velocity, u_{av}, is found to be :

$$u_{av} \simeq m\,(1 - n - 3n^2 - c_1) \qquad 3.44$$

Thus, given the specific discharge at x=0, the flow depth is easily obtained.

(b) Vertical velocity : The distribution of the normal velocity component over y is obtained by integrating alternatively Equation 3.33 or 3.34,

$$v(y) \simeq \begin{cases} \dfrac{v_w[(y-1)\ (1 + \ln y_o) - y \ln y]}{[y_o - 1 - \ln y_o]} & 3.45 \\ \dfrac{v_w\ (1-y)\ (1 - n - 3n^2 + n\ \sqrt{y-c_1})}{(1-y_o)\ (1 - n - 3n^2 + n\ \sqrt{y_o-c_1})} & 3.46 \end{cases}$$

(c) Shear stress distribution : From the velocity distribution and the eddy viscosity model used, the shear stress distribution is derived,

$$\tau^+(y) = u_{*o}{}^{(2-a)}\ (1-y)\ [mn\kappa(y^n - 3n\ \sqrt{y})]^a \qquad 3.47$$

$$\Longrightarrow \quad u_{*o} \simeq mn\kappa(y_o{}^n - 3n\ \sqrt{y_o}) \qquad 3.48$$

where $\tau^+ = \tau/(\gamma H_o S_o)$,

(d) Water Surface Profile : From Equation 3.21,

$$(S_o - \frac{dh}{dx}) \simeq S_o\ (1+ \alpha x)^2 \qquad 3.49$$

Using P icard integration and ignoring terms of order x^4 and more,

$$h \simeq 1 - \alpha\ S_o x^2\ [1 + \frac{\alpha\ x}{3}] \qquad 3.50$$

which may be considered accurate for $(\alpha x)^3$ and $(S_o x)^3$ numerically much less than 1.

3.1.6 Extension of results

It may be noted that while the present analysis gives an estimate of the hydrodynamic drag force on granular bed material

in a loose-boundary channel, it does not help in estimating the hydrodynamic lift force acting on bed grains. The lift force, which plays an important role in bed grain motion, may not be significantly affected by changes in the channel flow. Rather, it should depend on the vertical seepage pressure gradient as suggested by some researchers [eg, Brink and Oldenziel, 1974; Maclean and Willetts, 1986].

The present analytical results should hold good also for duct flows, though with reservations about the applicability of simple eddy viscosity models for the core flow region. In duct flows the question of free surface curvature does not arise, and $V = 0$ at the centreline for all X. Thus, for flow in rectangular ducts with uniform suction/injection through opposite boundaries, and with $\partial P/(\gamma \partial X)$ replacing S_o, the above results should hold identically. Since the flow is only approximately self-similar, the parameters v_w, u_{*o}, α, β, and the functions $f(y)$ and $g(y)$ would need to be evaluated continually (or at intervals) over X.

In many field situations involving seepage or infiltration through channel bed, the seepage rate may not be precisely constant. For the case of slowly varying suction or injection in open channel flow, $dv_w/dx = \lambda$,

$$v(x,y) = v_w (1 + \lambda x) \int_y^1 g(t)\, dt \qquad 3.51$$

and

$$u(x,y) = f(y) + \chi g(y) \left(1 + \frac{\lambda x}{2}\right) \qquad 3.52$$

The governing equations may be rederived as earlier to give

$$u_{*o} \chi y g' = 2\alpha - \beta + \phi_{(g+\lambda f)g} - \beta \phi_{fg} \quad , \; a=1 \qquad 3.53$$

Further approximations made herein are :

(iv) The flow is of high aspect ratio, and is incompressible, uniform and steady in the mean.

(v) Turbulent stresses τ_{xy} and τ_{xz} can be modelled in terms of an eddy viscosity and mean vorticity components in the z and y directions, respectively.

(vi) The mean streamwise and vertical velocity components vary periodically with Z in consonance with the variation of bed roughness.

The analytical approach here is similar to that of McLean [1981], but no attempt is made here for an exact solution of the cross-stream velocity components.

3.2.2 Formulation

Consider flow over a ribbon bed with mean depth, H_o, as indicated in Figure 3.2. The shape, strength and sense of the secondary flow cells are unknown. For the simple case of a sinusoidal variation of $\ln y_o$, where y_o is the dimensionless apparent origin of velocity distribution above bed level,

$$\ln y_o = \ln y_{om} [1 + \varepsilon \cos (kz)] \qquad 3.55$$

where $\ln y_{om}$ is the Z-averaged value of $\ln y_o$, $k = 2\pi / Zo$ is wave number with Z_o as the wavelength of ribbon spacing, and $z = Z_o/H$. It follows from assumption vi of the last section,

$$U(y,z) = U_o(y) + U_1(y) \cos (kz) \qquad 3.56$$

and $$V(y,z) = V_o(y) \cos (kz) \qquad 3.57$$

Considering all quantities invariant in the X-direction, th equations of motion are :

$$\frac{\partial v}{\partial y} + \frac{\partial w}{\partial z} = 0 \qquad 3.58$$

$$v\frac{\partial u}{\partial y} + w\frac{\partial u}{\partial z} = -1 + \frac{\partial}{\partial y}\tau^{+}_{xy} + \frac{\partial}{\partial z}\tau^{+}_{xz} \qquad 3.59$$

$$v\frac{\partial v}{\partial y} + w\frac{\partial v}{\partial z} = \frac{-\partial p}{\partial y} + \frac{\partial}{\partial y}\sigma^{+}_{y} + \frac{\partial}{\partial z}\tau^{+}_{yz} \qquad 3.60$$

$$v\frac{\partial w}{\partial y} + w\frac{\partial w}{\partial z} = \frac{-\partial p}{\partial z} + \frac{\partial}{\partial y}\tau^{+}_{yz} + \frac{\partial}{\partial z}\sigma^{+}_{z} \qquad 3.61$$

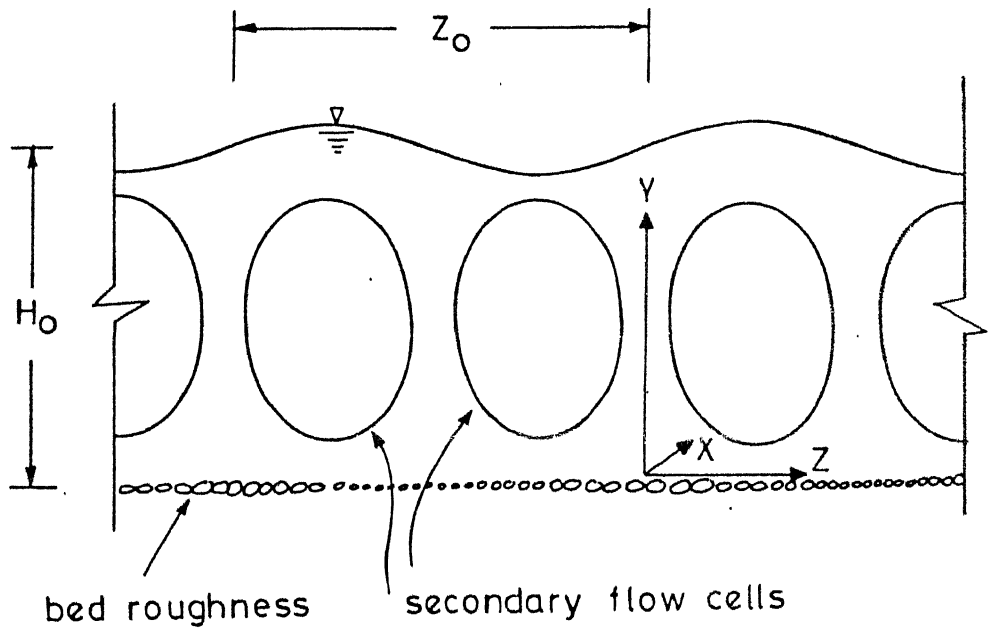

Figure 3.2 : Schematic of open channel flow over sand ribbons

where velocities have been normalized with $\sqrt{a_g H_o S_o}$, lengths with H_o, and pressure (P), normal stresses (σ) and shear stress (τ) with $\gamma H_o S_o$,

$$p = P/(\gamma H_o S_o),\ \sigma^+ = \sigma/(\gamma H_o S_o),\ \tau^+ = \tau/(\gamma H_o S_o)$$

Then from Equations 3.57 and 3.58,

$$w = \frac{-1}{k} \frac{dv_o}{dy} \sin(kz) \qquad 3.62$$

For the above set of equations, invoking a parabolic eddy viscosity formulation for modelling the turbulent stresses τ_{xy} and τ_{xz}, namely,

$$\tau^+_{xy} = u_* \chi y(1-y) \frac{\partial u}{\partial y} \qquad 3.63$$

$$\tau^+_{xz} = u_* \chi y\ (1-y) \frac{\partial u}{\partial z} \qquad 3.64$$

$$\text{implies} \quad u_* = \frac{U_*}{\sqrt{a_g H_o S_o}} = 1 + u_{*1} \cos(kz) \qquad 3.65a$$

$$\chi\ y_{om}\ (1-y_{om}) \left.\frac{du_o}{dy}\right|_{y_{om}} = 1 \qquad 3.65b$$

$$\chi\ y_{om}\ (1-y_{om}) \left.\frac{du_1}{dy}\right|_{y_{om}} = u_{*1} \qquad 3.65c$$

Hence an order of magnitude analysis of Equations 3.58 and 3.59 indicates

$$\frac{u_1(y)}{u_o(y)} \sim u_{*1} \sim \varepsilon \qquad 3.66$$

and $v \sim w \sim \varepsilon$

If σy, σz and τyz are also modelled similarly as τxy and τxz in terms of an eddy viscosity and the mean velocity gradients $\partial v/\partial y$, $\partial w/\partial z$ and $\partial v/\partial z + \partial w/\partial y$, then Equations 3.60 and 3.61 indicate that

$$\sigma_z \sim \tau_{yz} \sim \varepsilon$$

$$\Longrightarrow \quad \frac{\partial p}{\partial y} \sim \frac{\partial p}{\partial z} \sim \varepsilon \qquad 3.67$$

Hence the lateral variation of flow depth, ΔH, normalized by H_o, is of order

$$\Delta h = \varepsilon S_o \qquad 3.68$$

which is insignificant for small bed slopes.

3.2.3 ε - order solution

On substituting Equations 3.56, 3.57 and 3.62 through 3.65 in Equation 3.59 and simplifying,

$$\frac{d}{dy}\left[\varkappa y\,(1-y)\,\frac{du_o}{dy}\right] + \frac{d}{dy}\left[\varkappa\, y\,(1-y)\,u_{*1}\,\frac{du_1}{dy}\right]$$

$$+ \frac{d}{dy}\left[\varkappa\, y\,(1-y)\,\left(u_{*1}\,\frac{du_o}{dy} + \frac{du_1}{dy}\right)\right]\cos(kz)$$

$$+ \frac{d}{dy}\left[\varkappa\, y\,(1-y)\,u_{*1}\,\frac{du_1}{dy}\right]\cos^2(kz) =$$

$$= -1 + [v_o \frac{du_o}{dy} + k^2 \varkappa y (1-y) u_1] \cos(kz)$$

$$+ 2 [k^2 \varkappa y (1-y) u_{*1} u_1 - u_1 \frac{dv_o}{dy}] \cos^2(kz) \qquad 3.69$$

Separating terms of order cos(kz), $\cos^1(kz)$ and $\cos^2(kz)$,

$$\frac{d}{dy}[\varkappa y (1-y) \frac{du_o}{dy}] + \frac{d}{dy}[\varkappa y(1-y) u_{*1} \frac{du_1}{dy}] = 1 \qquad 3.70$$

order : [1] [ε^2] [1]

$$\frac{d}{dy}[\varkappa y(1-y)(\frac{du_1}{dy} + u_{*1} \frac{du_o}{dy})] = v_o \frac{du_o}{dy} + k^2 y(1-y)u_1$$

[ε] [ε] [ε] 3.71

$$\frac{d}{dy}[\varkappa y(1-y)u_{*1} \frac{du_o}{dy}] = 2k^2 \varkappa y(1-y)u_{*1} - 2u_1 \frac{dv_o}{dy} \qquad 3.72$$

order : [ε^2] [ε^2] [ε^2]

On comparing the orders of magnitude of each term of the above equations as indicated, if $\varepsilon^2 << 1$ then Equation 3.72 can be ignored altogether, and the second term of Equation 3.70 also vanishes. Hence the latter yields the conventional log-law,

$$u_o(y) = \frac{1}{\varkappa} \ln(\frac{y}{y_{om}}) \qquad 3.73$$

and Equation 3.71 simplifies to

$$\frac{d}{dy}[\varkappa y (1-y) \frac{du_1}{dy}] - k^2 \varkappa y (1-y) u_1 = u_{*1} + \frac{v_o}{\varkappa y} \qquad 3.74$$

The boundary conditions for the above are

$$\text{(i)}\quad \text{at } y = y_o, \quad u_1(y_o) = -\frac{\varepsilon}{\varkappa} \ln y_{om} \; ; \qquad 3.75$$

$$\text{(ii)}\quad \text{at } y = 1, \quad \varkappa\, y(1-y) \frac{du_1}{dy} = 0 \qquad 3.76$$

From the above set of equations, if $v_o(y)$ is known then $u_1(y)$ can be uniquely determined. The determination of $v_o(y)$ is however dependent on the modelling of turbulent stress terms of Equations 3.60 and 3.61. The conceptual difficulties attendant upon such modelling necessitate additional assumptions such as eddy viscosity formulae for these terms [cf. McLean, 1981]. Since the order of magnitude of these terms is small, errors in the modelling of these stresses in terms of the mean flow field are, however, likely to be significant. Partly for this reason and partly as computational shortcut, it is proposed to assume the form of $v_o(y)$ as

$$v_o(y) = a_o\, y^m (1-y)^n \qquad 3.77$$

where $m > 1$, $n > 0$ satisfying the boundary conditions

$$\text{(i)}\quad \text{at } y = y_o\,, \; v_o(y) = \frac{dv_o}{dy} = 0 \qquad 3.78$$

$$\text{(ii)}\quad \text{at } y = 1\,, \quad v_o(y) = 0 \qquad 3.79$$

Suitable values of the exponents m and n may be assumed based on empirical data. To determine the coefficient a_o of Equation 3.77, a second boundary condition on $u_1(y)$ may be defined based on empirical data, eg.,

$$u_1(y) = C\, u_1(y_o) \qquad 3.80$$

where C is a constant of proportionality.

3.2.4 Limitations

The above analysis is an approximate one. It is easily seen that, if ε is not very small, then

(i) Equation 3.70 shows that $u_o(y)$ does not follow the log-law;

(ii) Equations 3.71 and 3.72 may not give identical solutions for $u_1(y)$.

It follows from (ii) that the simple form of $u(y,z)$, which has only one sinusoidally varying component of z, is not valid. From a practical point of view lateral bed level variations due to projection of ribbons above mean bed level will also affect the secondary flow. Moreover, the assumption that $\ln y_o$ varies sinusoidally with z may be quite erroneous in the general case. Taking account of these factors, refinements in the above analysis may be neither useful nor easy in the absence of adequate experimental data to verify all analytical premises.

In Chapter 5 the analytical model has been calibrated with experimental data of Muller and Studerus [1979] in order to estimate the bed shear stress variation due to sand ribbons. The redistributed shear stress as computed has been employed hence in hydraulic and sedimentological analysis of sand ribbons generated in experiments described in the following chapter.

CHAPTER 4

EXPERIMENTS

To test the hypotheses and seek answers to the queries outlined in the previous chapter, two sets of experiments were conducted, -- one set with immobile bed to test the analytical model for suction/injection, and the other set to examine the morphological characteristics and hydrodynamic implications of sand ribbons and ridges. The experiments were carried out in a glass-sided tilting flume 8.0 m long, 0.4 m wide and 0.6 m high and provided with a 0.2 m long approach section. A honeycomb structure was used at the inlet to provide rectilinear flow, and a 0.7 m x 0.4 m flat plate with 3-4 mm gravel glued on it was placed at bed level at the inlet to ensure developed flow in the main flume section. The discharge in the flume, supplied from an overhead tank, was regulated by inlet valves and measured by a calibrated V-notch in a tank downstream of the flume. The flume water level was adjusted by tailgate and tail wier plates, and the water and bed levels were measured by point gauge of least count 0.1 mm. All experiments were conducted at subcritical flow conditions.

4.1 Experiments with suction/injection

The main aim of these experiments was to find out the flow depths with uniformly distributed suction/injection in a region where the water surface profile is approximately parallel to the bed. For this purpose a fine wire mesh was spread on a coarser screen covering a 7.0 m long and 0.15 m high structural frame placed on the floor of the flume. The two ends of the frame were

sealed with flat plates spanning the flume width. An inverted filter, 15mm thick, with coarse sand to medium gravel was laid on the wire mesh. A sand bed with medium sand size D_{50} = 0.53 mm and average thickness of 150 mm was prepared on the filter. During experiments on OC flow with suction/injection, the sand layer was topped with two to three layers of fine gravel, 2-4 mm diameter, which allowed for higher critical shear and normal stresses on the bed than the sand surface. Figure 4.1 shows relevant details of the experimental set-up.

To apply suction/injection to the channel flow, water was abstracted/supplied at a constant rate through three 76 mm diameter inlets at the flume bottom. The withdrawal/supply rate was effected by an open tank, Tank A, and adjusted by a common valve for all three inlets (see Figure 4.1). In experiments with injection water was pumped to the tank at a constant rate, adjusted to maintain the desired supply to the flume. For runs with suction, water was sucked from the flume by operating an outlet valve from the tank and measuring the volumetric outflow rate. In both cases the net influent/effluent seepage rate was cross-checked with the difference in measured flume outflow rates with and without seepage.

The water supplied by Tank A produced a constant pressure reservoir in the bottom 150 mm height of the flume (excluding the volume occupied by the frame). Since there will be a streamwise head drop in the channel flow due to free surface gradient (dH/dX), the seepage pressure head across the sand bed may be expected to vary with X. As mentioned by Pennell et al [1972] for pipe flows, this may result in non-uniform suction/injection rate

in the X-direction. To ensure uniform V_w the sand bed thickness, H_b, was varied in order to provide uniform vertical seepage gradient, $\partial H_p / \partial Y$, in every run. Towards this end, first suction/injection was applied to a uniformly thick (~ 150 mm), saturated sand bed with almost standing water in the flume. Pressure tappings in the flume walls at 1100 mm X-intervals, 30 mm Y-intervals and penetrating about 30 mm into the sand layer, as shown in Figure 4.1, indicated that $\partial H_p / \partial Y$ was independent of X. The mean V_w, computed from the net influent/effluent seepage flow and the sand surface area (6300 x 400 mm^2), was found to follow Darcy's law,

$$V_w = - K \frac{\partial H_p}{\partial Y} \qquad 4.1a$$

$$K = 0.268 \pm 0.011 \text{ mm/s} \qquad 4.1b$$

for $-1.05 < \partial H_p / \partial Y < 1.20$ where H_p is the local pressure head, and K is hydraulic conductivity of the sand bed. For $\partial H_p / \partial Y > 1.20$ V_w was less than that predicted by Equation 4.1 a suggesting nonlinear effects (non-Darcy flow). For $\partial H_p / \partial Y < -1.05$ the bed surface become unstable with boiling of sand at sporadic locations. Hence, to maximize suction/injection rates within practical limits, the seepage pressure gradients used were $\partial H_p / \partial Y \simeq - 0.80$ corresponding to $V_w \simeq 0.215$ mm/s for injection, and $\partial H_p / \partial Y \simeq 1.30$ corresponding to $V_w = -0.345$ mm/s for suction.

With application of suction/injection there was slight contraction/expansion of the sand layer. The sand bed thickness, H_b(mm) was found to vary with the seepage pressure gradient approximately as,

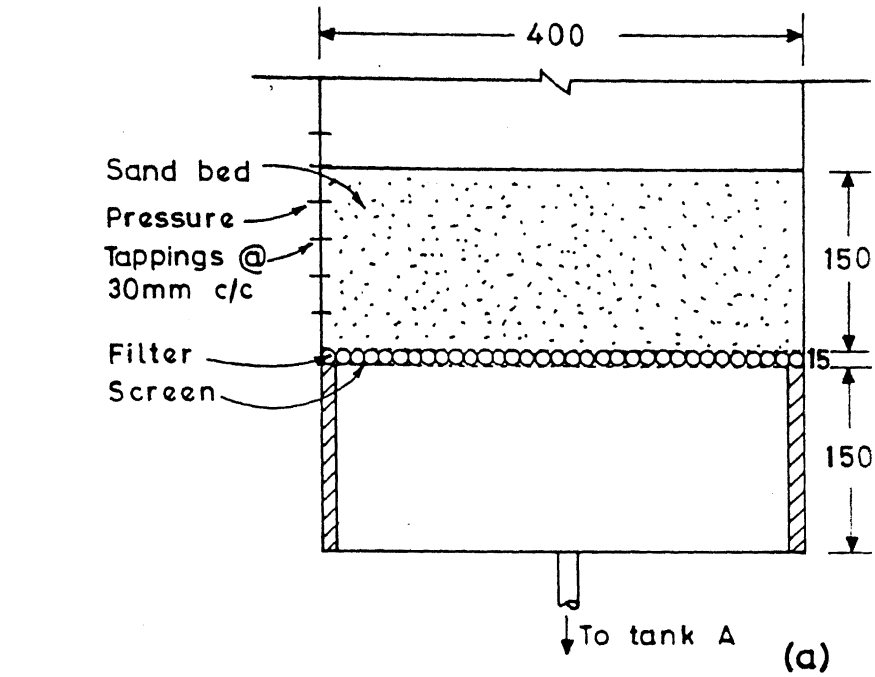

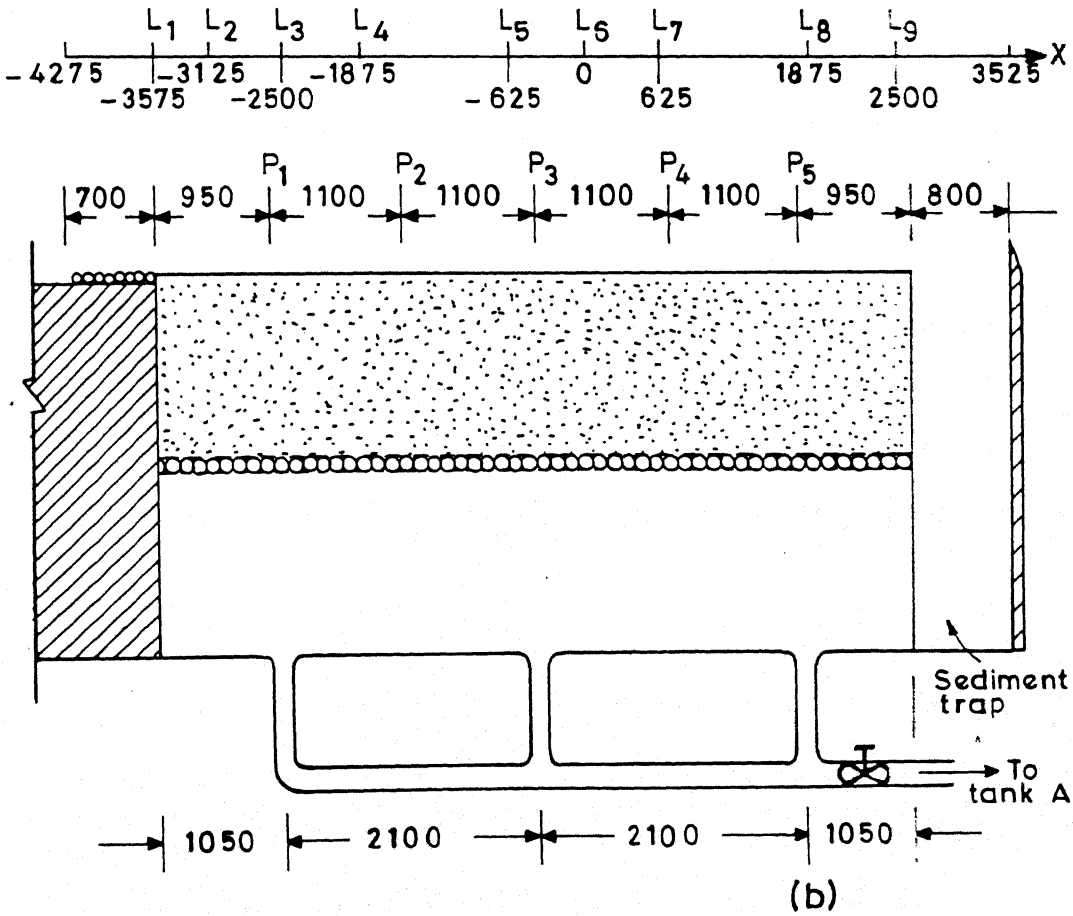

Figure 4.1 : Schematic of experimental set-up
(a) cross section;

$$H_b = H_{bi} - 1.8 \frac{\partial H_p}{\partial Y}\left(1 - 0.2 \frac{\partial H_p}{\partial Y}\right) \qquad 4.2$$

for $-1 \leq \partial H_p/\partial Y \leq 1.6$ where H_{bi} is the initial bed thickness. The variation of bed thickness at constant $\partial H_p/\partial Y$ was fairly uniform over the bed.

For each experimental run, assuming dH/dX of OC flow equal to $-S_o$, the sand bed thickness, $H_b(x)$, required to maintain constant $\partial H_p/\partial Y$ along X was computed for H_{bo} = 150 mm at X = 0,

$$H_b = H_{bo} - S_o X \frac{dY}{dH_p} \qquad 4.3$$

or,
$$H_b = \begin{cases} 150 + 1.25\, S_o X & : \text{injection} \quad 4.4a \\ 150 - 0.77\, S_o X & : \text{suction} \quad 4.4b \end{cases}$$

Before every run the sand bed thickness was adjusted to that of Equations 4.4. With quiescent flow in the flume, several cycles of injection and suction were applied, each cycle lasting about 15 to 60 minutes, in order to expel entrapped air from the sand bed. The process also produced slight compaction of the grain matrix. The sand permeability and bed expansion/contraction relations of Equations 4.1 and 4.2 are for this type of equilibrium bed condition.

On acheiving stable conditions, a few layers of 2-4 mm gravel were laid on the sand bed. The bed surface was smoothened with a wooden flat and bed levels measured at section L1 to L8 indicated in Figure 4.1. Flume discharge from the overhead tank was adjusted to the desired initial value, and suction/injection was applied. The tail gate was raised or lowered to vary the

flume water level. With every change in tail gate elevation the water surface profile, the seepage pressure gradient and the water level in Tank A took about 10 to 30 minutes to adjust to a mutually stable configuration. It was observed that while the water surface could have a rising, falling, or mixed profile, the profile was usually curved. When parallel to the bed near the middle of the flume the water surface had convex curvature (convex upwards) for injection and concave curvature for suction. In order to determine the self-preserving flow parameters in the region where $dH/dX = - S_o$, the location of optimum water level (the origin X=0 in Figure 4.1b) was chosen at 3575 mm from the point of commencement of suction/injection. Assuming the developing length of the flow with suction/injection to be less than 40H (vide Chapter 2), since H < 35 mm in all runs, the flow in the region - 2000 < X < 2000 mm could be assumed to be nearly self-similar.

In most runs, the water surface curvature was not sufficiently high as to determine the location of optimal flow depth precisely. Hence, a set of profiles with $dH/dX \simeq 0$ at X=0 were recorded by slightly adjusting the tailgate position, and the profile with dH/dX = 0 at X=0 was interpolated from these data. The outflow rate from the flume was also measured and its difference with the discharge at flume inlet, $\hat{Q}_i$, was checked with the inflow/outflow rate from/to Tank A. From the total sucked or injected flow rate, $\hat{Q}$, the suction/injection rate, V_w, and the flume discharge $\hat{Q}_o$ at X=0 were computed,

$$V_w = \frac{\hat{Q}}{6300 \times 400}$$

$$Q_o = Q_i + \frac{3575}{6300} Q$$

where Q is the discharge per unit width of flume in mm^2/s. Bed levels with suction/injection were measured at all sections L1 through L8 and verified against Equation 4.2. Finally, the discharge Q_o was run through the flume, and the normal flow depth, H_n, was determined. The water temperature was recorded during every experimental run.

All relevant experimental data are recorded in Tables 4.1 and 4.2. The table also gives the equivalent grain roughness, K_s, for the gravel bed computed for uniform flow Q_o from the log-low assuming $\kappa = 0.40$ and $B = 8.5$ (hydraulically rough bed).

4.2 Experiments on longitudinal bedforms

The experiments described here were conducted in order to determine the conditions of existence, morphological characteristics and hydrodynamic implications of ribbons or lineations on sand bed with equilibrium sediment transport. The experimental set-up is the same as that of the previous section, save that the sand bed composition was different and that, the bed was not overlaid with gravel or other material. Three different compositions of natural river sand, designated S1, S2 and S3, were used in these experiments. Whereas S1 was essentially fine to medium sand, S2 and S3 had increasingly higher amounts of coarse sand, with a small amount of very fine gravel being present in S3 sand. Thus both the median diameter and grading of the sands were

Table 4.1 : Observed Open Channel Flow Variables With Influent/Effluent Seepage

Run	Q_i mm^2/s	V_w mm/s	Q_o mm^2/s	S_o X1000	H_n mm	H_o mm	ν cp	K_s mm
R1	7097	-0.339	5885	4.26	21.4	20.65±0.2	0.93	6.02
R2	7928	-0.346	6691	3.80	23.3	22.05±0.2	0.93	5.25
R3	7160	-0.330	5980	2.82	24.1	22.9 ±0.3	0.92	5.73
R4	8782	-0.335	7584	2.36	28.7	26.95±0.3	0.92	5.27
R5	6491	-0.352	5233	1.76	24.9	23.1 ±0.5	0.91	4.79
R6	6342	-0.340	5127	1.22	27.2	25.0 ±0.5	0.91	4.62
R7	5845	0.208	6589	4.40	22.5	23.2 ±0.3	0.93	5.84
R8	6389	0.224	7190	3.72	24.5	25.15±0.3	0.93	5.37
R9	5453	0.216	6225	2.80	24.3	25.1 ±0.3	0.93	5.37
R10	5470	0.208	6214	2.34	25.4	26.5 ±0.4	0.91	4.90
R11	4653	0.219	5436	1.68	25.6	26.6 ±0.4	0.90	4.54
R12	4740	0.210	5491	1.20	28.7	30.1 ±0.6	0.90	4.95

Table 4.2 : Observed Water Surface Elevation (in mm) With Influent/Effluent Seepage : Optimum Elevation at X=0.

Stn.	L1	L2	L3	L4	L5	L6	L7	L8	L9
X(mm)	-3575	-3125	-2500	-1875	-625	0	625	1875	2500
Run									
R1	23.6	23.0	22.2	21.6	21.0	20.65	20.8	21.4	21.9
R2	25.2	24.2	23.2	22.6	22.1	22.05	22.1	22.6	23.7
R3	25.9	25.0	24.0	23.4	23.0	22.9	23.0	23.4	23.9
R4	30.4	28.8	27.9	27.4	27.0	26.95	27.0	27.3	27.7
R5	26.6	25.2	24.1	23.5	23.1	23.1	23.1	23.5	23.8
R6	30.1	27.6	25.8	25.3	25.0	25.0	25.0	25.3	25.6
R7	21.3	21.8	22.3	22.8	23.2	23.2	23.2	22.8	22.4
R8	23.3	23.9	24.5	24.8	25.1	25.15	25.1	24.9	24.5
R9	23.1	23.8	24.4	24.7	25.0	25.1	25.05	24.7	24.5
R10	24.5	25.2	26.0	26.2	26.5	26.5	26.5	26.25	26.0
R11	24.0	24.6	25.1	25.3	25.6	25.6	25.6	25.3	25.1
R12	26.4	27.4	28.1	28.5	28.7	28.7	28.7	28.5	28.4

increased from S1 to S2 to S3. The grain size distribution of S1, S2 and S3 sand samples based on sieve analysis are shown in Figure 4.2. For each sand type Kramer's uniformity coefficient, C_k, shown in Table 4.3 was computed from the formula [Garde and Raju, 1985] :

$$C_k = \frac{\sum_{0}^{50} D_i \, \Delta f_i}{\sum_{50}^{100} D_i \, \Delta f_i} \qquad 4.5$$

where Δf_i is the percentage interval on the ordinate of Figure 4.2 having representative (mean) size, D_i.

Table 4.3 Summary Data on Sand Bed Composition

Designation	Sand Type	Size range (mm)	D_{16} (mm)	D_{50} (mm)	D_{84} (mm)	D_{90} (mm)	C_k
S1	Fine to medium sand	0.09 to 0.70	0.15	0.28	0.445	0.50	0.48
S2	Fine to coarse sand	0.09 to 1.00	0.255	0.52	1.05	1.31	0.35
S3	Fine sand to very fine gravel	0.09 to 3.00	0.23	1.14	2.38	2.50	0.18

In each of the present experiments with suction/injection, the variation in sand bed thickness was partly carried out in the early part of the run by adding or removing sand at the downstream side while raising or lowering a plate embedded spanwise at the end of the sand bed. With flume discharge at about incipient

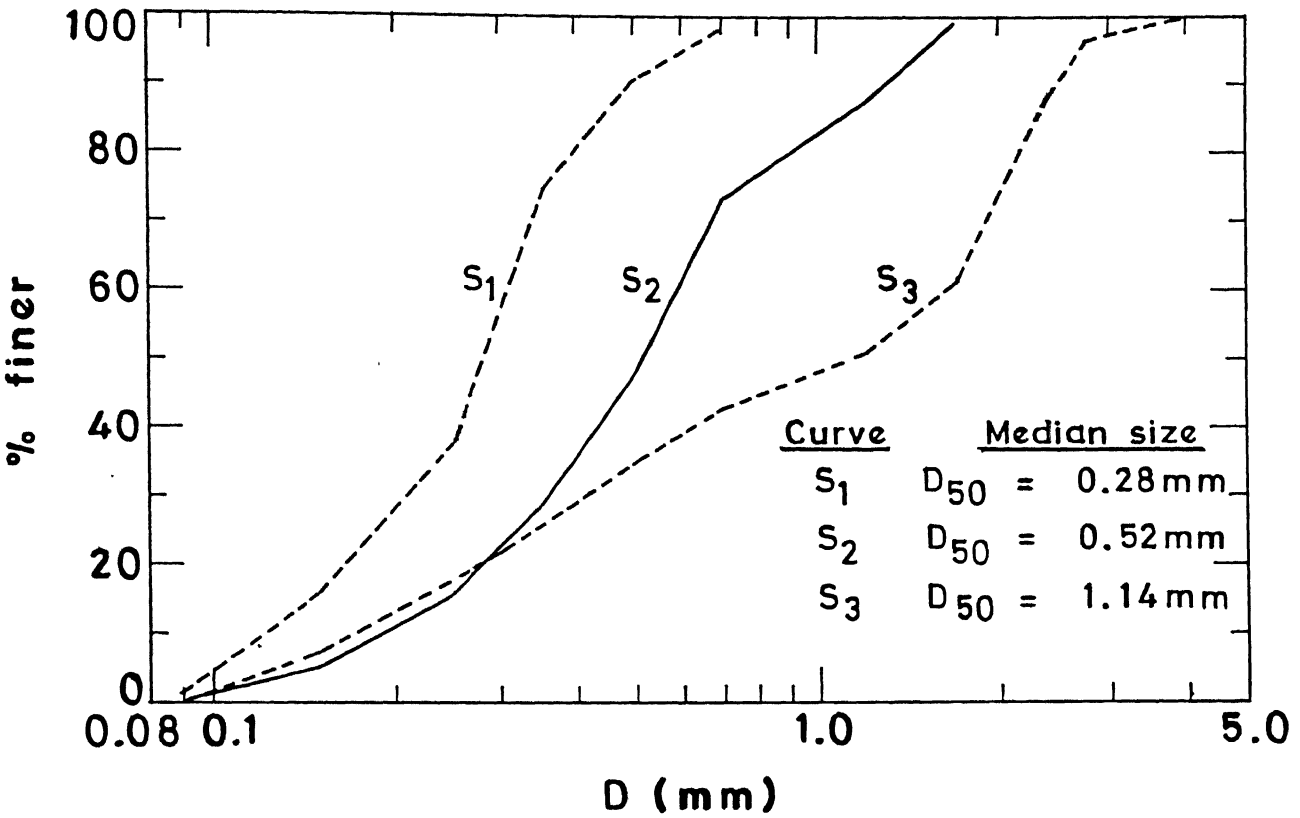

Figure 4.2 : Grain size distribution of sand bed.

Figure 4.3 : Photo of sand ribbons developed on the bed.

condition some amount of suspended material was initially washed away from the bed surface. Experiments with S1 sands were conducted at just above threshold conditions. It was observed that any significant sediment motion produced ripple bedforms, and neither suction nor injection promoted the development of any well developed lineations. In many experiments, however, fine streaky structures of very low relief were perceptible on the sand bed. These were in the form of longitudinal grooves, a few centimeters in length and of very small transverse and vertical dimensions (on the order of grain diameter). These striations often occurred in clusters on the bed, sometimes bifurcating or merging with neighbouring striations. Their visibility was slightly improved by adding a little chalk dust to the flow just before terminating the run so that the chalk powder tended to settle into the grooves. The only characteristic dimension of these striations that could be meaningfully measured was their transverse spacing, L_z.

The experiments with S2 and S3 sands were conducted with stable sediment transport rates. The bedload at the downstream sink was collected at every 15 minute intervals and fed gradually at the upstream end. During the first hour of the run the water and bed levels had to be adjusted slightly in order to maintain (nearly) uniform flow depth and seepage pressure gradient when suction/injection was applied.

In experiments with S2 and S3 sands, lineations or ribbons developed on the sand bed at modest bedload transport rates. The lineations, which commenced at or near the upstream end, ran down the entire flume length, being usually more well developed in the

downstream two-third length of the flume bed. The lineations appeared consistently uniform in size, spacing and surface texture after a few hours of run. They were characterized by both relief (ridge - groove combinations) and grain sorting (coarse and fine stripes). Figure 4.3 shows a typical photograph of sand ribbons developed on the flume bed. Though the applied suction/injection rates were less than those used in Section 4.1, V_w did have some perceptible influence on both sediment motion and bedform characteristics. In general, injection increased bedload while suction had the opposite effects. For S2 sand the longitudinal bedforms tended to disintegrate into primary ripples as described by Mantz (1978) at high bedload transport rates. Visually it was observed that moving bed grains mostly adhered to the sloping ridges rather than the valleys between ridges.

All experiments were terminated within 4 to 6 hours after stable flow, bedload and bedform conditions appeared to have been achieved. The flume water surface profile, water temperature and bed measurements were carried out in all runs. The latter included the lateral spacing between lineations (L_z) and the elevations of crests and troughs of the ridge-groove formations. The mean difference between the elevation of a crest and its two neighbouring valleys was designated as crest height, L_y. Sediment samples scraped from the surface of ridges and grooves respectively, and those sampled from the bedload collecting in the sink were oven-dried, and their sieve analysis was carried out. The experimental results are given in Tables 4.4, 4.5 and 4.6. For S1 sands the bedload was negligible. In other experiments the bedload (dry weight) transport rate, Q_s, is given in kg/m/hour.

Table 4.4 : Lineations on S1 sand bed

Run	Q_o (mm^2/s)	H_o (mm)	ν (cp)	S_o X1000	D_{16} (mm)	D_{50} (mm)	D_{84} (mm)	L_z (mm)
S101	5750	25.5	0.79	0.84	0.15	0.29	0.44	9.0
S102	9800	36.0	0.95	0.74	0.15	0.29	0.44	8.1
S103	10515	43.2	0.79	0.47	0.15	0.29	0.44	8.8
S104	10538	40.5	0.96	0.77	0.15	0.29	0.44	10.7
S105	11710	51.4	0.80	0.36	0.15	0.29	0.44	11.3
S106	11858	41.2	0.96	0.62	0.15	0.29	0.44	10.55
S107	12050	47.8	0.97	0.78	0.15	0.29	0.44	11.2

Table 4.5 : Hydraulic and sediment data for ribbons on S_2 sand bed.

Run	Q_o	H	S	ν	V_w	Q_s	L_z	L_y	Crest D_{50}	Trough D_{50}	Bedload D_{16}	Bedload D_{50}	Bedload D_{84}
	mm^2/s	mm	x1000	cp	mm/s	kg/m/h	mm	mm	mm	mm	mm	mm	mm
S201	8935	24.9	3.31	0.83	0.0	6.8	51.2	0.97	0.51	1.20	0.235	0.480	0.740
S202	9010	25.3	3.24	0.83	0.122	7.7	53.0	1.31	0.58	1.23	0.220	0.525	0.850
S203	8960	23.5	3.21	0.825	-0.210	6.1	46.8	1.04	0.49	1.22	0.250	0.470	0.700
S204	11355	28.6	3.05	0.85	0.0	7.3	55.3	1.09	0.51	1.02	0.175	0.465	0.790
S205	11225	29.1	3.12	0.84	0.150	8.5	59.6	1.26	0.54	1.13	0.230	0.500	0.815
S206	11240	28.7	3.00	0.84	-0.167	5.1	60.4	0.94	0.50	1.11	0.270	0.510	0.660
S207	13225	32.7	2.64	0.855	0.0	7.5	67.6	1.45	0.50	0.92	0.225	0.510	0.800
S208	13510	34.4	2.60	0.85	0.163	8.5	70.1	1.40	0.50	0.96	0.240	0.500	0.780
S209	13260	32.8	2.52	0.84	-0.154	6.1	63.7	1.26	0.46	1.05	0.250	0.490	0.740
S210	16380	40.0	2.20	0.92	0.0	7.1	85.5	1.29	0.50	1.20	0.190	0.480	0.810
S211	16400	40.2	2.33	0.92	0.142	8.4	82.5	1.58	0.51	1.26	0.250	0.465	0.850
S212	16325	39.6	2.25	0.92	-0.175	6.4	80.1	1.08	0.48	1.12	0.235	0.450	0.730
S213	20360	47.6	2.08	0.93	0.0	8.6	94.3	1.22	0.52	1.19	0.200	0.540	0.840
S214	20520	49.2	2.01	0.925	0.139	10.4	96.6	1.53	0.51	1.18	0.185	0.500	0.780
S215	20450	45.8	1.95	0.93	-0.182	7.0	91.1	1.20	0.55	1.10	0.240	0.530	0.780
S216	9415	25.2	3.10	0.95	0.0	7.1	51.2	0.90	0.55	0.97	0.225	0.465	0.680
S217	12950	34.9	2.68	0.95	0.0	7.4	71.4	1.28	0.48	1.07	0.255	0.510	0.750
S218	18760	46.3	1.65	0.94	0.0	5.9	93.4	1.10	0.49	0.86	0.260	0.510	0.770
S219	13090	31.9	2.85	0.85	0.0	12.8	---	---	---	---	0.225	0.575	0.970
S220	18660	36.5	2.42	0.86	0.0	13.6	---	---	---	---	0.245	0.560	0.880
S221	20940	39.9	2.19	0.92	0.0	11.4	---	---	---	---	0.230	0.540	0.900
S222	22570	45.1	1.97	0.93	0.0	12.2	---	---	---	---	0.260	0.545	0.810

Table 4.6 : Hydraulic and sediment data for ribbons on S3 sand bed.

Run	Q_o mm^2/s	H_o mm	S_o x1000	ν cp	V_w mm/s	Q_s kg/m/h	L_z mm	L_y mm	Crest D_{50} mm	Trough D_{50} mm	Trough D_{16} mm	Bedload D_{50} mm	Bedload D_{84} mm
S301	11240	30.6	4.10	0.90	0.0	14.8	63.0	1.74	0.81	1.27	0.23	0.600	2.30
S302	11185	31.3	4.08	0.895	0.144	16.1	62.4	1.98	0.80	1.40	0.235	0.645	2.40
S303	11220	29.4	4.02	0.895	-0.186	14.0	60.1	1.35	0.72	1.20	0.210	0.590	2.30
S304	14100	38.0	3.73	0.88	0.0	12.6	78.8	1.46	0.78	1.23	0.225	0.570	2.18
S305	14235	39.2	3.65	0.88	0.151	14.6	80.5	1.79	0.81	1.38	0.230	0.625	2.25
S306	13960	36.5	3.60	0.84	-0.206	12.0	73.6	1.38	0.86	1.26	0.230	0.560	2.15
S307	16635	38.8	3.82	0.855	0.0	15.7	79.6	1.72	0.89	1.31	0.245	0.610	2.35
S308	16610	39.3	3.76	0.85	0.140	17.9	83.7	1.85	0.87	1.53	0.230	0.680	2.55
S309	16620	38.1	3.82	0.85	-0.181	15.2	79.0	1.59	0.77	1.34	0.235	0.590	2.32
S310	19420	46.6	3.14	0.84	0.0	13.3	94.4	1.48	0.73	1.16	0.215	0.560	2.30
S311	19350	48.2	3.06	0.83	0.166	14.8	98.5	1.77	0.78	1.30	0.235	0.680	2.40
S312	19365	45.1	3.18	0.83	-0.170	12.7	91.3	1.30	0.77	1.26	0.220	0.630	2.35
S313	10170	25.5	5.47	0.92	0.0	15.9	53.6	1.68	0.79	1.30	0.220	0.590	2.37
S314	14325	33.2	4.80	0.91	0.0	16.2	69.5	1.81	0.88	1.42	0.235	0.660	2.55
S315	15850	40.5	3.95	0.915	0.0	13.6	79.3	1.54	0.83	1.33	0.215	0.650	2.30
S316	17215	36.4	4.92	0.910	0.0	17.1	65.5	1.63	0.86	1.47	0.240	0.715	2.25
S317	17840	48.0	3.06	0.910	0.0	12.7	94.0	1.50	0.81	1.22	0.200	0.630	2.40
S318	18060	39.8	4.03	0.910	0.0	15.6	83.1	1.72	0.80	1.30	0.205	0.655	2.20
S319	20490	51.3	3.03	0.900	0.0	18.0	98.7	1.65	0.84	1.45	0.220	0.660	2.55

CHAPTER 5

ANALYSIS OF RESULTS AND DISCUSSIONS

5.1 OC flow with suction/injection

The analysis of OC flow with suction/injection developed in Chapter 3 is semi-empirical in that it uses eddy viscosity formulations and assumed criteria for the apparent origin of turbulent velocity distribution, which need direct or indirect confirmation by experimental data. In the following sections the analytical results have been compared with experimental OC and TBL data, and significant aspects of the analytical model have been discussed in the context of wall flows, in general, and OC flows, in particular.

5.1.1 Free surface elevation

As described in Chapter 4 twelve sets of OC experiments were conducted on nominally rigid, hydraulically rough beds -- six sets with influent seepage (suction), and six sets with effluent seepage (injection). Each set consisted of an uniform subcritical flow (discharge = Q_o and flow depth = H_n) run, and another run with suction/injection for the same bed condition and same Q ($=Q_o$) and free surface slope ($S=S_o$) at a predetermined location (X=0). Determining the roughness scale, K_s, from an assumed log-law for the uniform flow experiment and holding it constant for the spatially varied flow, H(x) was computed from the model for $-2600 < X < 2600$. For the present experiments $|v_w| \ll 1$ and $(\emptyset_{fg})^2 \ll 1$ in most cases, and the mixing length (designated a = 2) and parabolic eddy viscosity (designated a = 1) models gave numerically close solutions.

Figure 5.1 shows plots of observed versus computed change in flow depth, ΔH ($=H_o-H_n$), at X = 0 due to suction/injection. The estimated error in measuring ΔH is indicated in the figure. It is seen from the figure that the analytical results for both a=1 and a=2 show fair to good agreement with experimental results within the limits of experimental error, though the mixing length model slightly overpredicts $|\Delta H|$ in the case of suction.

A comparison of the observed and computed water surface profiles (elevations with respect to H_o) is shown in Figures 5.2a and 5.2b for suction and injection respectively. The plotted points are the mean values from a set of measurements with slightly varying surface profiles, and the measurement error is expected to be small. The computed profiles are almost identical for a=1 and a=2; hence only one set of profiles is shown in the figure. The figure shows good agreement with experimental data for both suction and injection.

A comparison of the present model with one-dimensional OC analysis is in order. For the flow situation studied here the friction slope, S_f, used in OC hydraulics is easily determined. Setting dH/dX = 0 in Equations 2.36 and 2.39,

$$\frac{S_f}{S_o} = \begin{cases} 1 - 2\, C_m\, v_w\, u_{av}, & v_w > 0 \qquad 5.1a \\ 1 - C_e\, v_w\, u_{av}, & v_w < 0 \qquad 5.1b \end{cases}$$

With an assumed 1/7-th power law for u(y), $C_m \simeq 1.015$ and $C_e \simeq 1.045$. C_m and C_e which depend on the shape factor of u(y), could change slightly depending on the exact distribution of u(y), but the above values are adequate for comparison with the present analysis as $|v_w|$ is numerically small. Since the specific

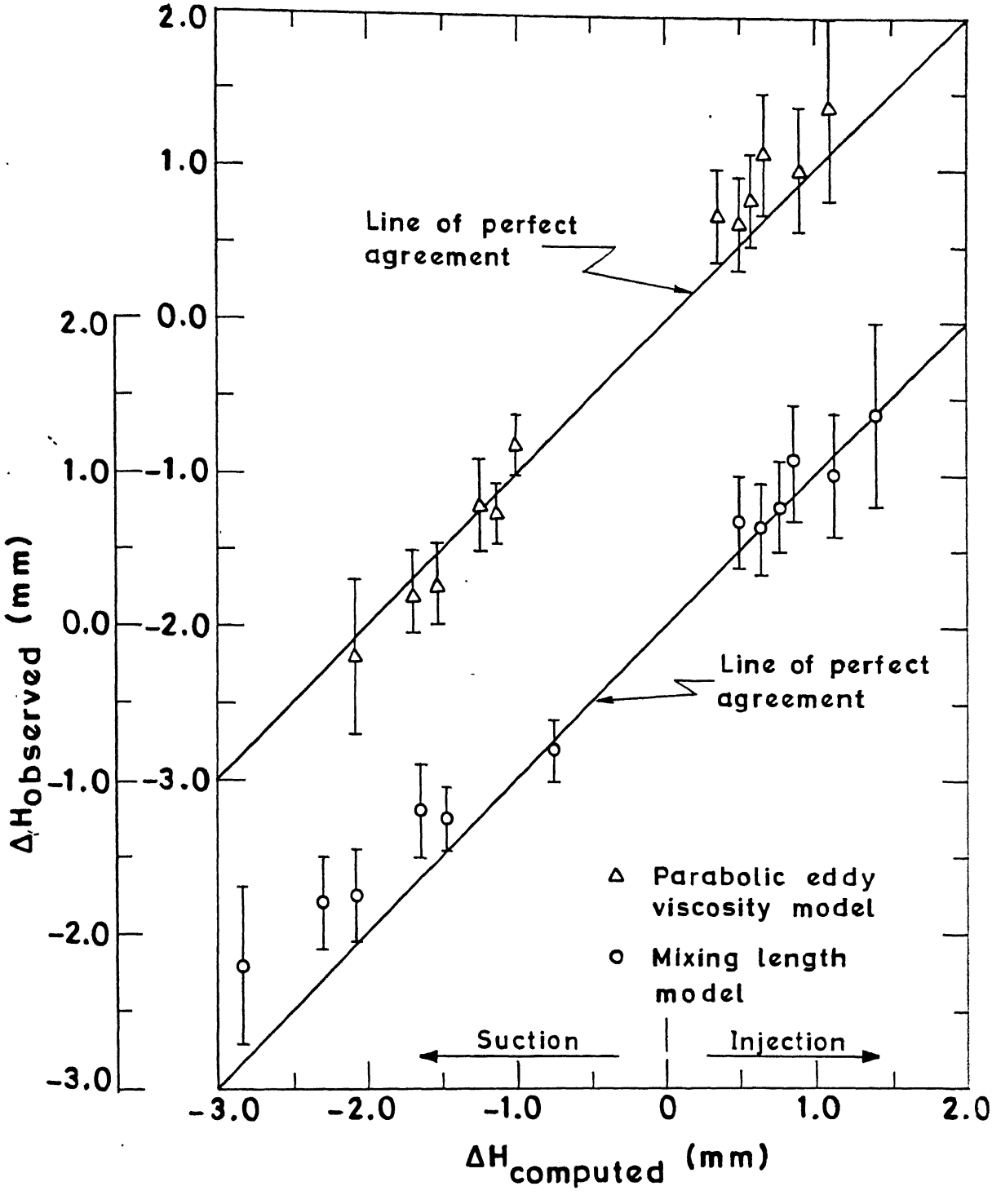

Figure 5.1 : Comparison of observed and computed change in flow depth due to suction/injection.

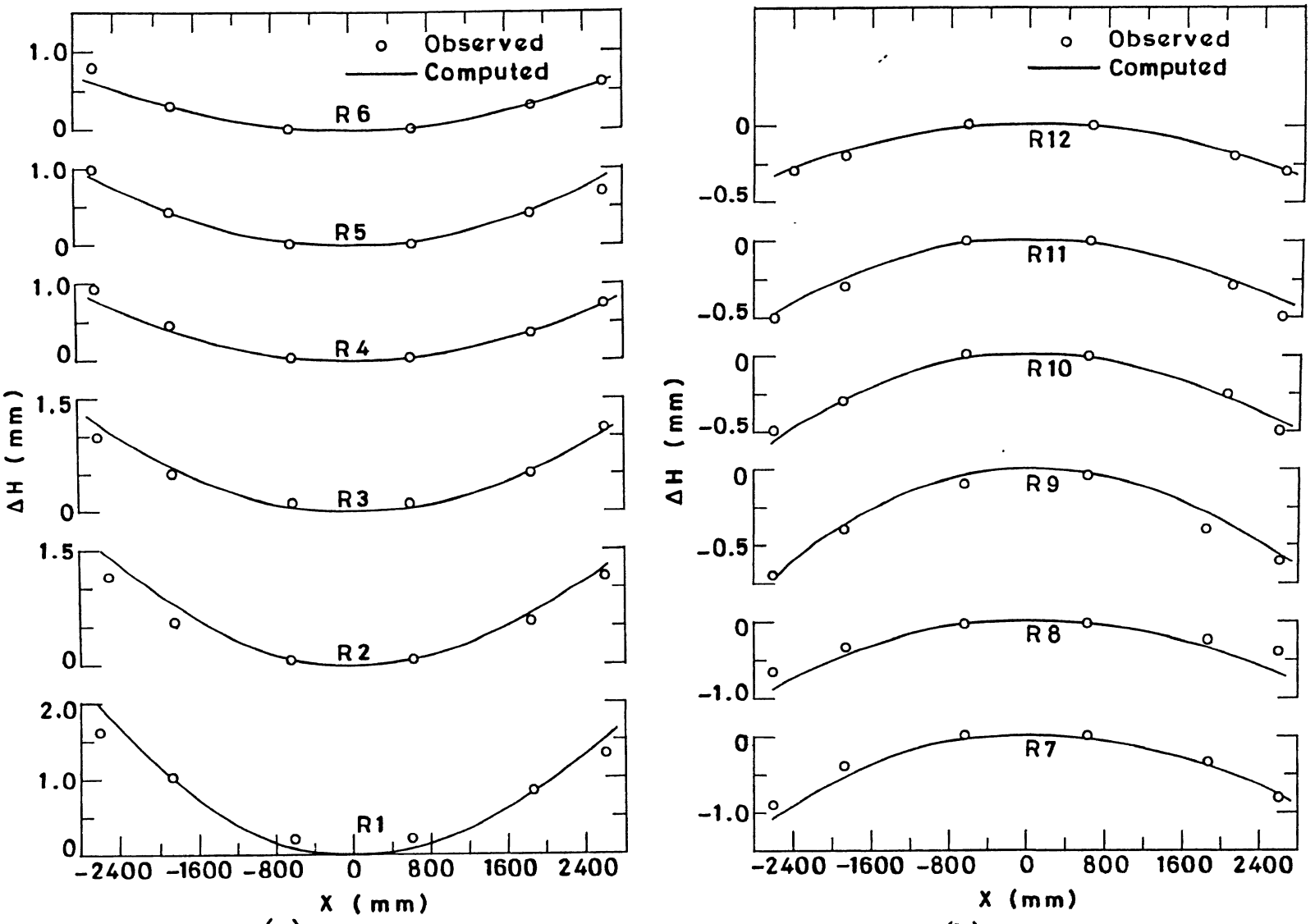

Figure 5.2 : Comparison of observed and computed water surface profiles : (a) suction ; (b) injection.

Table 5.1 : Computed parameters for self-similar smooth bed OC flow with suction/injection : parabolic eddy viscosity model (a=1).

R*	v_w	y_δ x1000	y_i x1000	n	Tao+ (S_F/S_o)	Alpha x1000	Beta x1000	H_δ/H_n	u_{av}
300.	-.0400	.15412	22.450	-.05456	3.416	-1.340	-.611	.727	29.84
300.	-.0350	.16744	23.914	-.05109	2.986	-1.250	-.632	.755	27.99
300.	-.0300	.18305	25.517	-.04697	2.599	-1.144	-.640	.784	26.23
300.	-.0200	.22318	29.192	-.03629	1.939	-.871	-.597	.848	22.95
300.	-.0100	.27964	33.603	-.02124	1.417	-.499	-.416	.918	20.03
300.	.0000	.36934	38.783	.00000	1.000	.000	.000	1.000	17.26
300.	.0100	.50550	45.380	.03008	.704	.662	.780	1.083	15.11
300.	.0150	.61681	49.054	.04945	.584	1.071	1.356	1.132	14.01
300.	.0200	.72632	53.124	.07266	.477	1.530	2.071	1.179	13.08
300.	.0250	.88916	57.590	.09991	.389	2.060	2.957	1.231	12.14
300.	.0300	1.08799	62.292	.13152	.317	2.666	4.024	1.287	11.25
1000.	-.0350	.04939	6.724	-.04769	3.364	-1.036	-.475	.738	33.78
1000.	-.0300	.05421	7.224	-.04412	2.889	-.953	-.490	.770	31.48
1000.	-.0250	.05995	7.780	-.03980	2.465	-.853	-.493	.804	29.30
1000.	-.0200	.06685	8.399	-.03458	2.089	-.734	-.475	.839	27.24
1000.	-.0100	.08504	9.853	-.02061	1.469	-.426	-.345	.917	23.49
1000.	.0000	.11080	11.635	.00000	1.000	.000	.000	1.000	20.27
1000.	.0050	.13238	12.771	.01386	.810	.266	.294	1.047	18.78
1000.	.0100	.16010	14.015	.03091	.649	.575	.696	1.096	17.39
1000.	.0150	.19559	15.445	.05207	.513	.931	1.227	1.147	16.12
1000.	.0200	.24247	17.087	.07864	.397	1.338	1.909	1.200	14.95
1000.	.0250	.30731	18.980	.11200	.302	1.808	2.763	1.256	13.83
10000.	-.0300	.00494	.643	-.03949	3.600	-.691	-.300	.732	43.39
10000.	-.0250	.00551	.702	-.03608	2.993	-.626	-.313	.770	39.94
10000.	-.0200	.00620	.770	-.03180	2.465	-.545	-.314	.811	36.71
10000.	-.0150	.00705	.847	-.02643	2.008	-.445	-.296	.855	33.70
10000.	-.0100	.00810	.937	-.01964	1.615	-.324	-.247	.901	30.90
10000.	-.0050	.00935	1.042	-.01102	1.281	-.176	-.154	.949	28.36
10000.	.0000	.01108	1.163	.00000	1.000	.000	.000	1.000	26.03
10000.	.0050	.01350	1.314	.01431	.759	.210	.238	1.055	23.85
10000.	.0100	.01693	1.497	.03330	.560	.457	.585	1.111	21.89
10000.	.0150	.02234	1.733	.05936	.396	.747	1.069	1.171	20.08
10000.	.0175	.02614	1.880	.07643	.324	.909	1.371	1.202	19.25

Table 5.2 : Computed parameters for self-similar smooth bed OC flow with suction/injection : mixing length model (a=2).

R*	v_w	y_o x1000	y_i x1000	n	Tao+ (S_f/S_o)	Alpha x1000	Beta x1000	H_b/H_n	u_{av}
300.	-.0175	.24598	27.977	-.02205	2.081	-.711	-.547	.814	24.61
300.	-.0150	.26499	29.589	-.01891	1.850	-.646	-.513	.842	23.22
300.	-.0100	.30168	32.734	-.01262	1.490	-.478	-.408	.896	20.90
300.	-.0050	.33564	35.775	-.00632	1.225	-.262	-.241	.946	19.05
300.	.0000	.36934	38.783	.00000	1.000	.000	.000	1.000	17.26
300.	.0050	.39214	41.562	.00633	.864	.308	.337	1.037	16.26
300.	.0100	.41405	44.321	.01266	.738	.659	.802	1.080	15.18
300.	.0150	.43124	46.993	.01900	.634	1.052	1.445	1.120	14.25
300.	.0200	.44367	49.584	.02535	.549	1.487	2.353	1.159	13.45
300.	.0250	.45144	52.099	.03171	.477	1.962	3.684	1.196	12.74
300.	.0300	.45462	54.541	.03806	.417	2.477	5.770	1.231	12.11
1000.	-.0150	.07744	8.476	-.01873	2.011	-.536	-.414	.826	27.96
1000.	-.0125	.08403	9.030	-.01561	1.760	-.476	-.382	.858	26.24
1000.	-.0100	.09048	9.577	-.01248	1.552	-.404	-.338	.889	24.73
1000.	-.0050	.10259	10.647	-.00624	1.232	-.225	-.205	.948	22.22
1000.	.0000	.11080	11.635	.00000	1.000	.000	.000	1.000	20.27
1000.	.0025	.11833	12.193	.00312	.903	.129	.136	1.029	19.35
1000.	.0050	.12271	12.692	.00624	.820	.269	.300	1.054	18.56
1000.	.0100	.13004	13.667	.01248	.683	.582	.734	1.103	17.20
1000.	.0150	.13536	14.611	.01871	.574	.935	1.369	1.150	16.04
1000.	.0200	.13864	15.524	.02495	.486	1.330	2.334	1.194	15.04
1000.	.0250	.13990	16.408	.03117	.414	1.763	3.910	1.237	14.18
10000.	-.0125	.00750	.823	-.01560	2.105	-.345	-.263	.818	36.22
10000.	-.0100	.00830	.892	-.01248	1.777	-.298	-.239	.858	33.51
10000.	-.0075	.00907	.962	-.00936	1.518	-.240	-.202	.896	31.20
10000.	-.0050	.00982	1.030	-.00624	1.309	-.171	-.152	.932	29.21
10000.	.0000	.01108	1.163	.00000	1.000	.000	.000	1.000	26.03
10000.	.0025	.01184	1.233	.00312	.877	.102	.109	1.035	24.60
10000.	.0050	.01240	1.300	.00624	.776	.214	.246	1.067	23.38
10000.	.0100	.01334	1.430	.01247	.616	.469	.644	1.129	21.31
10000.	.0150	.01398	1.558	.01870	.496	.765	1.311	1.188	19.60
10000.	.0175	.01419	1.621	.02181	.446	.928	1.829	1.217	18.85
10000.	.0200	.01432	1.683	.02493	.403	1.101	2.564	1.244	18.17

Table 5.3 : Computed parameters for self-similar OC flow over hydraulically rough bed with suction/injection : $\tilde{k}_{so}$ = 100, a = 1.

R*	v_w	y_o x1000	n	Tao+ (S_f/S_o)	Alpha x1000	Beta x1000	H_o/H_n	u_{av}
300.	.0400	11.124422	.14434	.438	8.006	5.796	1.109	6.90
300.	.0300	11.124422	.09806	.546	5.242	4.088	1.079	7.34
300.	.0200	11.124422	.05927	.674	3.038	2.564	1.049	7.80
300.	.0100	11.124422	.02697	.821	1.316	1.207	1.019	8.29
300.	.0000	11.124422	.00000	1.000	.000	.000	1.000	8.77
300.	-.0200	11.124422	-.04177	1.391	-1.688	-2.022	.932	9.89
300.	-.0400	11.124422	-.07183	1.890	-2.498	-3.606	.879	11.09
300.	-.0500	11.124422	-.08368	2.181	-2.687	-4.263	.854	11.73
300.	-.0600	11.124422	-.09386	2.500	-2.778	-4.843	.830	12.39
300.	-.0700	11.124422	-.10263	2.849	-2.796	-5.355	.807	13.07
300.	-.0800	11.124422	-.11022	3.230	-2.762	-5.807	.785	13.78
10000.	.0250	.333733	.11144	.312	2.771	1.818	1.149	13.75
10000.	.0200	.333733	.07665	.423	1.950	1.388	1.118	14.41
10000.	.0150	.333733	.05062	.546	1.283	.992	1.088	15.12
10000.	.0100	.333733	.03020	.682	.749	.630	1.057	15.87
10000.	.0050	.333733	.01367	.833	.327	.300	1.028	16.67
10000.	.0000	.333733	.00000	1.000	.000	.000	1.000	17.51
10000.	-.0050	.333733	-.01146	1.184	-.249	-.272	.970	18.40
10000.	-.0100	.333733	-.02119	1.387	-.433	-.517	.943	19.33
10000.	-.0200	.333733	-.03666	1.854	-.658	-.938	.891	21.32
10000.	-.0300	.333733	-.04824	2.410	-.750	-1.278	.842	23.47
10000.	-.0350	.333733	-.05293	2.724	-.765	-1.423	.819	24.60
10000.	-.0400	.333733	-.05704	3.064	-.765	-1.553	.797	25.76
1000000.	.0150	.003337	.06884	.297	.987	.640	1.140	23.45
1000000.	.0125	.003337	.04971	.395	.741	.517	1.118	24.19
1000000.	.0100	.003337	.03538	.499	.533	.400	1.095	25.03
1000000.	.0050	.003337	.01462	.731	.215	.186	1.047	26.92
1000000.	.0000	.003337	.00000	1.000	.000	.000	1.000	29.03
1000000.	-.0050	.003337	-.01091	1.313	-.138	-.160	.954	31.34
1000000.	-.0100	.003337	-.01930	1.677	-.221	-.295	.910	33.84
1000000.	-.0150	.003337	-.02590	2.096	-.265	-.411	.868	36.52
1000000.	-.0200	.003337	-.03115	2.575	-.284	-.508	.829	39.37
1000000.	-.0250	.003337	-.03538	3.119	-.286	-.590	.792	42.38

Table 5.4 : Computed parameters for self-similar OC flow over hydraulically rough bed with suction/injection : $\hat{k}_{so}$ = 1000, a = 1.

R*	v_w	y_o x1000	n	Tao+ (S_f/S_o)	Alpha x1000	Beta x1000	H_d/H_n	u_{av}
10000.	.0400	3.337327	.17817	.299	7.038	4.578	1.162	8.74
10000.	.0350	3.337327	.14284	.360	5.649	3.854	1.140	9.08
10000.	.0300	3.337327	.11258	.429	4.435	3.180	1.119	9.43
10000.	.0200	3.337327	.06437	.588	2.469	1.967	1.076	10.17
10000.	.0100	3.337327	.02807	.777	1.026	.914	1.035	10.95
10000.	.0000	3.337327	.00000	1.000	.000	.000	1.000	11.76
10000.	-.0100	3.337327	-.02217	1.251	-.701	-.790	.956	12.66
10000.	-.0200	3.337327	-.03995	1.544	-1.156	-1.470	.920	13.60
10000.	-.0300	3.337327	-.05437	1.878	-1.429	-2.055	.885	14.60
10000.	-.0400	3.337327	-.06617	2.257	-1.573	-2.557	.851	15.65
10000.	-.0500	3.337327	-.07589	2.682	-1.625	-2.986	.820	16.74
10000.	-.0600	3.337327	-.08395	3.157	-1.617	-3.354	.791	17.89
1000000.	.0175	.033373	.07497	.340	1.385	.928	1.134	18.86
1000000.	.0150	.033373	.05795	.418	1.091	.774	1.115	19.39
1000000.	.0100	.033373	.03257	.588	.612	.486	1.077	20.57
1000000.	.0050	.033373	.01413	.781	.257	.229	1.038	21.86
1000000.	.0000	.033373	.00000	1.000	.000	.000	1.000	23.27
1000000.	-.0050	.033373	-.01118	1.248	-.180	-.202	.963	24.78
1000000.	-.0100	.033373	-.02022	1.528	-.300	-.379	.927	26.39
1000000.	-.0150	.033373	-.02761	1.843	-.376	-.534	.892	28.09
1000000.	-.0200	.033373	-.03373	2.196	-.419	-.669	.860	29.89
1000000.	-.0250	.033373	-.03883	2.589	-.438	-.787	.829	31.77
1000000.	-.0300	.033373	-.04310	3.025	-.442	-.889	.799	33.74
1000000.	-.0350	.033373	-.04671	3.506	-.434	-.978	.771	35.79

discharge is roughly proportional to $H^{1.5}S^{0.5}$, Equations 5.1 give

$$\frac{H_o}{H_n} = \begin{cases} (1 - 2.03\ v_w u_{av})^{-1/3} & , v_w > 0 \quad 5.2a \\ (1 - 1.05\ v_w\ u_{av})^{-1/3} & , v_w < 0 \quad 5.2b \end{cases}$$

Equation 5.2a agrees fairly with both experimental and analytical results, but Equation 5.2b systematically underpredicts $|\Delta H|$.

The comparison between Equations 5.2 and the present theory can be more extensively made with reference to Tables 5.1, 5.2, 5.3 and 5.4 which give the flow parameters computed from the present model. Tables 5.1 and 5.2 give the computed parameters for smooth bed flow with a=1 and a=2 respectively, while Tables 5.3 and 5.4 are for hydraulically rough bed with $\tilde{k}_{so}$ = 100 and 1000 respectively, where $\tilde{k}_{so} = K_s \sqrt{a_g H_o S_o}/\nu$ and with a=1 . Between Tables 5.1 and 5.2 the computed parameters are seen to diverge with increase in $|v_w|$. This difference may be due to approximations in the analysis for a=2 wherein terms of order $(\phi_{fg})^2$, $(\phi_{fg})^3$, etc. where ignored. As evident from the magnitude of τ_w in Table 5.1, $(\phi_{fg})^2$ may became significant even at $|v_w|$ = 0.005 since $|\tau_w - 1|$ is not negligible. Hence in the rest of this chapter attention will mainly be focussed on the parabolic eddy viscosity model.

Comparison of Equations 5.2 with τ^+_w or S_f/S_o given in the above tables shows that the momentum equation generally gives comparable results for both suction/injection, whereas the energy equation yields lower values of $|S_f/S_o - 1|$ in both cases. It is therefore suggested that the application of energy equation (with the assumption of constant energy per unit mass) to OC flow with suction/injection may be incorrect, and the momentum equation is

recommended for both suction and injection when one dimensional analysis is used. This agrees with the recommendation by some earlier researchers [cf. El-Khashab and Smith, 1976]. It may be noted here that the one-dimensional analysis does not give any ready estimate of d^2H/dX^2 and dS_f/dX near X=0. Conventional one-dimensional analysis, wherein dS_f/dX is assumed to be zero, will indicate for both suction and injection that d^2H/dX^2 is negative for subcritical flows and positive for supercritical flows if $C_e = C_m = 1$, whereas the present analysis indicates negative curvature for injection and positive curvature for suction. The experimental results support the present model.

5.1.2 Shear stress and mean velocity distributions

The present analysis indicates that the velocity profile of u(y) is fuller for suction and more curved for injection. However, in the major part of the flow u(y) is higher for suction and lower for injection than the corresponding log-law velocity for R_*. These results qualitatively agree with the sample plots of u(y) with suction and injection given by Brink and Oldenziel [1974]. However, as mentioned in Chapter 2, their data are not adequate for comparison with the present results.

In order to elicit further empirical confirmation, computed values of $\tilde{U}(\tilde{y})$ have been normalized with U_* and plotted against $\tilde{y}$, where $\tilde{y} = yU_*/\nu$, in Figures 5.3a and 5.3b for two illustrative values of the parameters R_*, $R_* = 300$ and 10000 respectively, with hydraulically smooth bed conditions. The figures show that $\tilde{u}(\tilde{y})$ systematically deviates from the log-law with injection and suction. The deviation is positive for injection and negative

for suction, and in both cases increases with increase in $\tilde{y}$. These trends are qualitatively supported by the data of Maclean [1991] for flume experiments with abstraction through a perforated bottom. However, direct comparison with Maclean's results are not possible for the following reasons :

(i) Maclean's data are for $v_w/u_{av} > 0.04$, ie, for relatively high values of $|v_w|$, for which the present analytical results do not hold.

(ii) The length of the porous zone in Maclean's experiments was probably inadequate for full development of the inner boundary layer. In fact S and S_o were probably very different at the measuring station [cf. Maclean and Willetts, 1986].

(iii) U_* was determined by Maclean from an assumed relation between the spatially varied and uniform flow velocities at a reference height.

In the absence of adequate OC data, Stevenson's (or Dorrance and Dore's) velocity distributions for TBL flow with suction/injection have been compared with the present results in Figures 5.3a and 5.3b. Though the accuracy of Stevenson's equation is not accepted by all researchers [eg, Kays, 1972; Schetz and Nerney, 1977], it has been advocated by many others [eg, Schlichting] as it shows reasonable agreements with empirical data. As evident from Figures 5.3 $\tilde{u}(\tilde{y})$ for TBL flow deviates significantly from the log-law in the same manner as for OC flow. However the divergence from log-law is much more in the case of TBL flow. It may be pointed out here that Figures 5.3a and 5.3b

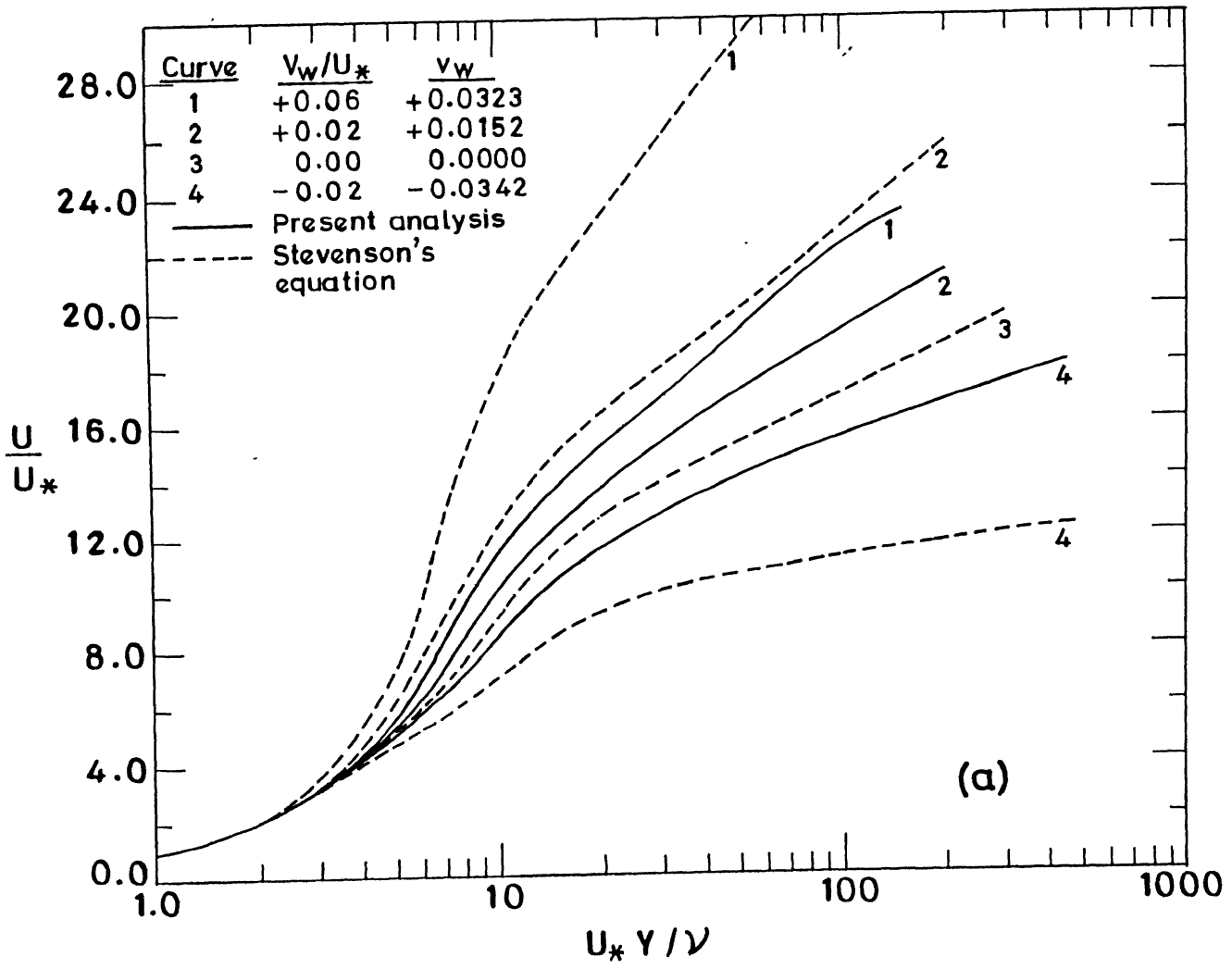

Figure 5.3 : Mean velocity distribution scaled with wall variables and comparison with TBL data (a) $R_* = 300$

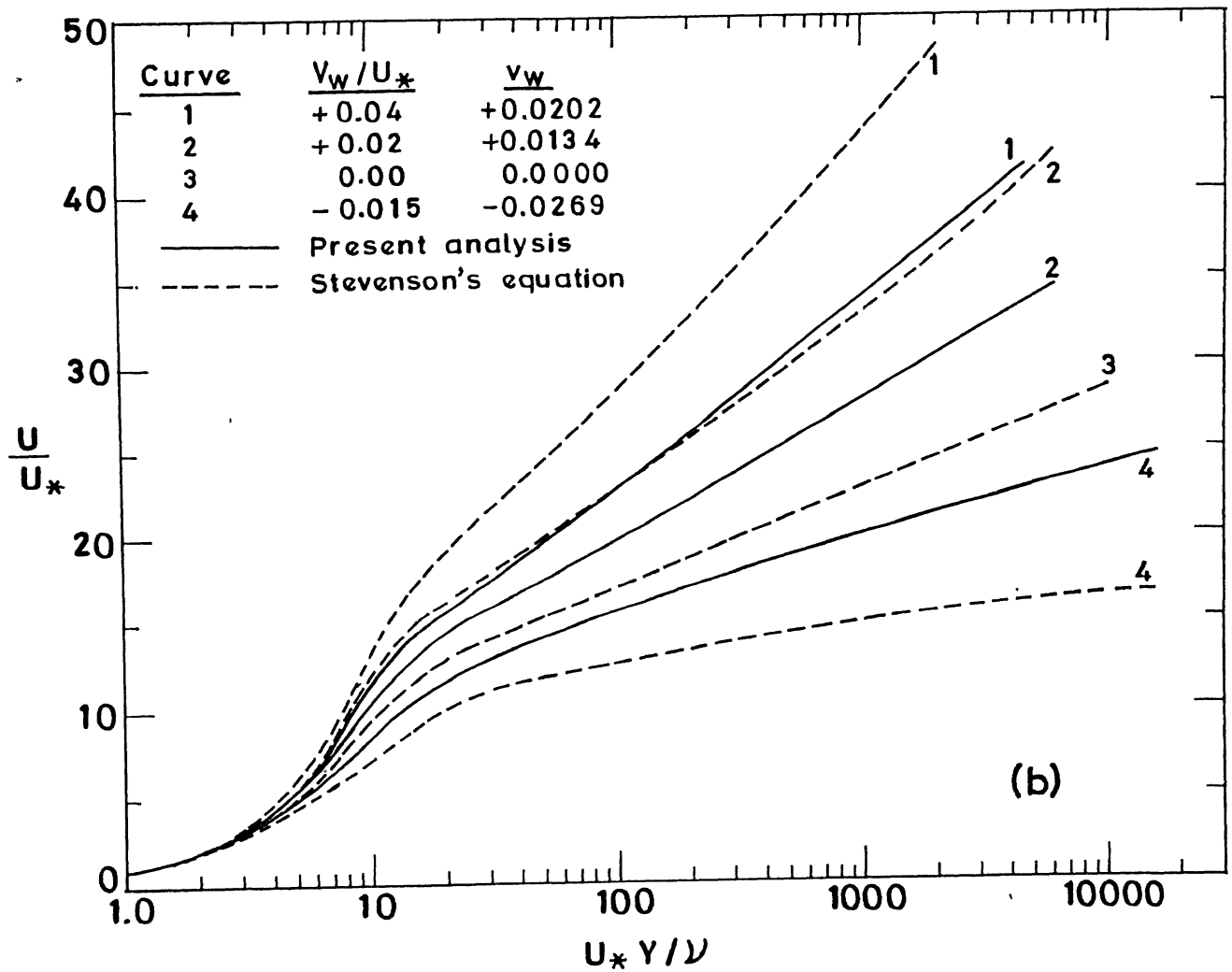

Figure 5.3 : Mean velocity distribution scaled with wall variables and comparison with TBL data (b) $R_* = 10,000$.

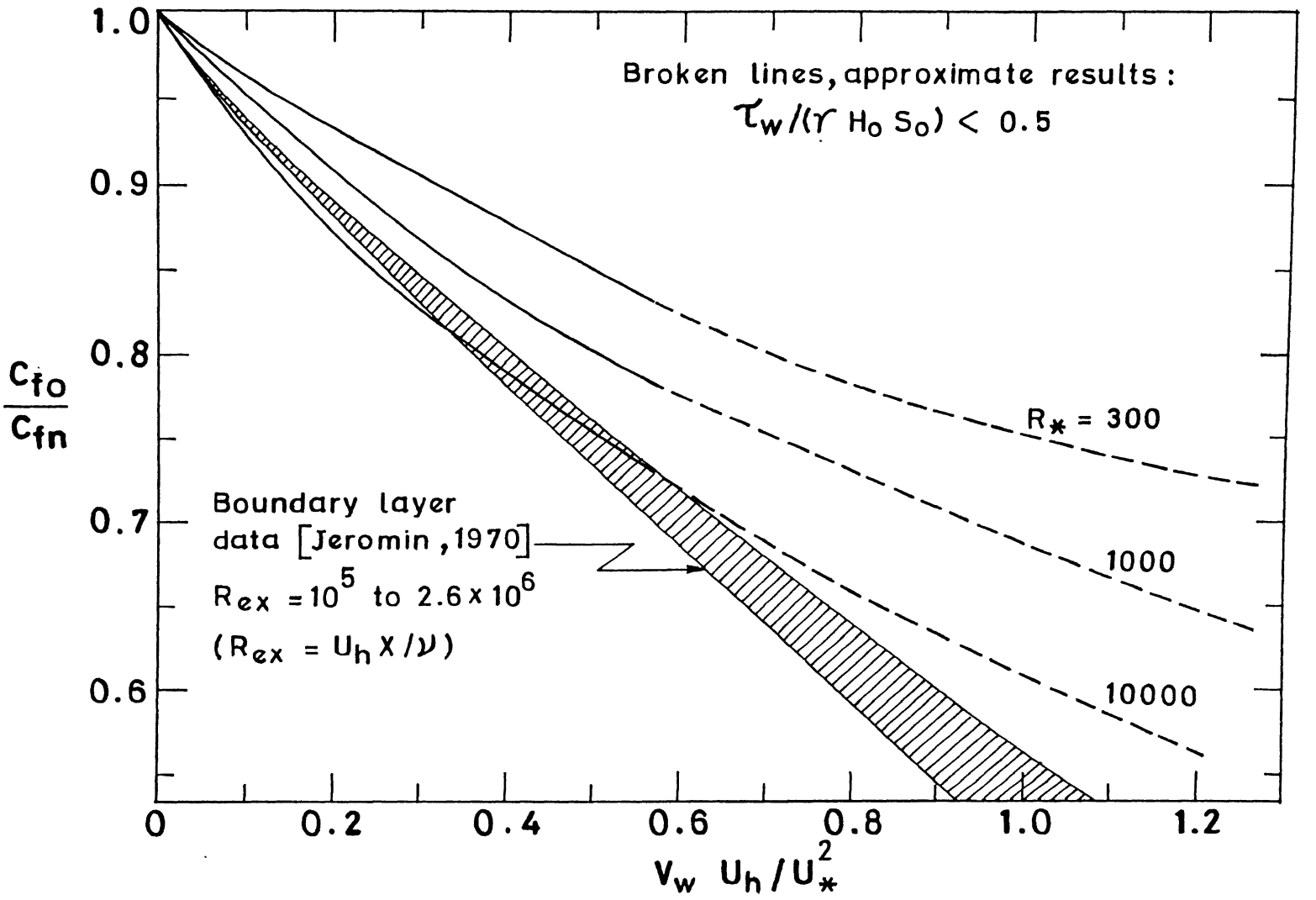

Figure 5.4 : Change in wall shear stress due to injection and comparison with TBL data.

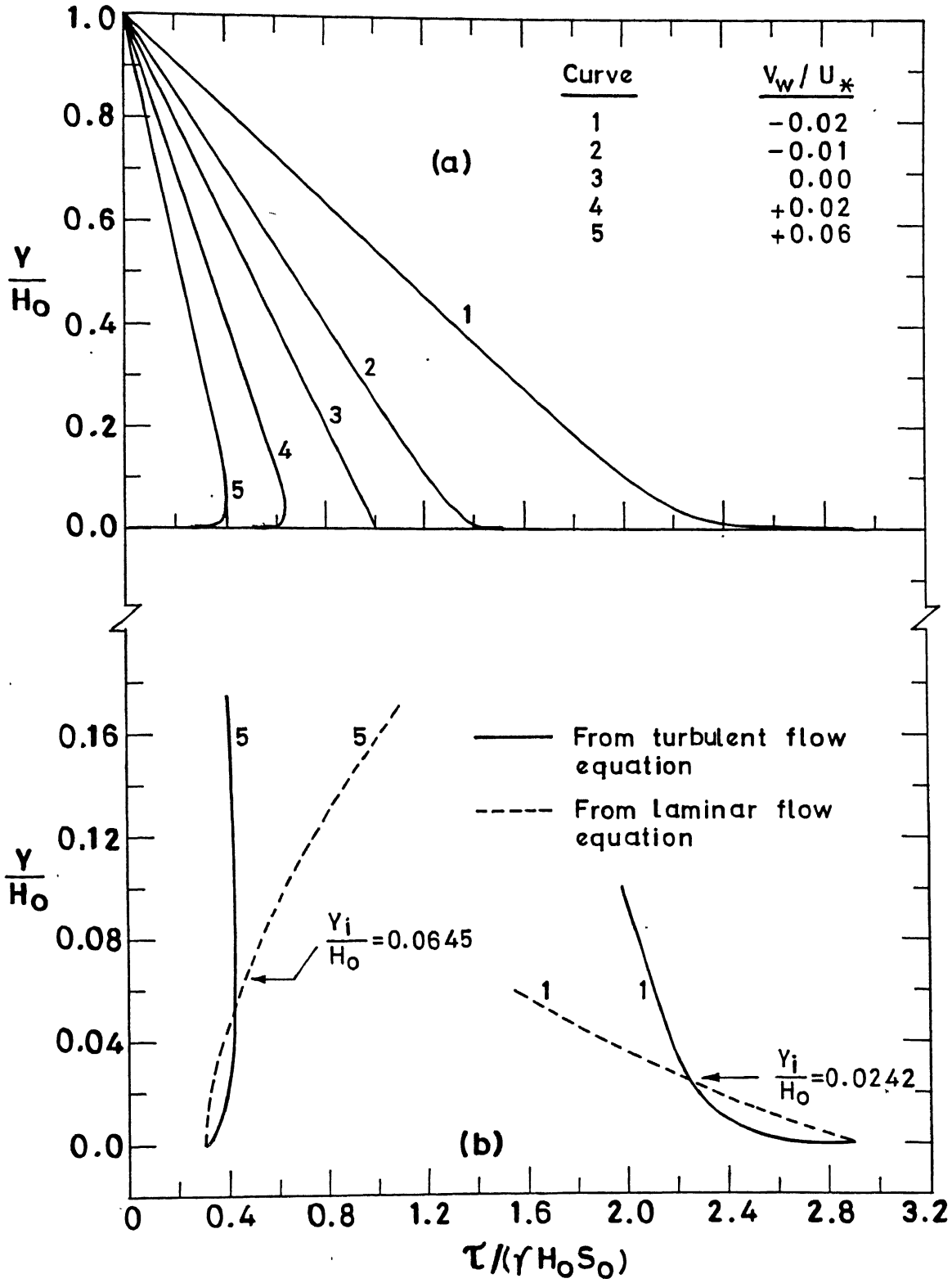

Figure 5.5 : Shear stress distribution over depth.

This result is also true for other values of R_* and v_w, indicating that the assumption of identical bed shear stress for the laminar and turbulent velocity distributions used in the present analysis is almost equivalent to assuming equal stresses at the interface.

It may be mentioned that the properties (deviations from uniform flow, trends, etc.) of the flow parameters noted above are true also for rough turbulent flows save that :

(i) the deviation from the uniform flow case decreases with increase in K_s/H_o for constant R_* and v_w; and

(ii) the apparent origin of the velocity, y_o, and y_i remain invariant for fully rough bed flows ($y_i=y_o$) if $K_s U_*/\nu > 70$, unless K_s/H_o changes.

On the basis of the comparisons in this and the previous section, it may be concluded that the premises and results of the present analysis are reasonably correct.

5.1.3 Physical significance for turbulent wall flows

The results cited and discussed in the previous section indicate that the effect of suction/injection on different types of wall-bounded flows should be, at least qualitatively, similar. Measurements reported in literature indicate that U(y) tends towards the laminar velocity profile in TBL, duct and OC flows when subjected to injection. The present work confirms this result and also indicates that the location of the sublayer-turbulent interface, y_i, shifts away from the wall in smooth-bed flows subjected to injection (see Tables 5.1 and 5.2). Conversely U(y) tends to more uniformity and the turbulence region extends closer to the wall with suction. Moreover, $\tau(y)$ increases/

decreases with suction/injection. On the face of it, these changes seem to suggest that suction/injection enhances/diminishes the turbulent nature of flow, which is contradicted by the observed reduction in flow turbulence reported in literature [refer eg. Elena, 1984; Fulachier et al, 1987]. The apparent conflict is resolved by observing that while suction/injection reduces/increases U'_{rms} and/or V'_{rms}, it may vastly increase/ decrease the correlation between U' and V'. This will cause increase in the turbulent shear stress with simultaneous decrease in turbulent normal stresses and turbulence generation with suction, and the converse for injection. Thus, suction can still be considered to promote the turbulent nature of the flow (increased ratio of turbulent to "laminar" shear stresses) at the cost of less turbulence or with apparent "laminarization" of the flow. This suggests that suction is likely to reduce the strength (or vorticity) and/or number of turbulence eddies while enhancing their directional preference and reducing their randomness. The opposite effects are implied for injection.

The present analysis makes use of eddy viscosity formulations based on Prandtl's approach. Theoretically, there is little to choose between any of these formulae as they are based on inadequate postulates or phenomenological hypotheses. It may also be mentioned that Prandtl's mixing length formula as well as the two eddy viscosity formulations used in this work give closely similar velocity distributions for the inner region of canonical TBLs that are well within the scatter of experimental data. Physically, Prandtl's formulation is based on the proportionality

of u' and v' with ydu/dy. The parabolic ν_t formula can be interpreted differently by assuming v' to be independent of du/dy. Empirical data [see eg. Hinze, 1975; Sabot et al, 1977] indicates that in many canonical wall flows

$$V'_{rms} \simeq C_1 U_* \sqrt{1-C_2 y} \qquad 5.3$$

where C_1 is of order 1 and C_2 is $\simeq 1$. C_2 is considerably less than 1 in duct flows, which may be due to turbulent fluctuations crossing over from one half to the other half of the duct. Nonetheless, the component of V' that correlates with U' may be expressed on the basis of Equation 5.3 as

$$V' = U_* \sqrt{1-y} \qquad 5.4$$

Since V' is mainly caused by ejection of wall fluid elements during turbulence bursts it is reasonable to consider V' as independent of U and instead scaling on U_*. On the other hand U' will be coupled to Y dU/dY with κ as a proportionality constant as in Prandtl's formulation. Thus the parabolic eddy viscosity formulation is readily obtained.

The above formulation suggests that any small change (perturbation) in wall variable is likely to be transmitted across the boundary layer by turbulence eddies with a mean vertical velocity approximating Equation 5.4. The time taken for the effect of the variable to permeate the flow depth will be $2H/U_*$. The mean distance, X_d, traversed by the flow during this time is

$$X_d = \frac{2U_{av}H}{U_*} \qquad 5.5$$

or, $x_d = 2u_{av}/u_*$, where X_d may be considered as the transition zone or the developing length of the inner boundary layer, U_* being the modified shear velocity after introduction of the wall disturbance/change. Similarly an inward growing layer can be visualized to develop from the boundary layer edge due to change in outer/freestream variable, and X_d derived as in Equation 5.5 with the difference that U_* is taken as the upstream shear velocity since the outer disturbance propagates inward through interaction with wall or inner region eddies. As an illustration, Table 5.5 gives the computed x_d for smooth bed OC flows with suction/injection [refer Table 5.2]. It is evident from the table that x_d increases/decreases with suction/injection and with increase/decrease in R_*. Similar results can be computed for hydraulically rough flows with suction/injection from Tables 5.3 and 5.4. The computed values of x_d are comparable to those reported in literature for TBL flow [Simpson, 1971].

Table 5.5 : Computed developing lengths, X_d/H, for OC flows with suction/injection

R_* \ v_w	-0.02	-0.01	0	0.01	0.02
300	33.0	33.65	34.5	36.0	37.9
1000	37.7	38.8	40.5	43.2	47.5
10000	46.8	48.6	52.1	58.5	--

As in the case of suction/injection, x_d can be computed for change in other wall variables if u_{av} and u_* are known. For example, with a step jump/reduction in wall roughness u_{av} is expected to decrease/increase and U_* is expected to increase/decrease. Hence the transition from a smooth to rough wall boundary layer is likely to be much faster than the opposite transition, which agrees with experimental obervations [cf. Smits and Wood, 1985]. Equation 5.4 can also give an estimate of the dimensions of the inner layer as it developes if U(y) is known. As an approximation, if U(y) is nearly uniform, $U(y) \simeq U_{av}$, then

$$h_i \simeq \frac{u_* x}{2u_{av}} \left(1 - \frac{u_* x}{4u_{av}}\right) \qquad 5.6$$

which shows that the thickness of the internal layer, h_i, varies quadratically with x.

Taking the above arguments further it may be reasoned that when a wall input is small such that

(i) U(y) is nearly self-similar when scaled with either U_* or an outer flow velocity scale, and

(ii) the fractional change in U(y) is comparable to the fractional change in U_* over the length x_d,

then the flow is nearly self-preserving not only in terms of its mean flow but also with respect to coherent structures and the turbulence field. This follows from the unique relation between the mean and turbulent flow fields underlying parabolic ν_t. Thus, in the case of suction/injection applied at low rates to OC flow, the present work gives the relations :

$$U(x,y) \simeq U(o,y)\,[1 + \alpha\, x],\quad \alpha = \frac{v_w}{u_{av}}$$

$$U_*(x) \simeq U_*(o)\,[1 + \beta x],\quad \beta = \left(\frac{1-v_w u_{av}}{1-2v_w u_{av}}\right)$$

Since the mean flow is nearly self-similar for $|v_w| \ll 1$,

$$\frac{U(x_d,y)}{U(o,y)} - \frac{U_*(x_d)}{U_*(o)} = -\frac{2v_w^2\, u_{av}}{u_*(1-2v_w u_{av})} \qquad 5.7$$

If, and only if, the right side of Equation 5.7 is numerically significant, then it implies different scales of evolution of U' and V' ie, the coherent flow structures may change significantly in the flow direction. Though the present arguments are speculative in nature, and it does not appear possible to demonstrate from the turbulence energy equation that the flow will remain nearly self-preserving in all turbulence moments and at all scales of turbulence [in the sense discussed by George, 1989] if the right side of Equation 5.7 is numerically much less than 1, this result follows from the phenomenological premises of parabolic ν_t formulation. Similar results as Equation 5.7 can be derived for gradually varying (quasi-uniform) or slowly developing wall turbulent flows (under the influence of small variations in wall inputs) if a nearly self-simiar mean velocity solution can be found with an appropriate eddy viscosity model. The wall inputs may include wall heating since theoretical considerations (Reynolds analogy) and experimental data [eg. Fulachier and Dumas, 1975; Fulachier, et al, 1987; Kays, 1972] suggest that the mechanism and diffusivities of heat and momentum transfer are comparable.

5.1.4. Practical implications for alluvial channels and duct flows

Most unlined canals and natural channel are subjected to infiltration and seepage losses through the channel boundary over long stretches and long periods of time. The rate of infiltration, depending on the difference in head of channel water with ambient ground water table and the soil porosity, may vary with time, but are generally small. The present anaysis shows that in such cases u(y) will tend to be more uniform and u_{av} higher than the corresponding log-law velocity. Since, even small changes in v_w of the order of 10^{-2} can change S_f/S_o significantly, particularly for $k_s << 1$, the use of a constant friction slope, or Manning's 'n', or Chezy's 'C', can give erroneous results if the seepage rates vary with time. If there is mass efflux through the channel boundary -- this may occur for instance, due to excess bank storage or due to groundwater recharge by prolonged precipitation in a catchment or by over-irrigation -- the channel water level may be significantly higher than predicted. This can compound other problems such as the likelihood of a channel to overflow its banks during the passage of flood waves.

Alluvial channels have erodible boundary and carry sediment load. While the present analysis shows that infiltration increases the time-average bed shear stress, this does not necessarily imply that grain mobility and sediment load are enhanced. Firstly, the present work gives the mean τ_w, but not the fluctuating component of τ_w, which is probably more important in grain erosion and motion. Secondly, grain erosion is

strongly affected by hydrodynamic lift force. Eddy viscosity models do not give any estimate of the near-wall pressure or lift force on surface grains. The change in lift force is probably more strongly related to the vertical seepage pressure gradient than the OC velocity fluctuations. Thus the combined effect of suction on bed grains would be an increase in drag force and reduction in lift force which have opposite effects on grain erodibility. Going by empirical data [eg. Brink and Oldenziel, 1974], it seems fairly certain that suction decreases grain velocity and bedload in a channel, while injection or effluent seepage has the opposite effects.

As noted in the earlier section the water surface profile is convex with effluent seepage and concave with influent seepage. Since $|v_w| << 1$ in most channels, the curvature of the water surface would be barely noticeable in field situations. However, over long stretches, the curvature effect may change the flow depth and U_{av} considerably, provided $S \simeq S_o$. One possible consequence of this over a long period of time may be some adjustments of channel geometry such as channel width or bed slope. It may be noted that many graded or regime channels exhibit exponentially decreasing bed slope over long stretches. Several possible causes have been attributed to this phenomenon [see eg., Garde and Raju, 1985]. Another possible reason suggested here is long-term channel adjustment of bed slope corresponding to the concave water surface produced by infiltration from the channel into the bed. Thus if bed slope, S, changes as

$$S = S_o \exp(-2Cx)$$

then $$h_{bed} = h_{bed,o} + C S_o x^2$$

which shows that bed elevation, H_{bed}, changes at the same rate as water surface elevation if $C = -\alpha = -V_w/U_{av}$ (cf. Equation 3.49). Hence the flow will be apparently uniform as the flow depth remains constant if $V_w S/(U_{av} S_o)$ is constant along X. Such channel adjustment leading to nearly self-similar flow may be a natural mechanism for channels to adjust to nonuniform flow. The suggestion made here is tentative, and obviously needs further examination based on field data and a valid variational principle of channel adjustment.

A direct extension of the present analysis to flow in ducts is possible if eddy viscosity formulations are assumed to be valid for the entire flow region. Replacing S by $\partial P^+/\partial x$ in the OC flow equations, the results for flow in rectangular ducts with uniform suction/injection through opposite boundaries will be similar to those for OC flow. Some quantitative difference will arise due to the flow depth being constant in duct flow. However, it may be expected that, in order to carry a certain Q_o at a given section, the centreline pressure gradient will be significantly higher/lower for injection/suction as compared to the case for $v_w = 0$. The ratio of pressure gradients should roughly be about $(H_o/H_n)^3$ in OC flow for $|v_w| << 1$. Moreover, $\partial P/\partial x$ can be expected to decrease/increase over x at the rate $\alpha = v_w/u_{av}$. On the other hand, the wall shear may increase/decrease slightly with suction/injection but will decrease/increase along x with suction/injection. Qualitatively similar results can be expected

for axisymmetric duct flows. It may be pointed out here that Eckert and Rodi's measurement [refer Narasimhan and Sreenivasan, 1979] showed clearly an increasing trend for C_f with x in turbulent pipe flow with injection. This partly confirms the above observations. However, a surer confirmation could be forthcoming from direct measurements of the centreline pressure gradient which, as of now, does not appear to have been reported in literature. Lacking such confirmation the observations made herein on duct flows should be considered tentative, or at least approximate, since the application of parabolic eddy viscosity model does not seem to be accurate even for canonical (ie, uniform) duct flows.

5.2 Hydraulics of sand ribbons

5.2.1 Scaling of lineations

The experiments described in the previous chapter showed that S1 sand beds comprising fine to medium sands developed bed ripples at a little above threshold conditions, while the relatively coarser S2 and S3 sand beds produced longitudinal bedforms or ribbons for a wide range of flow conditions. For S1 sands at just above incipient state fine striae were observed in some cases. On scaling the lateral spacing, L_z, of these striations with wall variables it was found that they are of dimensions on the order of sublayer streaks. As indicated in Table 5.6, $\tilde{d}_{50} < 6.0$, and the bed may be considered hydraulically smooth. The bed roughness Reynolds number $\tilde{d}_{50} = D_{50}\ U_*/\nu$ was computed after correcting the bed shear velocity for sidewall effect [Vanoni, 1975]. The measured values of $\tilde{l}_z$, varying between

~ 130 to 200, are higher than sublayer streaks spacings, but this could be due the striations not developing at all streak locations, or due to all striations not having been clearly observed during the measurements, or due to striations being related to buffer layer streaks which have higher spacing as compared to sublayer streaks [Smith and Metzler, 1977]. On the whole, the striations appear to conform to the low-speed streak model of parting lineations and bedload streaks.

Table 5.6 : Lateral spacing of bed striations scaled with wall variables

Run	S101	S102	S103	S104	S105	S106	S107
$\tilde{d}_{50}$	5.20	4.77	4.98	5.09	4.65	4.60	5.52
$\tilde{d}_{84}$	7.88	7.24	7.55	7.72	7.06	6.98	8.38
$\tilde{l}_z$	161	133	155	188	181	167	206

The sand ribbons on S2 and S3 sand beds were more well-marked and stable structures. Scaling with wall variables did not reveal any specific property of the ribbons. When normalized with flow depth, however, L_z was found to be fairly constant with an average $\overline{l}_z = L_z/H \simeq 2.03 \pm 0.1$. This value differs from some values reported in literature suggesting $\overline{l}_z \simeq 3$ to 4, particularly for ribbons observed in natural settings. This difference may be due to the confining effects of sidewalls; but, as the aspect ratio of flow was high (about 8 to 16) it is unlikely that sidewalls may have restricted the lateral spacing of ribbons. Overall, the consistently uniform value of L_z scaled on flow depth

confirms the secondary flow model for sand ribbons.

The vertical dimension, L_y, of sand ribbons does not appear to scale with either wall or outer variables. $L_y << L_z$, and in general L_y is about 2 to 3 times the median grain diameter of sand ribbons or median bedload grain size. Since bedload motion was observed during the experiments to occur mainly over and along the edge of ribbons, L_y probably represents the thickness of the upper two or three layers of moving bedload. Effluent/influent seepage, which had no perceptible effect on L_z, appeared to increase/decrease L_y slightly.

5.2.2 Bed shear stress distribution

The analysis of secondary flow in Chapter 3 assumed a specific type of roughness variation, and corresponding sinusoidally varying components of U, U_* and V,

$$\ln y_o = \ln y_{om} [1+\varepsilon \cos(kz)]$$

$$u = u_o(y) + u_1(y) \cos(kz)$$

$$u_* = 1 + u_{*1} \cos(kz)$$

and $$v(y) = a_o y^m (1-y)^n \cos(kz)$$

The solution set for $u_1(y)$, u_{*1} and a_o depends on the assumed values of m, n, and C_1, where C_1 relates $u_1(1)$ to $u_1(y_o)$, $u_1(1) = C_1 u_1(y_o)$. Numerical solution of Equation 3.74 showed that while a_o and $u_1(y)$ are significantly affected by C_1, m and n, u_{*1} depends mostly on ε and k, and to a lesser extent on $\ln y_{om}$, C_1, m and n. Since the analysis is only approximate, and since the aim here is to obtain a rough estimate of the bed stress distribution, variations in C_1, m and n may not significantly affect the use of the model results in the present study.

In order to calibrate the model the data of Muller and Studerus [1979] and Studerus [1982] were used. In their experiments with simulated bed ribbons, 60 mm wide roughness strips were placed at 160 mm centre to centre having 100 mm wide smooth zones between the strips. The flow depth being 80 mm, z_o=2 or k=π in their experiments. Replacing their bed roughness by an equivalent sinusoidally varying roughness such that the cross-sectionally averaged mean velocities match, their velocity and shear stress measurements can be compared with the analysis for different assumed C_1, m and n. As an illustration some comparisons are shown for C_1 = 0, m = 2 and n = 4 in Figures 5.6 through 5.8. Figure 5.6 shows fairly good matching between the observed and computed secondary flow velocities. The isovels for mean streamwise velocity shown in Figure 5.7 also indicate reasonable agreement for y<0.4 but diverge from measured values in the upper half of the flow region. This can be corrected by assigning a negative value to C_1. Figure 5.8 shows a plot of measured and computed shear stress over the rough and smooth zones. Though the measured and computed stresses have similar trends of variation over depth the ccomputed stresses are much less above the smooth zone. This can be rectified partly, but not entirely, by adjusting C_1, m and n.

It may be noted that in the experiments of Muller and Studerus, $\varepsilon \simeq 0.2$ is not very small. Hence ignoring terms of order ε^2 in the analysis may have produced significant error for this flow situation. Partly for this reason and partly because the main aim here is to estimate the bed shear stress variation

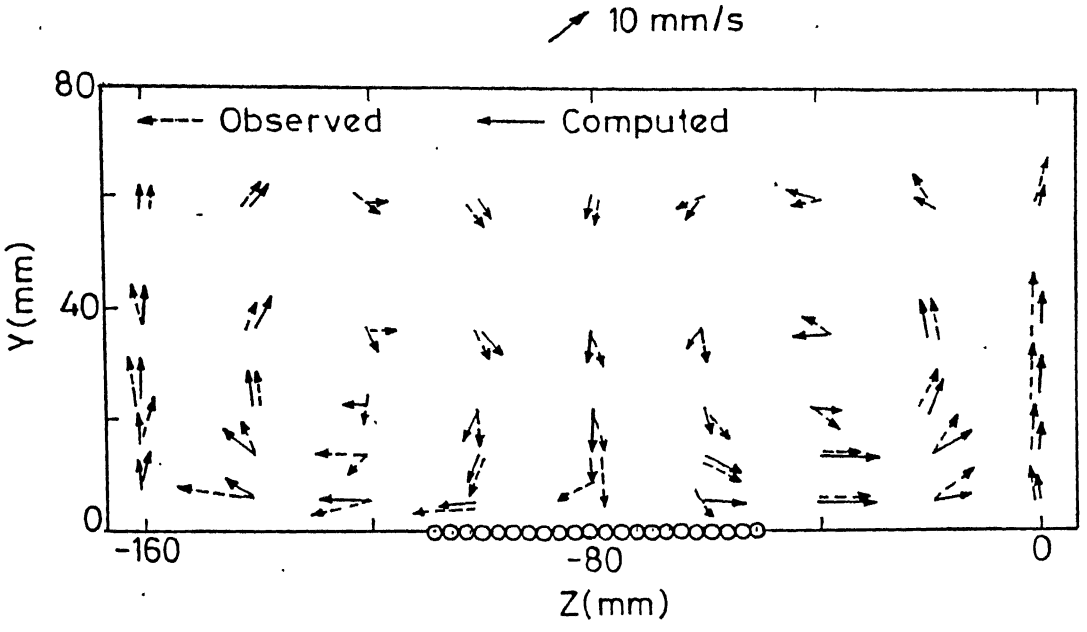

Figure 5.6 : Comparison of observed and computed secondary flow velocities on bed with roughness strips.

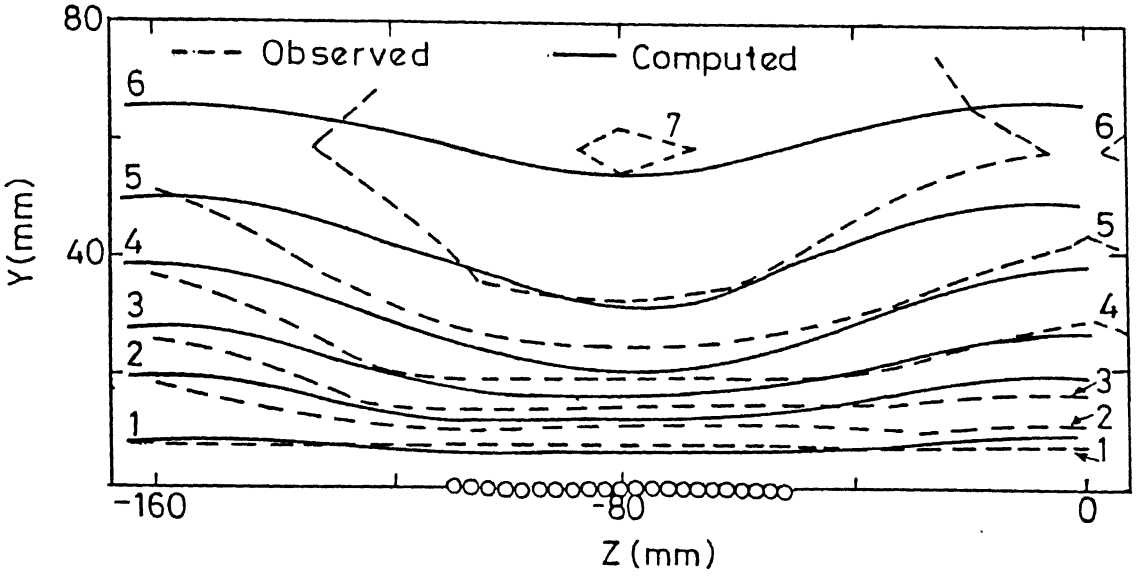

Curve	1	2	3	4	5	6	7
U/U	0·80	0·90	0·95	1·00	1·05	1·10	1·15

Figure 5.7 : Comparison of observed and computed mean velocity contours on bed with roughness strips.

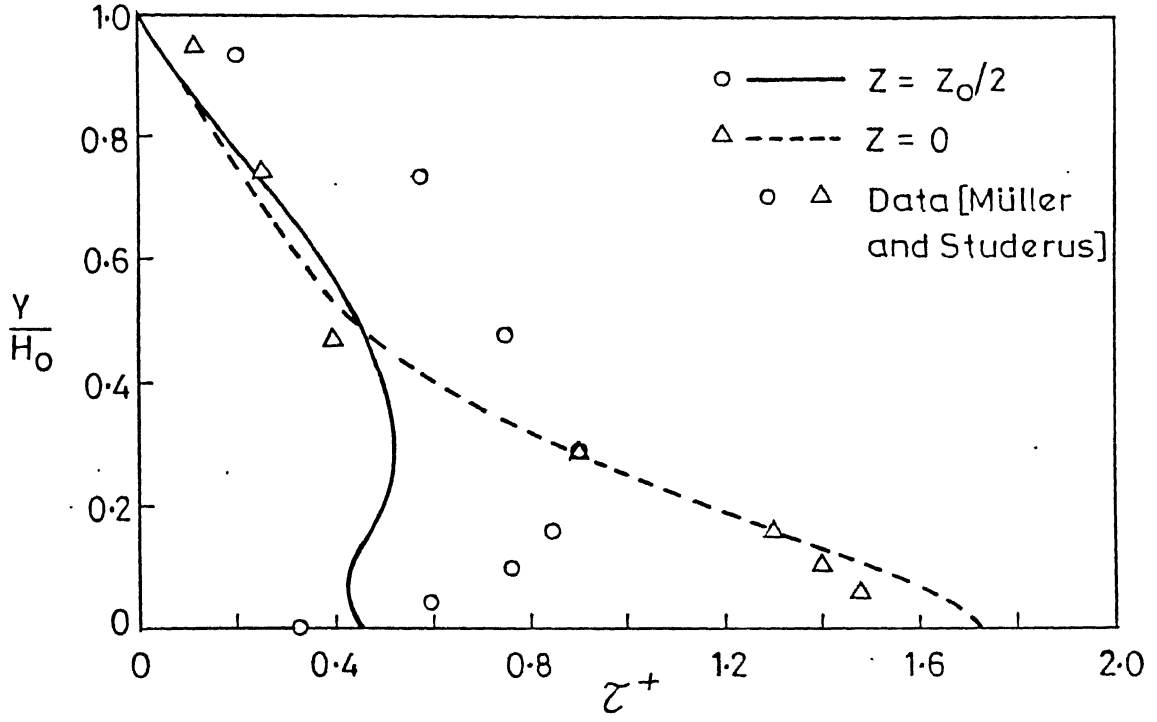

Figure 5.8 : Comparison of observed and computed shear stress over smooth and rough strips

for small values of ε, accurate calibration of the model parameters have not been attempted. Since the sand ribbons generated spacing of about $2H_o$, u_{*1} and a_o were computed for different values of ε and ln y_{om} with k=2 and C_1, m and n as above. The computed values are shown in Table 5.7.

Table 5.7 Computed values of u_{*1} and a_o for flow over sand ribbons with k=2, C_1=0, m=2 and n=4.

y_{om}	0.01	0.005	0.002	0.001	0.0005
ln y_{om}	-4.605	-5.298	-6.215	-6.908	-7.601
a_o/ε	268	213	180	167	157
u_{*1}/ε	-2.88	-2.29	-1.92	-1.78	-1.67

5.2.3 Bedform regime criteria and sand ribbons

The experiments with S1, S2 and S3 sands showed that sand ribbons formed readily for flow with equilibrium sediment load over a non-uniform sand bed comprising medium to coarse sand or sand-gravel mixtures, but not with fine-medium sand mixtures. Several bedform regime criteria have been proposed in sediment transportation literature, eg., Garde and Albertson, Simons and Richardson [refer Garde and Raju, 1985; Vanoni, 1975], van Rijn [1984]; several other criteria are in use in geophysical and sedimentological analysis. Since all these criteria are empirical, it will suffice to compare the sand ribbons' existence conditions with only one of these in order to show that the bedform regime criteria are not valid for sand ribbons.

Figure 5.9 shows a plot of the regime data of sand ribbons on Simons and Richardson's graph of stream power $\tau_w U_{av}$ versus fall diameter of ribbon sand, where τ_w is the estimated stress over ribbons. As evident from the figure the sand ribbons occupy a considerable area of the lower (dune) and transition bedform regime. Likewise, comparison of the hydraulic regime of sand

ribbons with other bedform regime criteria indicate that with non-uniform sand beds containing sufficient amounts of coarse or very coarse sand or gravel the development of ripple or dune bedforms are considerably inhibited. Physically, this may be attributed to possible mutual cancellation of three-dimensional or streamwise disturbances associated with suspended motion (of fine and medium sands), saltation (of coarse sand) and bedload motion (of very coarse sand and gravel). Since the present experiments where conducted at subcritical flow conditions, the results complement Chiew's [1991] finding of no antidune formation on non-uniform sand bed at near-critical or supercritical flow conditions.

5.2.4 Sediment transport with sand ribbons

Since sand ribbons are flow-aligned and are of low relief, they do not offer any significant form resistance. Hence the equilibrium sediment transport rate, Q_s, over a bed of sand ribbons may be expected to differ from that over a dune or ripple bed. Though the suggested bedload transport equations for sand mixtures are different from those of uniform sand, the Einstein-Brown relation [refer Vanoni, 1975] for uniform bedload size has been used here as an yardstick for comparison. Accordingly,

$$\phi_s = \frac{Q_s}{F_1 \sqrt{a_g (\gamma_s - \gamma) d_s^3}} \qquad 5.8$$

$$\tau_* = \frac{\gamma H S}{(\gamma_s - \gamma) d_{50}} \qquad 5.9$$

where $F_1 = \sqrt{0.666667 - f_1} - \sqrt{f_1}$ 5.10a

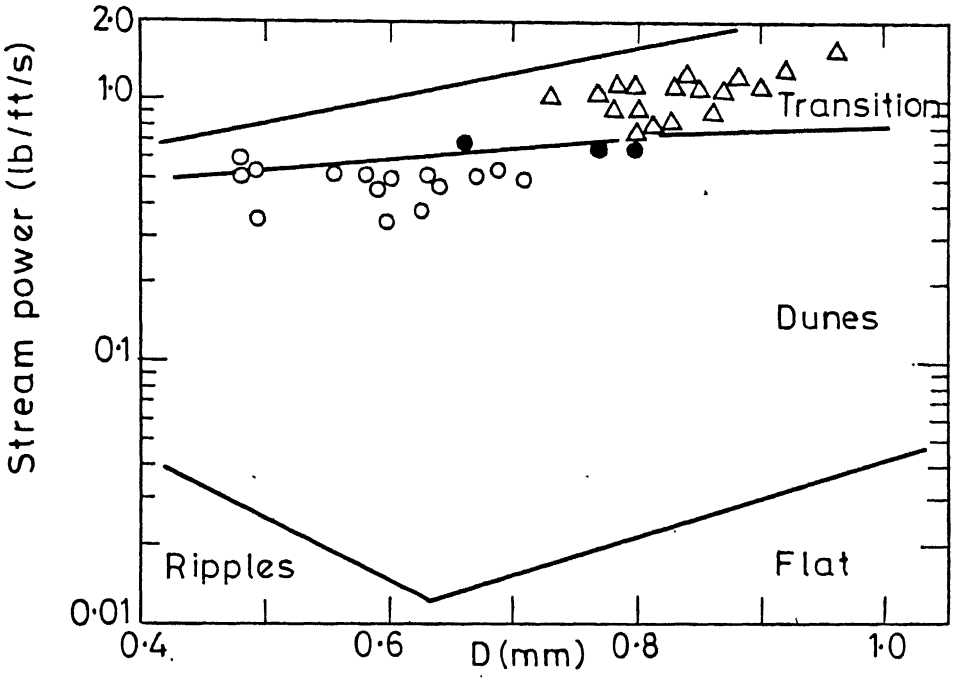

Figure 5.9 : Comparison of sand ribbons with Simons and Richardson's regime criteria.

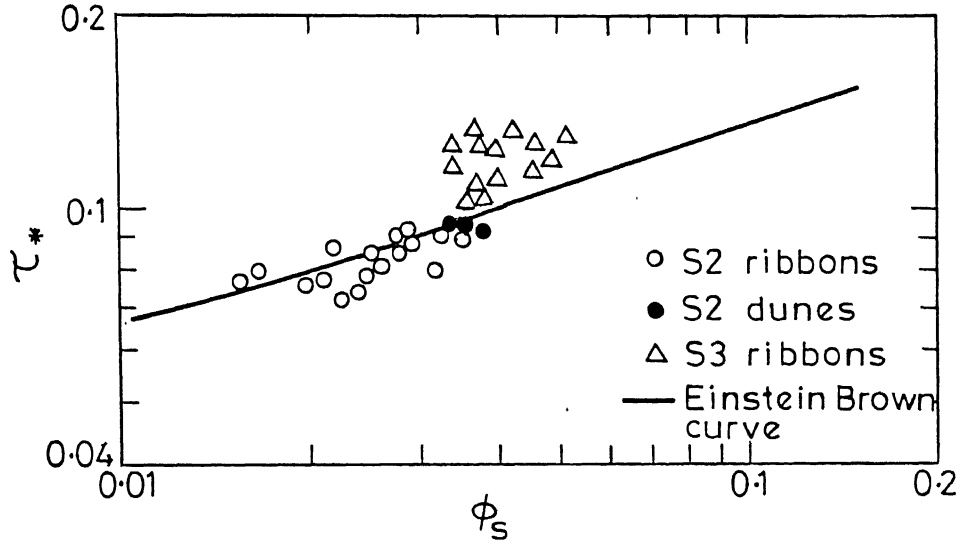

Figure 5.10 : Sediment transport over sand ribbons compared with Einstein-Brown relation.

$$\text{and} \qquad f_1 = \frac{36\,\rho\,\nu^2}{d_s^3\,(\gamma_s - \gamma)} \qquad 5.10b$$

have been plotted in Figure 5.10. As evident from the figure some of the data of S3 sand indicate lower bedload than predicted from the Einstien-Brown relation for $\tau_* > 0.09$,

$$\phi_s = \frac{40}{\tau_*^3} \qquad 5.11$$

There ia also slight increase in bedload with injection and decrease with suction (not shown in figure). This difference can be rectified by including a lift force component in Equation 5.9 to account for change in sediment mobility with suction/ injection [cf. Brink and Oldenziel, 1974; Maclean and Willetts, 1986].

5.3 Concluding remarks

The present work shows that eddy viscosity or mixing length models can be successfully applied to OC flows where the secondary velocity components, V and W, are numerically much less than the streamwise velocity, U. In such cases U(x,y,z) can be split into separate components

$$u(x,y,z) \simeq u_o(y) + f(x)\,u_1(y) + g(z)\,u_2(y) \qquad 5.12$$

where $u_o(y)$ is the canonical (log-law) velocity, and f(x), g(z), $u_1(y)$ and $u_2(y)$ are determined from the equations of motion with suitable assumptions on the form of f(x) and g(z) from boundary conditions. Evidently, the approach is likely to fail when the secondary velocities or velocity gradients are significant in

comparison to the streamwise velocity or velocity gradient, eg., flow near corners or sidewalls in a rectangular channel, or spatially varied OC flow with high rates of inflow or outflow. Though the analysis of TBL flow, spatially varied pipe flow and other slowly developing wall flows is beyond the scope of this work, it is suggested that eddy viscosity modelling together with the assumption of Equation 5.12 may be found analytically useful in many such flow situations.

CHAPTER 6

SUMMARY AND CONCLUSIONS

6.1 Summary

Isotropic eddy viscosity modelling of Reynolds stresses has been applied to open channel flow

(i) subjected to uniformly distributed suction/injection, and

(ii) over sand ribbons of lateral grain sorting.

In the former case the equations of motion are reduced to two coupled ordinary differential equations by assuming the mean streamwise velocity and the outer and inner velocity scales (energy gradient velocity and bed shear velocity) to be piecewise linear in X. For low rates of suction/injection and water surface nearly parallel to the bed, the flow was found to be nearly self-similar, and the velocity and shear stress distributions were obtained. The analysis indicates higher/lower mean velocity (hence lower/higher flow depth) and positive/negative water surface curvature with suction/injection as compared to an equivalent uniform flow. Flume experiments conducted on rigid, hydraulically rough bed showed good agreement with the model. The results also compare with boundary layer data while indicating quantitative differences.

Experimental study of sand ribbons showed stable flow-aligned sand ribbons at the exclusion of ripples and dunes in subcritical flow with equilibrium sediment load on a bed of sand-gravel or fine-coarse sand mixtures. The spanwise spacing of ribbons was about 2 times the flow depth and their relief was about twice the median grain diameter. The analytical model indicated secondary flow cells and spanwise shear stress variation

at the rate of 2 to 3 times the rate of log-law velocity shift due to bed roughness variation.

6.2 Conclusions

The following conclusions are drawn in the present study :

(i) $U_*^2/(a_g H_o S_o)$, or S_f/S_o where S_f is friction slope, increases/decreases with suction/injection in agreement with one-dimensional OC analysis and TBL data.

(ii) α and β are comparable, but deviate as $|v_w|$ increases.

(iii) Dimensionless velocity u(y) increases and has a fuller profile for suction, and conversely for injection.

(iv) $\tau(y)$ sharply increases/decreases near the bed with suction/injection.

(v) The above changes magnify with increase in $H_o \sqrt{a_g H_o S_o}/\nu$ and with decrease in relative roughness, K_s/H_o.

(vi) Water surface has concave/convex curvature for suction/injection. Flow depth varies as

$$H \simeq H_o \left[1 - \alpha S_o x^2 \left(1 + \left(\alpha / 3\right)x\right)\right] \qquad (3)$$

(vii) The analysis suggests that in duct flow dP/dX decreases/increases with suction/injection for same discharge.

(viii) From a physical interpretation of parabolic eddy viscosity distribution it is reasoned that the flow is nearly self-preserving in all respects -- mean flow, turbulence field and coherent structures -- if $|v_w^2 U/U_*| \ll 1$, and an estimate of inner boundary layer length with change in wall inputs is suggested.

(ix) It is suggested that effluent seepage increases flow depth and enhances chances of flood waves overflowing stream banks, while infiltration may be the cause of exponentially decreasing bed slope in graded streams.

(x) Sand ribbons, that are hydrodynamically similar to flat bed, are a stable phenomenon associated with coarse sand-fine sand or sand-gravel mixtures.

(xi) Sand ribbons and secondary flow cells develop by mutual reinforcement, secondary flow causes bedload deflection towards the ribbons, while the ribbons themselves produce lateral shear stress variation and secondary flow by creating transverse velocity gradients, and hence lateral shear stress gradients.

(xii) Sand ribbons do not grow into well-developed ridge-groove structures (except under degrading bed conditions) probably because the lateral stresses are not very high, and because developed ridges will have the opposite effects as grain-sorting, thereby weakening the secondary flow and shear stress variation.

(xiii) The breakdown of ribbons to primary ripples or dunes in sand mixtures may be inhibited due to insufficiency of fine sand(suspended and saltating sediment grains).

(xiv) The existence of sand ribbons in subcritical flow defies the existence criteria of ripples, dunes, etc., for uniform sand, but complements Chiew's finding of no antidune bed for sand mixtures in supercritical flow.

(xv) From the point of view of paleocurrent analysis lineations with lateral grain sorting should indicate past flow with non-uniform bedload, whereas uniform bedding surface texture may be the imprint of sublayer flow structure.

6.3 Recommendations

(i) The scope of the present analytical solution for suction/injection can be improved by considering arbitrary water surface slopes or higher suction/injection velocities. This will necessitate numerical solution of coupled equations derived from the equations of motion (boundary layer equations).

(ii) The effect of suction/injection on grain mobility and sediment transport rates has been studied by several researchers empirically. These studies may be combined with the present analytical results.

(iii) An extension of the present analysis to duct flows and TBLs may be studied theoretically and experimentally by adopting an appropriate eddy viscosity formula.

(iv) The sand ribbons studied here were generated in the laboratory. Field studies may be a useful addition to the knowledge of these structures.

(v) The study of the breakdown of sand ribbon to ripples or dunes (associated with flow disturbances propagating downstream) may be a stimulating problem that can throw light on the mechanism of generation of ripples and dunes.

REFERENCES

ACKERS,P.[1983]. "Sediment transport problems in irrigation systems design," in NOVAK, P. (ed.), Developments in Hydraulic Engineering-I, Appl. Sci. Publ., London, 151-195.

ALFREDSSON,P.H., JOHANSSON,A.V., HARITONIDIS,J.H., and ECKELMAN,H.[1988]. "The fluctuating wall shear stress and the velocity field in the viscous shear sublayer," Phys. Fluids, 31(5), 1026-1033.

ALLEN,J.R.L.[1969]. "Erosional current marks of weakly cohesive mud beds," J. Sed. Petrol., 39, 607-623.

ALLEN,J.R.L.[1982]. Sedimentary Structures,I, Elsevier, Amsterdam, 237-270.

AKAN,A.O. and YEN,B.C.[1981]. "Mathematical modeling of shallow water flow over porous media," J. Hydr. Engg., 115 (6), 825-830.

ASCE Task Committee [1988]. "Turbulence modeling of surface water flow and transport," Parts 1 to 5, J. Hydr. Engg., 114(9), 970-1073.

BAYAZIT,M.[1976]. "Free surface flow in a channel of large relative roughness," J. Hydr. Res., 14 (2), 115-126.

BEAVERS,G.S. and JOSEPH,D.D.[1967]. "Boundary conditions at a naturally permeable wall," J. Fluid Mech., 30(1), 197-207.

BLACKWELDER,R.F. and ECKELMAN,H.[1979]. "Streamwise vortices associated with the bursting phenomenon," J. Fluid Mech., 94, 577-594.

BLAKE,W.K.[1970]. "Turbulent boundary-layer wall pressure fluctuations on smooth and rough walls," J. Fluid Mech., 44, 637-660.

BLINCO, P. H. and PARTHENAIDES, E. [1971]. "Turbulence characteristics of free surface flows over smooth and rough boundaries," J. Hydr. Res., 9(1), 43-69.

BRINK,W.E. and OLDENZIEL,D.M.[1974]. "Influence of suction and blowing on entrainment of sand particles," J. Hydr. Div., Proc. ASCE, 100(HY7), 935-949.

CANTWELL,B.J.[1981]. "Organized motion in turbulent flow," Ann. Rev. Fluid Mech., 13, 457-515.

CARDOSO,A.H., GRAF,W.H., and GUST,G.[1989]. "Uniform flow in a smooth open channel," J. Hydr. Res., 27(5), 603-616.

CHEN,C.-L.[1991]. "Unified theory on power laws for flow resistance," J. Hydr. Engg., 117(3), 371-389.

CHIEW,Y.W.[1991]. "Bed features in nonuniform sediments," J. Hydr. Engg., 117(1), 116-120.

CHOW,V.T.[1959]. Open-Channel Hydraulics, McGraw-Hill, N.Y., 680p.

COLEMAN,N.L.[1981]. "Velocity profiles with suspended sediment," J. Hydr. Res., 19(3), 211-229.

COLEMAN,N.L.[1991]. Discussion on "Turbulent velocity profiles for smooth and rough open channels," J. Hydr. Engg., 117(9), 1219-1221.

DAVID,K.J.[1980]. "The effect of non-uniformity in grain size on the roughness of sand beds," Ph.D. Thesis, IIT, Kanpur, 356 p.

DENGEL,P. and FERNHOLZ,H.H.[1990]. "An experimental investigation of an incompressible turbulent boundary layer in the vicinity of separation," J. Fluid Mech., 212, 615-636.

ELENA,M.[1984]. "Suction effects on turbulence statistics in a heated pipe flow," Phys. Fluids, 27(4), 861-866.

EL-KHASHAB,A. and SMITH,K.V.H.[1976]. "Experimental investigations of flow over side weirs," J. Hyd. Div., ASCE, 102(HY9), 1255-1268.

FIEDLER,H.E. and FERNHOLZ,H.-H.[1990]. "On management and control of turbulent shear flows," Prog. Aerosp. Sci., 27, 305-387.

FOLK,R.L.[1976]. "Rollers and ripples in sand, streams and sky : rhythmic alternation of transverse and longitudinal roll vortices," Sedimentol., 23, 649-669.

FULACHIER,L., BENAGID,T., ANSAELMET,E., ANTONIA,R.A., and KRISHNAMOORTHY,L.V.[1987]. "Behaviour of coherent structures in a turbulent boundary layer with wall suction," Proc. First European Turb. Conf., Advances in Turbulence, Springer, Berlin, 399-407.

FULACHIER,L. and DUMAS,R.[1976]. "Spectral analogy between temperature and velocity fluctuations in a turbulent boundary layer," J. Fluid Mech., 76(2), 257-277.

FULACHIER,L., VEROLLET,E., and DEKEYSER,I.[1977]. "Experimental results on a turbulent boundary layer with wall suction and heating," Int. J. Heat Mass Trans., 20(7), 731-739.

GAD-EL-HAK,M. and BLACKWELDER,R.F.[1989]. "Selective suction for controlling bursting events in a boundary layer," AIAA J., 27(3), 308-314.

GALBRAITH,R.A.McD. and HEAD,M.R.[1975]. "Eddy viscosity and mixing length from measured boundary layer developments," Aeron. Quart., 26, 133-154.

GANGADHARAIAH,T., DAVID,K.J. and ROY,G.[1991]. "Effect of non-uniformity of sand grains on roughness scale, "Nat. Sem. -- Rec. Trends Water Res. Engg., IIT, Kanpur, M1-M5.

GARDE,R.J. and RAJU,K.G.R.[1985]. Mechanics of Sediment Transportation and Alluvial Stream Problems, Wiley Eastern, New Delhi, 618 pages.

GEORGE,W.K.[1989]. "The self-preservation of turbulent flows and its relation to initial conditions and coherent structures," in George, W. K. and Arndt, R. (eds.), Advances in Turbulence, Hemisphere, New York, 39-73.

GLENNIE,K.W.[1987]. "Desert sedimentary environments, present and past -- a summary," Sed. Geol., 50, 233-256.

GRASS,A.J.[1971]. "Structural features of turbulent flow over smooth and rough boundaries," J. Fluid Mech., 50, 233-256.

GUPTA,A.K., LAUFER,J. and KAPLAN,R.E.[1971]. "Spatial structure in the viscous sublayer," J. Fluid Mech., 50, 493-512.

GUPTA,G.D., PARKASH,B. and GARDE,R.J.[1987]. "An experimental study of fabric development in plane-bed phases," Sed. Geol., 53, 101-122.

GUPTA,A.D. and PAUDYAL,G.N.[1985] "Characteristics of free surface flow over gravel bed," J. Irr. Drain. Engg., 111(4), 299-318.

HANNA,S.R.[1969]. "The formation of longitudinal sand dunes by large helical eddies in the atmosphere," J. Appl. Meteor., 8, 874-883.

HARITONIDIS,J.E.[1989]. "A model for near-wall turbulence," Phys. Fluids-A, 1(2), 302-306.

HEAD,M.R. and BANDYOPADHYAY,P.[1981]. "New aspects of turbulent boundary-layer structure," J. Fluid Mech., 107, 297-338.

HINZE,J.O.[1975] Turbulence, McGraw-Hill, New York, 790 p.

HO,L.T. and GELHAR,L.W.[1983]. "Turbulent flow over undular permeable boundaries," J. Hydr. Engg., 109(5), 741-756.

JACKSON,R.G.[1976]. "Sedimentological and fluid dynamic implications of the turbulent bursting phenomenon in geophysical flows," J. Fluid. Mech., 77, 511-560.

JEROMIN,L.O.F.[1970]. "The status of research in turbulent boundary layers with fluid injection," Prog. Aeron. Sci., Pergamon, Oxford, 10, 65-189.

JOBSON,H.E. and SAYRE,W.W.[1970]. "Vertical transfer in open-channel flow," J. Hydr. Div., Proc. ASCE, 96(HY3), 703-724.

KARCZ,I.[1967]. "Harrow-marks, current-aligned sedimentary structures," J. Geol., 75, 113-120.

KAYS,W.M.[1972]. "Heat transfer to the transpired turbulent boundary layer," Int. J. Heat Mass Trans., 15(5), 1023-1044.

KENYON,N.H.[1970]. "Sand ribbons in European tidal sea," Mar. Geol., 9, 25-39.

KLINE,S.J., REYNOLDS,W.C., SCHRAUB,F.A. and RUNSTADLER,P.W.[1967]. "The structure of turbulent boundary layers," J. Fluid Mech., 30, 741-773.

KOCHERYZHENKOV,G.V. and MATVEYEV,S.K.[1977]. "Improved law of the wall and its application to the calculation of turbulent boundary layers with injection (or suction)," Fluid Mech. -- Sov. Res., 6(3), 53-65.

KOMORI,S., UEDA,H., OGINO,F. and MIZUSHIMA,T.[1982]. "Turbulent structure and the transport mechanism at the free surface in an open channel flow," Int. J. Heat Mass Trans., 25(4), 513-521.

MACLEAN,A.G.[1991]. "Open channel velocity profiles over a zone of rapid infiltration," J. Hydr. Res., 29(1), 15-27.

MACLEAN,A.G. and WILLETS,B.B.[1986]. "Measurement of boundary shear stress in non-uniform open channel flow," J. Hydr. Res., 24(1), 39-51.

MANTZ,P.A.[1978]. "Bedforms produced by fine cohesionless, granular and flakey sediment under subcritical water flows," Sedimentol., 25, 83-103.

MARTIN,C.S.[1970]. "Effect of a porous sand bed on incipient sediment motion," Water Resour. Res., 6(4), 1162-1174.

MARTIN,C.S. and ARAL,M.M.[1971]. "Seepage force on interfacial bed particles," J. Hydr. Div., Proc. ASCE, 97(HY7), 1081-1100.

MCBEAN,E.A. and AL-NASSIRI,S.[1988]. "Uncertanity in suspended sediment transport curves," J. Hydr. Engg., 114(1), 63-74.

MCLEAN,S.R.[1981]. "The role of non-uniform roughness in the formation of sand ribbons," Mar. Geol., 42, 49-74.

MITTAL,P.K.[1977]. "Roughness of non-uniform sand beds," M. Tech. Thesis, IIT, Kanpur.

MITTAL,S.[1978]. "Roughness of sands having non-uniform grain size distributions," M. Tech. Thesis, IIT, Kanpur.

MULLER,A. and STUDERUS,X.[1979]. "Secondary flow in an open channel," Proc. 18th Cong. IAHR, Cagliari, Paper B.a.3, 19-24.

NAKAGAWA,H.[1984]. "Interaction between flow over a granular permeable bed and seepage flow," J. Hydrosc. Hydr. Engg., 2(2), 1-10.

NARASIMHA,R. and SREENIVASAN,K.R.[1979]. "Relaminarization of fluid flows," Adv. Appl. Mech., 19, 221-309.

NEZU,I., NAKAGAWA,H. and TOMINAGA,A.[1985]. "Secondary currents in a straight channel flow and the relation to its aspect ratio," in Bradbury, L.J.S. et al (eds.), Turbulent Shear Flows, 4, Springer-Verlag, Berlin, 246-260.

NEZU,I. and RODI,W.[1986]. "Open channel flow measurements with a laser doppler anemometer," J. Hydr. Engg., 112(5), 335-355.

NOURMOHAMMADI,K., HOPKE,P.K. and STUKEL,J.J.[1985]. "Turbulent air flow over rough surfaces. II. Turbulent flow parameters," J. Fluid Engg., 107(1), 55-60.

ODGAARD,A.J.[1984]. "Shear-induced secondary currents in channel flows," J. Hydr. Engg., 110(7), 996-1004.

PENNELL,W.T., ECKERT,E.R.G. and SPARROW,E.M.[1972]. "Laminarization of turbulent pipe flow by fluid injection," J. Fluid Mech., 52, 451-464.

PERKINS,H.J.[1990]. "The formation of streamwise vorticity in turbulent flow," J. Fluid Mech., 44, 721-740.

PERRY,A.E., HENBEST,S., and CHONG,M.S.[1986]. "A theoretical and experimental study of wall turbulence," J. Fluid Mech., 165, 163-199.

PERRY,A.E., SCHOFIELD,W.H., and JOUBERT,P.N.[1969]. "Rough wall turbulent boundary layers," J. Fluid Mech., 37, 383-413.

RASHIDI,M. and BANERJEE,S.[1990]. "Streak characteristics and behaviour near wall and interface in open channel flow," J. Fluid Engg., 112(2), 164-170.

RAUDKIVI,A.J.[1990]. Loose Boundary Hydraulics, Pergamon, Oxford, 538 p.

RICHARDSON,C.P. and PARR,A.D.[1991]. "Friction and free surface flow over porous media," J. Hydr. Engg., 117(11), 1496-1512.

RIJN, L. C. VAN [1984]. "Mathematical model for sediment concentration profiles in steady flow," Euromech 192 : Transport of Suspended Solids in Open Channels, 49-68.

ROBINSON,S.K.[1991]. "Coherent motions in the turbulent boundary layer," Ann. Rev. Fluid Mech., 23, 601-639.

SABOT,J. and COMTE-BELLOT,G.[1976]. "Intermittency of coherent structures in the core region of turbulent pipe flow," J. Fluid Mech., 74, 767-796.

SABOT,J., SALEH,I., and COMTE-BELLOT,G.[1977]. "Effect of roughness on the intermittent maintenance of Reynolds shear stress in pipe flow," Phys. Fluids, 20(10), S150-155.

SAMAGA,B.R., RAJU,K.G.R., and GARDE,R.J.[1986]. "Suspended load transport of sediment mixtures," J. Hydr. Engg., 112(11), 1019-1035.

SCHETZ,J.A. and NERNEY,B.[1977]. "Turbulent boundary layer with injection and surface roughness," AIAA J., 15(9), 1288-1294.

SCHLICHTING,H.[1979]. Boundary-Layer Theory, McGraw-Hill, New York, 817 p.

SCHMITZ,G.H. and SEUS,G.J.[1992]. "Mathematical zero-inertia modeling of surface irrigation : advance in furrows," J. Irr. Drain. Engg., 118(1), 1-18.

SCHOFIELD,W.H.[1981]. "Equilibrium boundary layers in moderate to strong adverse pressure gradients," J. Fluid Mech., 113, 91-122.

SHAH,D.A. and ANTONIA,R.A.[1989]. "Scaling of the bursting period in turbulent boundary layer and duct flows," Phys. Fluids A, 1(2), 318-325.

SIMPSON,R.L.[1971]. "The effect of discontinuity in wall blowing on the turbulent incompressible boundary layer," Int. J. Heat Mass Transf., 14(12), 2083-2097.

SIMPSON,R.L., MOFFAT,R.J., and KAYS,W.M.[1969]. "The turbulent boundary layer on a porous plate : experimental skin friction with variable injection and suction ," Int. J. Heat Mass Transf., 12, 771-789.

SINGH,S.P.[1981]. "Roughness of sand beds : development of models," M.Tech.Thesis, IIT, Kanpur, 77 p.

SMITH,C.R. and METZLER,S.P.[1983]. "The characteristics of low-speed streaks in the near-wall region of a turbulent boundary layer," J. Fluid Mech., 129, 27-54.

SMITS,A.J. and WOOD,W.H.[1985]. "The response of turbulent boundary layers to sudden perturbations," Ann. Rev. Fluid Mech., 17, 321-358.

SPEZIALE,C.G.[1991]. "Analytical methods for the development of Reynolds-stress closures in turbulence," Ann. Rev. Fluid. Mech., 23, 107-157.

STREET,R.L.[1979]. "Turbulent heat and mass transfer across a rough air-water interface : a simple theory," Int. J. Heat Mass Trans., 22, 885-899.

STUDERUS,X.[1982]. "Sekundärasträmungen in offenen Gerinne über rauhen Längsstreifen," Ph.D. Thesis (in German), ETH, Zurich, 186 p.

STUKEL,J.J., HOPKE,P.K., and NOURMOHAMMADI,K.[1984]. "Turbulent air flow over rough surfaces : mean flow parameters," J. Fluid Engg., 106(4), 405-409.

SUBRAMANYA,K.[1986]. Flow in Open Channels, Tata McGraw-Hill, New Delhi, 372 p.

TOMINAGA,A. and NEZU,T.[1992]. "Velocity profiles in steep open channels," J. Hydr. Engg., 118(1), 73-90.

TOWNSEND,A.A.[1976]. The Structure of Turbulent Shear Flow, Cambridge University Press, Cambridge, 429 p.

TSUJIMOTO,T.[1989]. "Longitudinal stripes of sorting due to cellular secondary currents," J. Hydrosc. Hydr. Engg., 7(1), 23-34.

UEDA,H., MOLLER,R., KOMORI,S., and MISZUSHIMA,T.[1977]. "Eddy diffusivity near the free surface of open channel flow," Int. J. Heat Mass Trans., 20(7), 1127-1136.

UMEYAMA,M. and GERRITSEN,F.[1992]. "Velocity distribution in uniform sediment-laden flow," J. Hydr. Engg., 118(2), 229-245.

VANONI,V.A.(ed.)[1977]. Sedimentation Engineering, American Society of Civil Engineers, New York, 745 p.

VEDULA,S. and ACHANTA,R.R.[1985]. "Bed shear from velocity profiles : a new approach," J. Hydr. Engg., 111(1), 131-143.

WARK,C.E. and NAGIB,H.M.[1991]. "Experimental investigations of coherent structures in turbulent boundary layers," J. Fluid Mech., 230, 183-208.

WATTERS,G.Z. and RAO,M.V.P.[1971]. "Hydrodynamic effects of seepage on bed particles," J. Hydr. Div., Proc. ASCE, 97(HY3), 421-439.

WEEDMAN,S.D. and SLINGERLAND,R.[1985]. "Experimental study of sand streaks formed in turbulent boundary layers," Sedimentol., 32, 133-145.

WERNER,F., UNSOLD,G., KOOPMANN,B., and STEFANON,A.[1980]. "Field observations and flum experiments on the nature of comet-marks," Sed. Geol., 26, 233-262.

WHITE,F.M.[1974]. Viscous Fluid Flow, McGraw-Hill, New York,725p.

WILLIAMS,P.B. and KEMP,P.H.[1971]. "Initiation of ripples on flat sediment beds," J. Hydr. Div., Proc. ASCE, 97(HY4), 505-522.

WILLIS,J.C.[1985]. "Near-bed velocity distributions," J. Hydr Engg., 111(5), 741-753.

WILLMARTH,W.W.[1975]. "Pressure fluctuations beneath turbulent boundary layers," Ann. Rev. Fluid Mech., 7, 13-38.

WILSON,K.C.[1989]. "Mobile bed friction at high shear stress," J. Hydr. Engg., 115(6), 825-830.

YEFIMTSOV,B.M., KUZNETSOV,B.V., and SYSOYEV,V.A.[1983]. "Turbulent fluctuations of shear stress at the wall," Fluid Mech. -- Sov. Res., 12(2), 121-131.

ZAGNI,A.F.E. and SMITH,V.H.[1976]. "Channel flow over permeable beds of graded spheres," J. Hydr. Div., Proc. ASCE, 102(HY2), 207-222.

ZIPPE,H.J. and GRAF,W.H.[1983]. "Turbulent boundary layer flow over permeable and non-permeable rough surfaces," J. Hydr. Res., 21(1), 51-65.